博士学位論文

Doctoral Dissertation

Water Diffusion-Governed Thermal History of Self-Healing Hydrogels and Their Applications for Dynamic Materials

水拡散によって支配される自己修復ハイドロゲルの熱履歴現象とその動的材料への応用

By

余 承涛

YU Chengtao

Supervisor: Jian Ping Gong

北海道大学大学院生命科学院

Graduate School of Life Science, Hokkaido University

2020 年 12 月

December 2020

Contents

Abstract

Thermal responsive hydrogels have been subject to extensive research for smart applications. The existing thermal responsive hydrogels, no matter with upper critical solution temperature or lower critical solution temperature, usually show obvious changes in transparency, volume and mechanical performance at the critical temperature, which is independent on the experienced thermal history. In this dissertation, we reported that self-healing hydrogels containing abundant physical bonds, such as ionic bonds and hydrogen bonds, show transparency change upon cooling at arbitrary temperature, with negligible changes in size and mechanical performance, which is distinctly different from the temperature-induced polymer solubility change in conventional thermal responsive hydrogels. Moreover, this thermal responsive behavior is thermal history dependent, and it is fast and sensitive, as thermal responsive behavior originates from the structure frustration upon cooling. The frustrated structure is formed by temporarily free water aggregating. As the free water gradually diffuses out of the gel, the frustrated structure spontaneously decays with the transparency change. Furtherly, we demonstrated that such new thermal responsive behavior has applications as dynamic materials in designing dynamic memory with forgetting ability, drug release, thermal imagery, and security paper. The finding of using hydrogels containing abundant physical bonds as a new type of thermal responsive hydrogels revealed here expands the applications of thermal responsive hydrogels and inspires future researches on this unusual thermal responsive behavior.

Nomenclature

1. Materials:

AMPS 2-acrylamido-2-methylpropanesulfonic acid

DMAEA-Q Methyl chloride quarternized *N*,*N*-dimethylamino ethylacrylate

MAAc Methacrylic acid

MATAC Methacrylatoethyl-trimethylammonium chloride

MBAA *N*,*N*′-methylene-bis-acrylamide

MPTC 3-propyl -trimethylammonium chloride

NaSS Sodium *p*-styrenesulphonate

UMA 2-ureidoethyl methacrylate

P(NaSS-*co*-DMAEA-Q) Poly(sodium *p*-styrenesulphonate-*co*-methyl chloride quarternized *N*,*N*-dimethylamino ethylacrylate)

P(NaSS-*co*-MATAC) Poly(sodium *p*-styrenesulphonate-*co*-methacrylatoethyl-trimethylammonium chloride)

P(UMA-*co*-MAAc) Poly(2-ureidoethyl methacrylate-*co*-Methacrylic acid)

***α*-keto** *α*-ketoglutaric acid

AAm Acrylamide

2. Measurement

DSC Differential scanning calorimetry

SAXS Small-angle X-ray scattering

SEM Scanning electron microscopy

UV-*vis* spectrophotometry Ultraviolet and visible spectrophotometry

3. Main parameters

C_m Total monomer concentration

C_p Heat capacity

d Thickness

d_0 Thickness at the beginning

d_t Thickness at swelling/shrinking time t_v

d_∞ Thickness at equilibrium

d_0 Characteristic length

D Diameter

D_0 Diameter at the beginning

D_t Diameter at swelling/shrinking time t_v

D_∞ Diameter at equilibrium

$\mathbf{D_{co}}$ Cooperative diffusion coefficient

$\mathbf{D_{sh}}$ Cooperative diffusion coefficient for shrinking

$\mathbf{D_{sw}}$ Cooperative diffusion coefficient for swelling

$\boldsymbol{E}$ Young's modulus

$\mathbf{G'}$ Storage modulus

$\mathbf{G''}$ Loss modulus

$\boldsymbol{m}$ Weight

$\boldsymbol{m_{gel}}$ Weight of hydrogel

$\boldsymbol{m_{dry}}$ Weight of dry hydrogel

$\mathbf{R}$ Radius

$\mathbf{R_0}$ Radius at the beginning

$\mathbf{R_t}$ Radius at swelling/shrinking time t

$\mathbf{R_\infty}$ Radius at equilibrium

$\mathbf{T}$ Temperature

$\mathbf{T_L}$ Learning temperature or higher temperature

$\mathbf{T_F}$ Forgetting temperature, lower temperature, or quenched temperature

$\mathbf{t}$ Time

$\mathbf{t_F}$ Forgetting time or recovery time

$\mathbf{t_L}$ Learning time or heating time

$\mathbf{t_v}$ Swelling/shrinking time

$\mathbf{\tan \delta}$ Loss factor

$\mathbf{W_{BW}}$ Content of bound water

$\mathbf{W_{FW}}$ Content of free water

$\mathbf{W_T}$ Total water content

$\boldsymbol{W_{extf}}$ Work of extension at fracture

$\boldsymbol{\tau}$ Characteristic time

$\boldsymbol{\tau_{sh}}$ Characteristic time for shrinking

$\boldsymbol{\tau_{sw}}$ Characteristic time for swelling

$\boldsymbol{\rho}$ Density

$\boldsymbol{\lambda}$ Thermal conductivity

$\boldsymbol{\lambda_c}$ Critical stretch ratio

$\boldsymbol{\varepsilon_b}$ Fracture strain

$\boldsymbol{\sigma_b}$ Fracture stress

$\boldsymbol{\Phi_p}$ Polymer volume fraction

$\boldsymbol{\Gamma}$ Fracture energy

Chapter 1-General Introduction

1.1 Conventional thermal responsive hydrogels

Hydrogels, consisting of three-dimensional polymer network and abundant water, have drawn increasing attentions due to their prime importance and promising applications in diverse fields, such as tissue engineering [1-4], bio-inspired engineering [5-8], and soft electronics [9-13]. Recently, many research attempt to the intellectualization of hydrogels, like stimuli-responsive hydrogels, which can respond or self-adapt the change of environmental factors, *e.g.*, heat, light, and pH [14-21]. Among the stimuli-responsive hydrogels, the thermal responsive hydrogels are the most classic ones and have been subject to extensive research, in which their optical property, mechanical behavior, or volume can be regulated by heat [22-26]. Examples of their smart applications are switchable hydrophilic/hydrophobic surface, temperature-induced drug release, and thermo-switchable optical devices [27-29].

The representative thermal responsive hydrogels are the hydrogels with an upper critical solution temperature (UCST gels) and with a lower critical solution temperature (LCST gels) [30]. Based on the temperature-dependent molecular reorganizations and interactions between the polymer chains and water [31], both UCST and LCST gels only trigger phase transition to show obvious transparency change when the temperature is lower or higher to the critical temperature. The critical temperature is related to the components of hydrogels and the solution condition (*e.g.*, salt and pH) [32, 33], independent on thermal history. For example, when the temperature decreases

from high temperature T_H to low temperature T_L and T_L is lower than the critical temperature, the UCST gels turn their optical appearance from transparency to opaque [31-37], accompanying with dramatic volume shrinkage [38-40] and mechanical performance change [41]. However, these UCST gels cannot response the change of temperature that T_H and T_L are both higher or lower than the critical temperature. Therefore, synthesizing hydrogels with new components or tuning the solution condition is necessary but tedious to change the critical temperature for practical requirement. In other words, these reported thermal responsive hydrogels just trigger the response by the specific temperature point, not a temperature difference.

1.2 Hydrogels containing dynamic bonds

Hydrogels containing dynamic bonds (DB gels) means the hydrogels have abundant dynamic physical bonds, such as ionic bonds and hydrogen bonds [42-44]. The DB gels can be divided as two groups: One is the pure physical hydrogels without chemical crosslinkers; the other is the physical hydrogels with a slight chemical crosslinkers. These hydrogels both have abundant physical associations, which can easily break to dissipate energy during deformation and can reform after fracture, due to their dynamic and reversible nature. Therefore, DB gels usually have high toughness and good self-healing [16, 42, 45-94].

1.3 Polyampholyte hydrogels

Polyampholyte (PA) hydrogels are the hydrogels which is made by ionic bonds. Recently, we found a series of self-healing and tough PA hydrogels that have a hierarchical structure, consisting of reversible ionic bonds at the 1 nm scale, permanent polymer network at the 10 nm scale, and bi-continuous phase network at the 100 nm scale [95-97]. This bi-continuous phase-separation structure consists of a soft phase network and a hard phase network due to the difference in polymer density. This structure is critical for the toughness and fatigue resistance of PA gels, as demonstrated by the recent uniaxial loading and fatigue loading experiments [95, 98].

The role of the phase-separation structure in toughness of PA gels was revealed in a uniaxial loading experiment [95]. Upon loading, the bicontinuous phase network first shows a large affine deformation, during which the nanoscale chain conformation changes with ionic bond breaking to dissipate energy. At a certain large deformation, the strands of the hard phase network start to rupture, and the load is transferred to the soft phase network. The soft phase network sustains the load, which effectively reduces the stress concentration and prevents the catastrophic crack propagation. Upon further increasing the deformation, the soft phase finally ruptures, leading to the global failure of the gel. Such a multiscale rupture process dissipates a significant amount of energy and results in the high toughness of PA gels. The role of the phase-separation structure in fatigue resistance was revealed in a cyclic loading experiment [98]. Upon cyclic loading, the bi-continuous phase network orients along the stretching direction to induce a pronounced crack blunting and crack deceleration effect, resulting in an

extremely slow crack growth even above the energy release threshold. The relative strength of soft and hard phases has also been demonstrated to be important for the mechanical behavior of PA gels [96].

1.4 Overview of this thesis

In **Chapter 1**, we briefly introduced the characteristics and applications of conventional thermal responsive hydrogels and polyampholyte (PA) hydrogels.

In **Chapter 2**, we chose the hydrogels containing dynamic bonds (DB gels, *e.g.*, ionic bonds and hydrogen bonds) as model systems, and mainly described the synthesis process of various kinds of PA gels and hydrogen bonding hydrogels.

In **Chapter 3**, we reported an unusual thermosensitive behavior in DB gels, and their transmittance change is thermal history dependent, unlike the conventional thermosensitive hydrogels, such as UCST and LCST gels. The cooling rate, heating temperature, and cooling temperature all influence the transparency of the DB gels after cooling. The transparent-to-opaque transition of the gels is fast and does not have a specific critical temperature, unlike the UCST and LCST gels. The gel with turbid appearance is induced by the formation of frustrated structure that is unstable, so spontaneously occurs opaque-to-transparent transition from the surface to the center of the gel. Even though the opaque appearances of the gels with or without frustrated structure are very different, it makes no obvious influences on the mechanical performance.

In **Chapter 4**, we demonstrated the DB gels had the asymmetry of swelling kinetics during heating and shrinking kinetics during recovery. The cooperative diffusion coefficient for swelling is nearly 2 orders larger than that for shrinking. This obvious asymmetry is formed owing to the formation of large-scale frustrated structure. Moreover, the chemical crosslinkers can decrease the heterogeneity of this frustrated structure, and the asymmetry of swelling/shrinking kinetics turns to worse.

In **Chapter 5**, the DB gels has been applied as the memorizing-forgetting materials based on the fast swelling kinetics and slow shrinking kinetics upon thermal stimulus (**Chapter 4**), as well as thermal history dependent transparency change of these gels (**Chapter 3**). The gels can memorize various information by thermal learning, and the distinct turbidity change of these hydrogels after sudden cooling provides a facile mechanism to retrieve the memorized information. Interestingly, the memorized information decays spontaneously, without any external stimuli. As the forgetting time of the memorized information is proportional to the learning strength, the forgetting process can be programmable by controlling the learning time and learning temperature.

In **Chapter 6**, we further expand the applications of this thermal history dependent responsive behavior in PA gels, such as in controllable drug release, two-dimensional thermal imagery, and security paper for recording temporary information. The applications of using the PA gels revealed here can inspire more research on this unusual thermal responsive behavior.

In **Chapter 7**, concluding remarks of this dissertation are summarized.

Chapter 2-Fabrication of hydrogels containing dynamic bonds

2.1 Introduction

Recently, a novel class of tough and self-healing hydrogels containing reversible ionic bonds and hydrogen bonds have been successfully synthesized [42-44, 93]. For example, polyampholyte (PA) hydrogels were synthesized by random copolymerization of anionic and cationic monomers at charge balanced point. The heterogeneous structure in these gel with structural length in tens or hundreds nanometers scale has been reported, like PA system in water [95]. According to atomic force microscopy and time-resolved small-angle X-ray scattering (SAXS), our group demonstrated that PA gels have a hierarchical structure of several length scale: at the monomer scale, the positive and negative charges associate to form ionic interactions; at the nanoscale, the charged chains aggregate into soft and hard regions, which differ in modulus and polymer density; in the mesoscale, the soft and hard regions form a bicontinuous double network structure (**Fig. 2.1**) [95]. This multiscale structure leads to a multiscale energy dissipation during deformation, which endows extraordinarily high toughness, fatigue resistance and self-healing ability to PA gels [95, 98]. Therefore, these gels are good candidates as soft and wet biomaterials. In this chapter, we mainly introduced the synthesis of hydrogels containing dynamic bonds (DB gels), such as ionic bonds and hydrogen bonds.

2.2 Hydrogels containing ionic bonds

2.2.1 Materials

Cationic monomers, methyl chloride quarternized *N*,*N*-dimethylamino ethylacrylate (DMAEA-Q; 79.2 *wt*%, MT AquaPolymer, Inc.), methacrylatoethyl-trimethylammonium chloride (MATAC; Wako Pure Chemical Industries, Ltd.), and 3-(methacryloylamino)propyl-trimethylammonium chloride (MPTC; Wako Pure Chemical Industries, Ltd.); anionic monomer, sodium *p*-styrenesulphonate (NaSS; Wako Pure Chemical Industries, Ltd.); chemical cross-linker, *N*,*N*′-methylene-bis-acrylamide (MBAA; Wako Pure Chemical Industries, Ltd.; ultraviolet (UV) initiator, *α*-ketoglutaric acid (*α*-keto; Wako Pure Chemical Industries, Ltd.) were used as received (**Fig. 2.2**). Millipore deionized water was used for all experiments.

2.2.2 Synthesis

PA gels were synthesized by one-step random radical copolymerization of anionic and cationic monomers at charge balance point in a concentrated aqueous solution, following our previous work [42, 95, 96, 98, 99]. The prescribed amounts of cationic monomer (DMAEA-Q, MATAC, or MPTC), NaSS, *α*-keto, and MBAA were dissolved in deionized water. Here, we used parameters C_m, f, $C_{\alpha\text{-keto}}$, and C_{MBAA} denoted the total monomer concentration of NaSS and cationic monomer (DMAEA-Q, MATAC, or MPTC), the molar ratio of NaSS, the concentrations of MBAA relative to C_m, and the concentrations of *α*-keto relative to C_m, respectively. Then, the solution was injected

into a reaction cell consisting of a pair of glass plates with a spacer of varying thickness values, and the reaction cell was irradiated with UV lights (~365 nm) for 10 h under argon atmosphere. Subsequently, the as-prepared gels in a platelet shape were immersed in a large amount of pure water for 1 month to remove the counterions. The gel at equilibrium state has a water content of around 45 *wt*%. The code P(NaSS-*co*-DMAEA-Q) denoted the gels were synthesized by NaSS and DMAEA-Q monomers, and the suffix -C_m-C_{MBAA} after the name of copolymer denotes C_m and C_{MBAA}. The code P(NaSS-co-MATAC) and P(NaSS-co-MPTC) gles denoted the gels were synthesized by NaSS and MATAC monomers, and NaSS and MPTC, resprectively. Their components were list in **Table 2.1**. These gels were all synthesized with chemical crossliker, therefore these gels were chemical hydrogels with aboundant ionic bonds.

2.3 Hydrogels containing Hydrogen bonds

2.3.1 Materials

2-ureidoethyl methacrylate (UMA) was kindly provided by Osaka Organic Chemical Co., Ltd. and Methacrylic acid (MAAc) was purchased from Wako Pure Chemical Industries, Ltd. Their chemical structures were represented in **Fig. 2.2**.

2.3.2 Synthesis

Hydrogen bonding hydrogels were synthesized in dimethyl sulfoxide solution containing a prescribed amount of monomers 2-ureidoethyl methacrylate (UMA),

methacrylic acid (MAAc), and α-keto [100]. The total monomer concentration C_m of UMA and MAAc was 2.0 M, and the molar ratio of UMA:MAAc was 0.73:0.27. The concentration of α-keto was 0.1 mol% relative to C_m. The UV reaction was conducted in reaction cells under argon atmosphere with 365 nm UV lights for 10 h. After polymerization, the as-prepared gels were dialyzed in a large amount of pure water for 2 weeks to reach equilibrium. We used the code P(UMA-*co*-MAAc) to denote this gel. Here, we know P(UMA-*co*-MAAc) gels are physical gels without chemical crosslinker.

2.4 Figures and tables

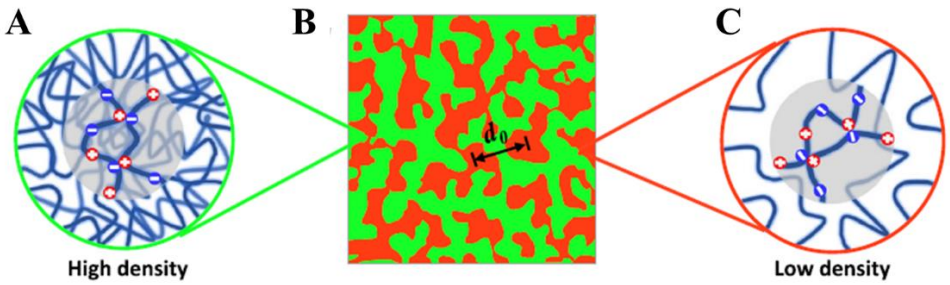

Fig. 2.1. Illustrations of the multiscale structure of PA gels: bicontinuous network structure consists of hard, dense regions (green) and soft, sparse regions (red) with a characteristic length in hundred nanometers (**B**), aggregated polymer chains of dense (**A**) and sparse (**C**) regions at nanoscale, and ionic bonds at monomer scale [insets in (**A**) and (**C**)] [95].

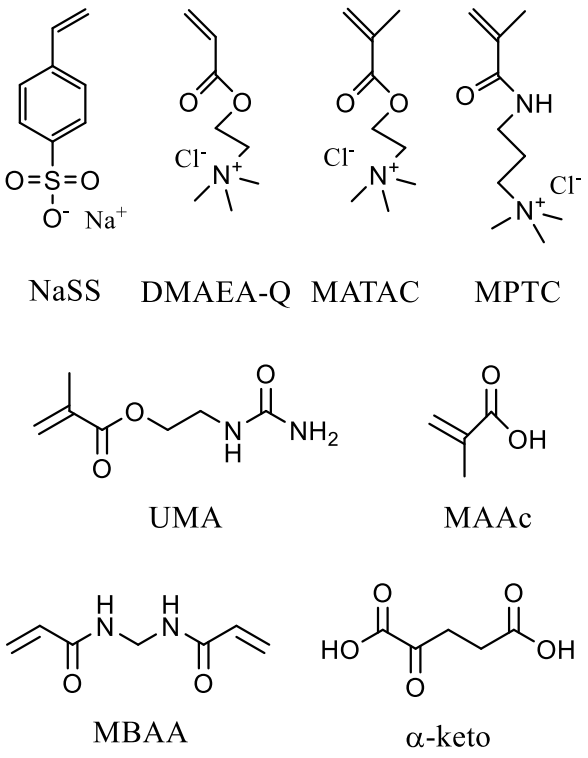

Fig. 2.2. Chemical structures of the monomers, chemical cross-linker, MBAA, and UV initiator, *α*-ketoglutaric acid that were used to synthesize the hydrogels.

Table 2.1. Formulation of hydrogels.

Hydrogels	C_m (M)	f	$C_{\alpha\text{-keto}}$ (mol%)	C_{MBAA} (mol%)
P(NaSS-*co*-DMAEA-Q)-2.0-0.1	2.0	0.514	0.1	0.1
P(NaSS-*co*-DMAEA-Q)-2.5-*x*	2.5	0.514	0.1	*x*
P(NaSS-*co*-MATAC)	2.0	0.525	0.1	0.1
P(NaSS-*co*-MPTC)	2.1	0.522	0.25	0.2

C_m, total monomer concentration; f, molar ratio of NaSS; $C_{\alpha\text{-keto}}$, initiator concentration (mol%) in relative to C_m; C_{MBAA}, chemical crosslinker concentration (mol%) in relative to C_m. x, C_{MBAA} of P(NaSS-*co*-DMAEA-Q)-2.5-x gels, x = 0, 0.1, 0.3, 0.5, 1.0, 3.0, and 5.0, respectively.

Chapter 3-Thermal history dependent responsive behavior

3.1 Introduction

Smart materials are the materials that can respond to the change of external stimuli [14, 21, 58, 101-104]. Thermal responsive hydrogels are a type of smart materials exhibiting thermal sensitive phase transition [23, 105-108], which have applications in many fields, such as *in vivo* drug release [40, 109-111], intelligent display [29, 112, 113], and functional materials with switchable hydrophilic/hydrophobic surface [114-117]. These gels are usually characterized by a sharp phase transition at a temperature defined as the lower critical solution temperature (LCST) [30, 117-121] or upper critical solution temperature (UCST) [31-34, 37, 122]. In case of LCST gels, the polymers below the LCST are water soluble and in swelled state, but above are less or no water soluble and in collapsed form [118, 123]. Such a phase transition induced by the solubility change of polymers is usually featured by a transparent/opaque transition in optical appearance and dramatic changes in the size and mechanical performance of the gels [124-126]. The UCST gels show a similar thermal responsive behavior but with an opposite temperature dependence [38, 39, 41]. However, in both LCST and UCST gels, the phase transition only occurs at the critical temperature, limiting their applications to a specific temperature. Moreover, the dramatic changes in size and mechanical performance around the critical temperature also hinder their applications.

In this chapter, we reported the DB gels (*e.g.*, PA and hydrogen bonding gels) can universally respond the temperature difference during cooling by transparency variation,

without the critical temperature. We investigated that this transparency change is temporary and dependent on thermal history, which is distinctly different from the conventional thermosensitive gels (**Fig. 3.1A**). Furtherly, we demonstrated that the transparency change is owing to the formation of large-scale frustrated structure, induced by the aggregation of free water, which has no interactions with polymer network, so this frustrated structure makes no obvious effects on the mechanical performance of the gels. This work favors the understanding of the nonequilibrium frustrated structure in hydrogels for developing novel thermal responsive hydrogel materials with obvious transparency change by slight changes of volume and mechanical behaviors.

3.2 Measurement

Total water content (W_T). The W_T of PA gels were measured by a moisture balance (MOC-120H, SHIMADZU Co.), defined as $W_T = (1 - m_{dry}/m_{gel}) \times 100$ %, where m_{gel} was the weight of PA gels and m_{dry} was in the dry state. Every sample was repeatedly tested for 3 times.

Transmittance measurement. The light transmittance of the sample was characterized using a Shimadzu UV spectrophotometer (UV-1800) at a wavelength of 550 nm. The gel was put into a quartz cuvette filled with water during measurement.

SAXS analysis. SAXS measurement was performed at BL19U2 beamline of National Facility for Protein Science (NFPS), Shanghai Synchrotron Radiation Facility (SSRF), Shanghai, China. The energy and wavelength of X-ray were 12 keV and 0.9184 Å, respectively. The sample-to-detector distance was 5934.0 mm. A Pilatus 1 M detector with a resolution of 981×1043 pixels and the pixel size of 172 μm was used to record the 2D SAXS patterns. The 1D scattering profiles were obtained by integrating the 2D patterns *via* Fit2D software. The temperature of the samples was controlled by a Linkam THMS 600 hot stage.

Differential scanning calorimetry (DSC). DSC analysis was performed by employing a Model DSC22 instrument (SII Nano Technology Inc.) connected to a thermal analysis system (SSC 5100). The samples (8-12 mg) were first cooled to -80 °C with a cooling rate of 50 °C/min, and maintained at -80 °C for 10 min; then heated to 25 °C with a heating rate of 5 °C/min to observe the melting behavior of water in PA gels. Every sample was repeatedly tested for 3 times.

Rheology test. The rheological measurement was performed with a parallel-plate geometry using an ARES-G2 rheometer (TA Instruments, USA). The frequency sweep varying from 0.1 to 100 Hz was carried out under a constant strain of 0.1 % at 25 °C. The disc-like sample with a diameter of 10 mm was adhered to the parallel plates with the superglue and surrounded with deionized water during testing.

Uniaxial tensile test. The uniaxial tensile test was carried out at 25 °C, performed by an Instron 5965 tensile tester (Instron Co.) under vapor atmosphere to avoid the water loss of the samples. The tensile speed was 100 mm/min, which gave a nominal strain rate of 0.14 s^{-1}. Every sample was repeatedly tested for 5 times.

A single-edge notch test. A single-edge notch test was performed under vapor atmosphere at 25 °C to obtain fracture energy[127, 128]. The rectangular samples with a length l = 20 mm, a width w = 10 mm, and without notch or with a notch length c = 2 mm were used. The stretch speed was 100 mm/min. The fracture energy Γ was calculated by $\Gamma=2\frac{3}{\sqrt{\lambda_c}}cW(\lambda_c)$, where $W(\lambda_c)$ was the stain energy density of an unnotched sample and λ_c was the stretch ratio at which the fracture started for the notched sample. Every sample was repeatedly tested for 3 times.

3.3 No transmittance change during heating

Fig. 3.1B represents a practical example of the transparency change in P(NaSS-*co*-DMAEA-Q)-2.5-0.1 gels. We maintained T_L = 25 °C for convenience to carry out various measurements. The original gel was initially at T_L = 25 °C for equilibrium; then, it was heated at T_H = 80 °C for 2 h (heated gel); finally, the turbid gel was obtained by quenching to T_L = 25 °C. The heating time (t) at T_H = 80 °C was chosen as 2 h, because this time period was sufficient for PA gels to acquire equilibrium state at T_H = 80 °C. This turbid gel spontaneously recovered to transparent over time (recovered gel). From

Fig. 3.1B, we can see the transparency change of PA gel occurs in two processes. One is the cooling process that the gel is moved from T_H = 80 to T_L = 25 °C, showing transparency-to-opaque transition. The other is the recovery process that the turbid gel spontaneously occurs opaque-to-transparency transition at T_L = 25 °C. However, the optical appearance has no obvious change between the original gel and the heated gel, indicating the PA gel keeps transparent during heating. To confirm this, the optical appearances of PA gels after heating at different temperature T_H have been recorded in **Fig. 3.2A**, and the transmittance change of the original gel during heating from 25 to 80 °C with different heating rate has also been observed in **Fig. 3.3**. As a result, no distinct transmittance change occurs. This is different from the UCST and LCST gels, which respectively show opaque-to-transparency transition and transparency-to-opaque transition as the temperature increases to beyond the critical temperature. Therefore, we used the PA gels to investigate the characteristic of transparency change in cooling process and in recovery process, as a model system of DB gels.

3.4 No critical temperature in transmittance change

At first, there is no specific critical temperature for PA gels in transparency-to-opaque and opaque-to-transparency transitions, unlike the conventional UCST and LCST gels. **Fig. 3.2B(i)** shows the transmittance change of PA gels when they are cooled from different heating temperatures T_H under the same cooling rate (1 °C/min). At the beginning of cooling process, their transmittances are almost the same, which is consistent with the result as shown in **Fig. 3.2A**. For comparison, we consider the

inflection point of the transmittance curve in this work as the cloud point [33, 129], and the corresponding temperature as the cloud temperature. As **Fig. 3.2B(ii)** shown, when the PA gels are cooled from 80, 70, 60, 50, and 40 °C, the cloud temperatures are 67, 59, 50, 41, and 32 °C, respectively. We can see the cloud temperatures are completely different, dependent on the heating temperature, and the PA gels have the higher cloud temperature when they are cooled from the higher heating temperature T_H. Subsequently, we examined the transmittance change of PA gels under different cooling rate when the PA gels were cooled from the same heating temperature T_H = 80 °C (**Fig. 3.2C**). **Fig. 3.2C(i)** displays the transmittance change is related to the cooling rate, and **Fig. 3.2C(ii)** also represents the could temperature is dependent on the cooling rate, and the could temperature decreases from 68 to 49 °C with the cooling rate decreasing from 2 to 0.1 °C/min. Above results suggest that the could temperature in transparency-to-opaque transition of PA gels during cooling is dependent on the heating temperature and the cooling rate, showing thermal-history dependence.

Moreover, the same method was employed to study the opaque-to-transparency transition in PA gels during heating. Before testing, the gels are obtained by quenching to T_L = 25 °C after heating at different temperature T_H (= 40, 50, 60, 70, and 80 °C) for t = 2 h, and all the gels show turbid appearance (**Fig. 3.2D**). Therefore, these gels have low transmittance as shown in **Figs. 3.2E(i)** and **3.2F(i)** at the beginning of heating process. Similarly, the could temperature of opaque-to-transparency transition in the heating process also depends on the heating temperature and heating rate (**Figs. 3.2E(ii)** and **3.2F(ii)**). Furtherly, we can find the change of the cloud temperature in both

transparency-to-opaque and opaque-to-transparency transitions is liner to the heating temperature (**Figs. 3.2B(ii)** and **3.2E(ii)**), which provides a facile way to tune the cloud temperature. For the UCST and LCST gels, changing the components of hydrogels and/or the solution condition is necessary to control the could temperature (or critical temperature) [32, 33].

3.5 Thermal history dependent transmittance change

Interestingly, not only the cloudy temperature, but also the transmittance of the PA gel after quenching is dependent on the thermal history. The PA gels with various transmittance can be obtained by tuning the heating time *t* (**Fig. 3.4A**), high temperature (or heating temperature) T_H (**Fig. 3.4B**), and/or low temperature (or cooling temperature) T_L (**Fig. 3.4C**). **Fig. 3.4A(i)** shows the optical images of the PA gels quenched to T_L = 25 °C after heating at T_H = 60 °C for different time *t*, and their corresponding transmittance are recorded in **Fig. 3.4A(ii)**. The PA gel is transparent at the beginning (*t* = 0). When the heating time is less than 5 min, it is semi-transparent, and its transmittance turns more and more lower with increased heating time. It becomes turbid since the heating time is 8 min or more. The optical images of the PA gels quenched to 25 °C after heating at different temperature T_H for *t* = 5 min is presented in **Fig. 3.4B(i)**. The transmittance of the PA gel is influenced by the heating temperature, and turns worse with the increase of heating temperature. When the heating temperature is higher than 70 °C, it becomes completely turbid (**Fig. 3.4B(ii)**). **Fig. 3.4C** represents the

optical images of PA gels quenched to different low temperature T_L for 1 min after heating at T_H = 80 °C for *t* = 2 h (**Fig. 3.4C(i)**) and corresponding transmittance (**Fig. 3.4C(ii)**). Similarly, the gel can obtain high transmittance as it is quenched to higher T_L. From **Figs. 3.4B** and **3.4C**, we can see the transmittance change can mirror the temperature difference between the heating temperature T_H and cooling temperature T_L; the sample with lower transmittance is obtained by larger difference between T_H and T_L. Except PA gels, above phenomenon is universal in other DB gels, like another PA gel system P(NaSS-*co*-MATAC) gel and hydrogen-bonding P(UMA-*co*-MAAc) hydrogel (**Fig. 3.5**).

3.6 Advantages of PA gels used as thermal responsive materials

As a potential candidate for thermal responsive materials, PA gels have many advantages. The first advantage is quick response. An example is shown in **Fig. 3.6A**. A PA gel is initially heated at T_H = 80 °C for *t* = 2 h; Then, this PA gel is moved to T_L = 25 °C and turns to turbid within 4 s, and it becomes transparent when moved back to 80 °C within 4 s. The response for transparency change only takes several seconds. The second advantage is high sensitivity. In theory, tiny change of temperature can induce the transparency change of the sample as implied in **Figs. 3.2B** and **3.2C**. For observing by naked eyes, the temperature difference of 3 °C is sufficient. **Fig. 3.6B** shows an example: A PA gel is initially heated at T_H = 28 °C for *t* = 4 h; Then, this PA gel is moved to T_L = 25 °C and occurs obvious transparency change, and it returns to

transparent when moved back to 28 °C. The third advantage is that the distinct transparency change just requires a slight volume change. **Fig. 3.6C** represents the volume change of PA gels with heating temperature. The volume expands with the heating temperature, but the increase of volume is small. The volume of the gel after heating at T_H = 80 °C for t = 2 h is just 1.27 times larger than that at 25 °C equilibrium state; for T_H = 40 °C, it decreases to 1.07. It is surprising that so obvious transparency change is only caused by a considerably small change of volume, while the LCST or UCST gels shows large volume change (tens or hundreds of times in volume) at the critical temperature [38-40], which brings difficulty to construct devices.

3.7 Instability of PA gels with turbid appearance

In **Fig. 3.1**, we have referred that the PA gels with turbid appearance (or turbid gels) is unstable and recovers to transparent spontaneously, where this point is also distinct to the UCST gels. This result shows the structure, making the gel have a turbid appearance, is unstable, and shows a spontaneous nonequilibrium-to-equilibrium structural transition. This spontaneous structural transition is one of the important roles to design hydrogel materials with dynamic memorizing-forgetting behavior, which will be represented in **Chapter 5**.

Here, we continue to demonstrate the recovery time (or the recovery process) still depends on the thermal history. **Fig. 3.7A** displays the transmittance change in recovery process of PA gels quenching to T_L = 25 °C after heating at different T_H for t = 2 h (**Fig.**

3.7A(i)), and the corresponding characteristic recovery time (t_c, **Fig. 3.7A(ii)**). The characteristic recovery time t_c was defined as the corresponding time at the inflection point of transmittance curve. t_c is apparently prolonged by the increase of the heating temperature. When the heating temperature T_H = 40 °C, t_c is approximately 285 min. t_c becomes 1202 min for T_H = 80 °C, which is about 4.2 times longer than that for T_H = 40 °C. Likewise, we studied the transmittance change in recovery process of PA gels quenching to T_L = 25 °C after heating at T_H = 60 °C for different heating time t (**Fig. 3.7B(i)**), and the corresponding characteristic recovery time t_c (**Fig. 3.7B(ii)**). When the heating time t is less than 90 min, t_c keeps increasing. However, the transmittance curves overlap and their t_c's are constant for $t \geq 90$ min. This is because the gel in this condition reaches to the equilibrium state in heating process.

Although we know the turbid gel is unstable and changeable over time, the recovery time of opaque-to-transparency transition as shown in **Fig. 3.7** is much longer than the characterization time for performance of the turbid gels (several seconds or minutes), so in the following measurement we neglect the effect of structural change during characterization.

3.8 Structure and structural evolution in transparency-change process

According to above analysis, we know the transparency change of PA gels, both from transparent to turbid and from turbid to transparent, is thermal history dependent, and the gels with turbid appearance are unstable and turn to transparent gradually. Then, we consider to step forward to explore the structural characteristic behind the original and

the turbid gels.

The gel shows turbid appearance after the temperature jumps from T_H = 80 °C to T_L = 25 °C (**Fig. 3.1B**), suggesting the formation of large-scale structure caused by sudden cooling. The formation of large-scale heterogeneous structure is further confirmed by SEM. SEM images of cross section of the original gel, with transparent appearance as shown in **Fig. 3.1B**, exhibits a smooth appearance in cross section showing in **Fig. 3.8A(i)**. In contrast, the turbid gel shows a porous like structure and heterogeneous distribution of polymer, and the porous diameter is roughly 400 nm (**Fig. 3.8A(ii)**). This porous like structure implies the formation of numerous water aggregations and the temporary fluctuation of polymer concentration, called frustrated structure here. The transparency change of PA gels from transparent to turbid or from turbid to transparent is related to the formation or the decay of the frustrated structure. In order to evaluate this mechanism, moreover, we employed SAXS to examine the structures of the original, heated, turbid, and recovered gels (**Figs. 3.1B** and **3.8B**). The original gel has a scattering peak at q around 0.1 nm^{-1} in 1D SAXS profile, demonstrating the phase separation structure of PA gels with a length size of about 60 nm, in consistent with our previous work [95, 96, 98]. In addition, our previous work also demonstrated that this small-scale heterogeneity is attribute to the formation of isotropic bicontinuous hard/soft phase networks in PA gels [95]. **Fig. 3.8B** shows an obvious characteristic is that this scattering peak maintains in the original, heated, turbid, and recovered gels, indicating the bicontinuous structure always exists in transparency-change process.

Comparing the original gel and the heated gel, we can see the intensity of the scattering peak of the heated gel is stronger than that of the original gel; this suggests the contrast between hard phase and soft phase becomes larger. As the gel absorbed water during heating and released water during recovery, we think the water absorbing capacity of hard phase and soft phase is different, and soft phase can absorb more water than hard phase during heating. Carefully, we can see the peak position of the heated gel slightly shift to small *q* area after comparing with that of the original gel (**Fig. 3.8B**), and we consider the slight increase of length size of PA gel during heating is induced by the expansion of its size, because of the water absorption.

As we mentioned before, the water molecules aggregate locally to form nonequilibrium frustrated structure in PA gel (turbid gel) after the heated gel is quenched to T_L = 25 °C (**Fig. 3.8A**). From 1D SAXS profile in **Fig. 3.8B**, the turbid gel has a sharp increase of scattering intensity at small *q* region. This also suggests the formation of another heterogeneous structure with large length scale, which is responsible for the opaque appearance of this gel. This large-scale frustrated structure finally transforms into equilibrium structure, as the recovered gel is observed by the disappearance of the strong scattering in small *q* region of SAXS profiles and its 1D SAXS profile nearly overlaps with the profile of original gel (**Fig. 3.8B**).

Now we can confirm the structural difference between the original gel and turbid gel. The transparency change of PA gels is due to the formation or decay of the large-scale frustrated structure, induced by water aggregation and diffusion. As the turbid gel is formed by the local aggregation of water molecules, we furtherly propose these water

molecules are free water, which has no interactions with polymer network. To confirm this hypothesis, DSC was performed to examine the types of water in the original gel and the turbid gel. For comparison, the dry PA gels and pure water were also performed under the same thermal procedure. The dry sample was obtained by evaporating the water in the gel at an elevated temperature of 120 °C [99]. The samples were initially cooled to -80 °C for 10 min to sufficiently allow the crystallization of free water in PA gels, as the bound water, which has a strong interaction with polymer network, cannot crystallize in this condition. On the basis of the DSC data from **Fig. 3.8C** the melting enthalpy (ΔH_m) of the original gel and the turbid gel, by integrating their areas of endothermic melting peaks, can be calculated, and they are 59.76 and 97.25 J/g, respectively (**Fig. 3.8D**). As shown in **Fig. 3.8D**, the contents of free water (W_{FW}'s) can be determined by comparing the melting enthalpy of the gels to that of pure water (330.00 J/g).

According to the data of W_{FW} and the total water content W_T, the bound water W_{BW} can be obtained by the equation of $W_{BW} = W_T - W_{FW}$ (**Fig. 3.8D**). As the weight of polymer in the transparent gel and turbid gel should be equal, the free water and bound water were normalized by the weight of polymer, W_{FW}/W_{poly} and W_{BW}/W_{poly} (**Fig. 3.8D**). Comparing with the values of W_{FW}/W_{poly} and W_{BW}/W_{poly} in the original gel and turbid gel, we find W_{FW}/W_{poly} of the turbid gel is nearly two times larger than that of the turbid gel, and their values of W_{BW}/W_{poly} are almost the same. This shows the free water varies significantly, while the bound water has no obvious change even though the gel occurs obvious transparency change. This result verifies that the water

aggregations in turbid gel is mainly free water.

3.9 Water absorption and formation of frustrated structure

Indeed, when the water absorption is prohibited during heating, for example, by sealing the sample with a plastic bag, the gel retains the transparency by sudden cooling from T_L to T_F, indicating no frustrated structure formation. As the water absorption is driven by osmotic pressure of polymer, it can also be prohibited by imposing a pressure on the sample. To demonstrate this, we used a disk-shape gel with a 5 mm radius and a 1.15 mm thickness. The gel in a 25 °C bath was initially sandwiched between two glass plates without pressure or with a prescribed pressure; then, it was moved to an 80 °C bath for thermal learning. During this process, only the periphery of the gel was in contact with water to allow water absorption (**Fig. 3.9A**). After a certain heating time t_L in the 80 °C bath, the sample was moved back to the 25 °C bath and the appearance of the sample was observed. For the gel without pressure during heating, the periphery of the gel became opaque and the area of opaque region increased with increasing time in the hot bath t_L, owing to the water absorbing from the periphery of sample. For the gel with a nominal stress of 0.1 MPa during the thermal learning, the opaque region was only observed at the periphery which did not increase with increasing t_L. Here, we define a parameter, $\beta = (R-R_{tr})/R$, to characterize the length ratio of the opaque region to that of the entire sample, where R and R_{tr} are radiuses of the entire sample and transparent region, respectively (**Fig. 3.9B**). As shown in **Fig. 3.9C**, for the gel without stress, β increased with t_L and it reached to 1 at t_L = 6 h, indicating that the entire sample

was swelled in this hot bath. For the gel with a stress of 0.03 MPa, β also increases with t_L, while it is significantly smaller than that of the gel without pressure when compared at the same t_L. This result suggests that the water absorption was significantly suppressed under a pressure of 0.03 MPa. When the applied pressure was increased to 0.1 MPa, β was about 0.2 and it almost did not change with t_L, suggesting that the water absorption was completely prohibited except at the periphery of the sample. The nonzero value of β at the stress of 0.1 MPa is due to the fact that, the periphery of the gel is in stress-free state and it can absorb water. This property permits us to control the heating regions in PA gels with a relatively sharp spatial resolution.

3.10 Effect of transmittance change on mechanical performance

From our previous work, we know the bicontinuous hard/soft phase structure of PA gel plays an important role in its mechanical performance, such as viscoelasticity, toughness, self-healing, and fatigue resistance [95, 96, 98]. From **Fig. 3.8B**, we have discussed the original gel and the turbid gel both keep the bicontinuous structure, and the length sizes of bicontinuous structure in the original gel and turbid gel are nearly the same. Moreover, the water aggregations in turbid gel are free water (**Fig. 3.8D**), which has no interactions with polymer network. According to above results, we propose that the formation of large-scale fractured structure in PA gel has no obvious influences on their mechanical performances. To evaluate this, we investigated the uniaxial tensile behavior, dynamic behavior, and fracture energy of the turbid gel and

the original gel.

Fig. 3.10A exhibits the typic uniaxial tensile stress-strain curves of the original gel and the turbid gel at 25 °C, and their Young's modulus E, fracture stress σ_b, and fracture strain ε_b , and work of extension at fracture W_{extf} are summarized in **Fig. 3.11**. We find σ_b and ε_b of the turbid gel and the original gel have no obvious differences, but E of the turbid gel is less than E of the original gel (**Fig. 3.11**). As the total water contents of the turbid gel (55.03 %) and the original gel (45.67 %) are different (**Fig. 3.8D**), we initially calculate their polymer volume fraction (Φ_p), determined by the equation $\Phi_p^{-1} = 1 + (\frac{W_{WC}}{1 - W_{WC}})\frac{\rho_P}{\rho_w}$, where ρ_P = 1.19 and ρ_W = 0.98 g/cm^3 are the density of PA and water at room temperature, respectively [130]. Φ_p's of the original gel and turbid gel are 0.50 and 0.41, respectively (**Fig. 3.12**). The change of Φ_p usually causes the change of the density of the polymer chain. For eliminating this effect, by assuming the polymer density change of the original gel and the turbid gel is homogeneous, the E, σ_b, and ε_b are related to Φ_p: $E = E^N \Phi_P$, $\sigma_b = \sigma_b^N \Phi_P^{2/3}$, and $\lambda_b = \lambda_b^N \Phi_P^{1/3}$, where E^N, σ_b^N, and λ_b^N are the values at the virtual reference state (Φ_p = 1) [131]. Here, $\lambda_b = \varepsilon_b + 1$ is the fracture stretch ratio. The results of the virtual reference state E^N, σ_b^N, and λ_b^N of the original gel and the turbid gel are shown in **Figs. 3.10(B-D)**. The E^N's of the original gel and the turbid gel are (0.22 ± 0.02) and (0.20 ± 0.02) MPa, respectively. We find their values of E^N's have no obvious difference, as well as σ_b^N and λ_b^N. This result suggests that only the difference of polymer density between the original gel and the turbid gel induces the difference of E, so their interactions in polymer network should be the same. This result is consistent with the DSC result: Their contents of bound water

are nearly the same (**Figs. 3.8C** and **3.8D**).

As the PA gels are viscoelastic, their mechanical behavior highly depends on the frequency. Strictly, above result only shows their tensile behaviors are nearly the same when the nominal strain rate is 0.14 s^{-1}, so we furtherly observed their dynamic behaviors under a frequency sweeping from 0.1 to 100 Hz. **Figs. 3.10E** represents the frequency dependence of storage modulus G′ and loss modulus G″ of the original gel and turbid gel at 25 °C. We can see G′ and G″ of the original gel and turbid gel both increase with frequency, and the value of G′, as well as G″, for the turbid gel is approximately equal to that of the original gel, showing the same dynamic behavior.

According to the stress-strain curves in Fig. 7a, if we use the work of extension at fracture W_{extf} as a parameter to characterize the toughness, we can see the W_{extf}'s of the original gel and turbid gel are almost the same (**Fig. 3.11**). Furtherly, the single-edge notch test was also performed to evaluate the toughness [127, 128] of the original gel and turbid gel. **Fig. 3.10F** shows the representative force-stretch ratio curves of notched and unnotched samples for the turbid gel. The toughness represented by fracture energy Γ can be estimated from the purple area in **Fig. 3.13**. Similarly, fracture energy Γ of the turbid gel at the virtual reference state (Φ_p = 1) is also obtained by $\Gamma=\Gamma^N\Phi_p^{2/3}$. The calculated value of Γ^N for the turbid gel is about (2.5±0.2) kJ/m^2; In same method, for the original gel, that is around (3.0±0.2) kJ/m^2 (**Fig. 3.10G**). Although numerous water aggregations in turbid gel probably behave like small defects, it has no distinct influence on the fracture energy because of the good crack resistance of PA gels (**Fig. 3.14**) [98]. These results clearly suggest that the frustrated structure in PA gels makes no obvious

effects on their mechanical performances.

3.11 Figures and tables

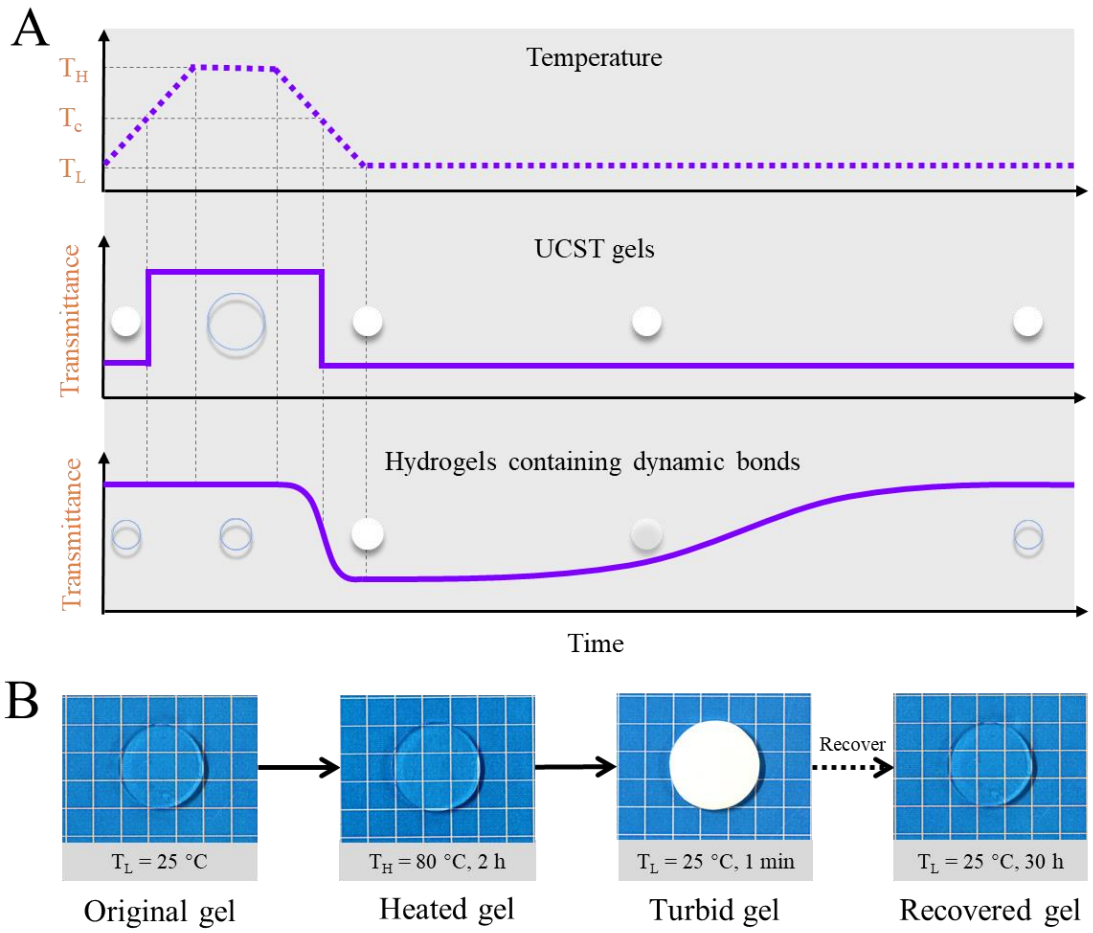

Fig. 3.1. Thermosensitive behaviors in UCST gels and hydrogels containing dynamic bonds (DB gels). **(A)** Scheme to show the transparency change of UCST gels and DB gels. For an UCST gel, it has turbid appearance at a low temperature of T_L, and becomes transparent sharply with a large swelling of volume when the temperature increases to the critical temperature T_c. It keeps transparent appearance at a high temperature of T_H ($T_H > T_c > T_L$). As the temperature returns back to T_L, it turns to turbid with a large shrinkage of volume at T_c, and keeps turbid appearance over time at T_L, without volume change. For DB gels, it keeps transparent even it is moved from the low temperature T_L to the high temperature T_H. After cooling to T_L, it first becomes turbid; then gradually

turns to transparent for equilibrium. The volume change in entire process is small. **(B)** Optical images to represent a real example of the transparency change and volume change in DB gels. The PA gel maintains the transparent appearance and slightly swells (heated gel) when it (original gel) is moved from T_L = 25 to T_H = 80 °C for heating time of t = 2 h. After a hot-to-cold jump (80 to 25 °C), this gel occurs transparency-to-opaque transition (turbid gel), and this turbid gel spontaneously recovers to transparent at T_L = 20 °C within 30 h (recovered gel). The background lattice is 5 mm.

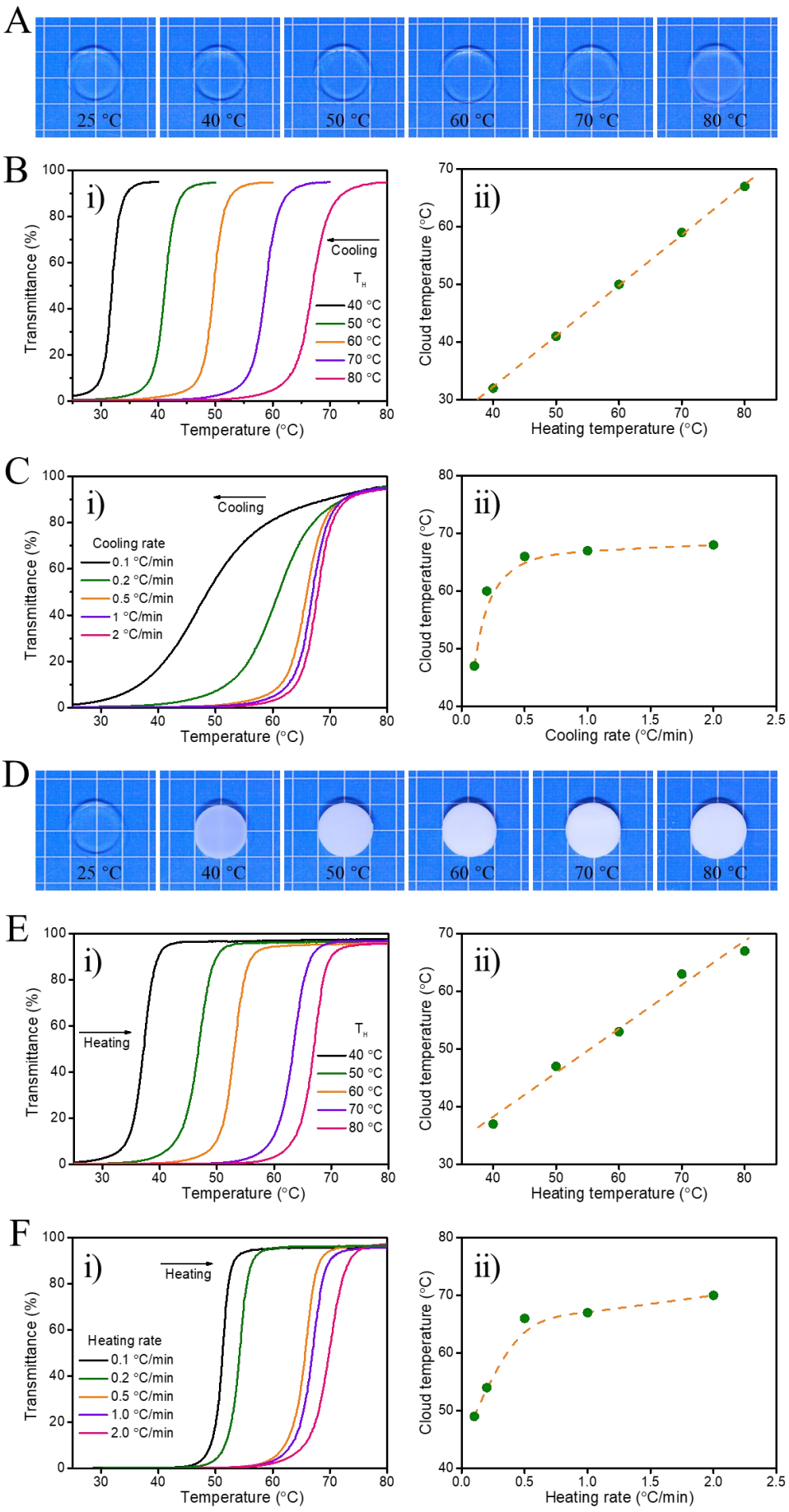
A
25 °C
40 °C
50 °C
60 °C
70 °C
80 °C
B
i)
Transmittance (%)
Temperature (°C)
Cooling
T_H
40 °C
50 °C
60 °C
70 °C
80 °C
ii)
Cloud temperature (°C)
Heating temperature (°C)
C
i)
Cooling
Cooling rate
0.1 °C/min
0.2 °C/min
0.5 °C/min
1 °C/min
2 °C/min
Transmittance (%)
Temperature (°C)
ii)
Cloud temperature (°C)
Cooling rate (°C/min)
D
25 °C
40 °C
50 °C
60 °C
70 °C
80 °C
E
i)
Heating
T_H
40 °C
50 °C
60 °C
70 °C
80 °C
Transmittance (%)
Temperature (°C)
ii)
Cloud temperature (°C)
Heating temperature (°C)
F
i)
Heating
Heating rate
0.1 °C/min
0.2 °C/min
0.5 °C/min
1.0 °C/min
2.0 °C/min
Transmittance (%)
Temperature (°C)
ii)
Cloud temperature (°C)
Heating rate (°C/min)

Fig. 3.2. Transparency-to-opaque and opaque-to-transparency transitions of PA gels without specific critical temperature. **(A)** Optical appearance of PA gels after heating at different temperature T_H for t = 2 h. **(B)** Transmittance change during cooling from different heating temperature T_H to 25 °C with a cooling rate of 1 °C/min **(i)** and corresponding cloud temperature **(ii)**. The gel was initially heated at T_H for t = 2 h before cooling. **(C)** Transmittance change during cooling from 80 to 25 °C with different cooling rate **(i)** and corresponding cloud temperature **(ii)**. The gel was initially heated at T_H = 80 °C for t = 2 h before cooling. **(D)** Optical appearance of PA gels obtained by quenching to T_L = 25 °C after heating at different temperature T_H for t = 2 h. **(E)** Transmittance change of the gel during heating from 25 to 80 °C with a heating rate of 1 °C/min **(i)** and corresponding cloud temperature **(ii)**. The gel was obtained by quenching to T_L = 25 °C after heating at different temperature T_H for t = 2 h. **(F)** Transmittance change of the gel during heating from 25 to 80 °C with different heating rate **(i)** and corresponding cloud temperature **(ii)**. The gel was obtained by quenching to T_L = 25 °C after heating at T_H = 80 °C for t = 2 h. All recorded transmittance change is at wavelength of 550 nm, and all background lattices are 5 mm.

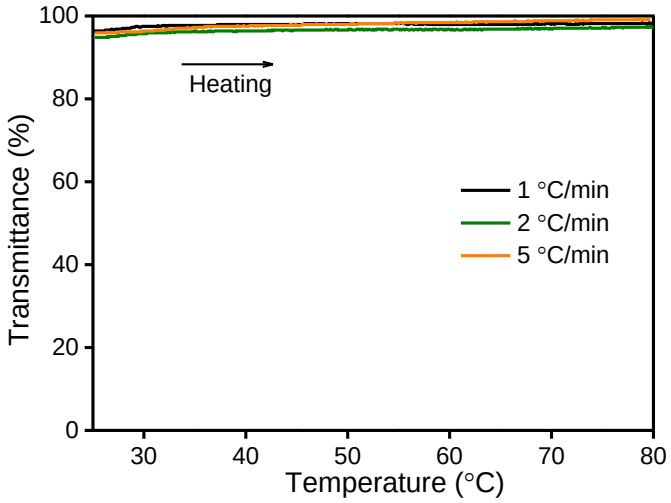

Fig. 3.3. Transmittance curve of the original gel during heating from 25 to 80 °C with different heating rate.

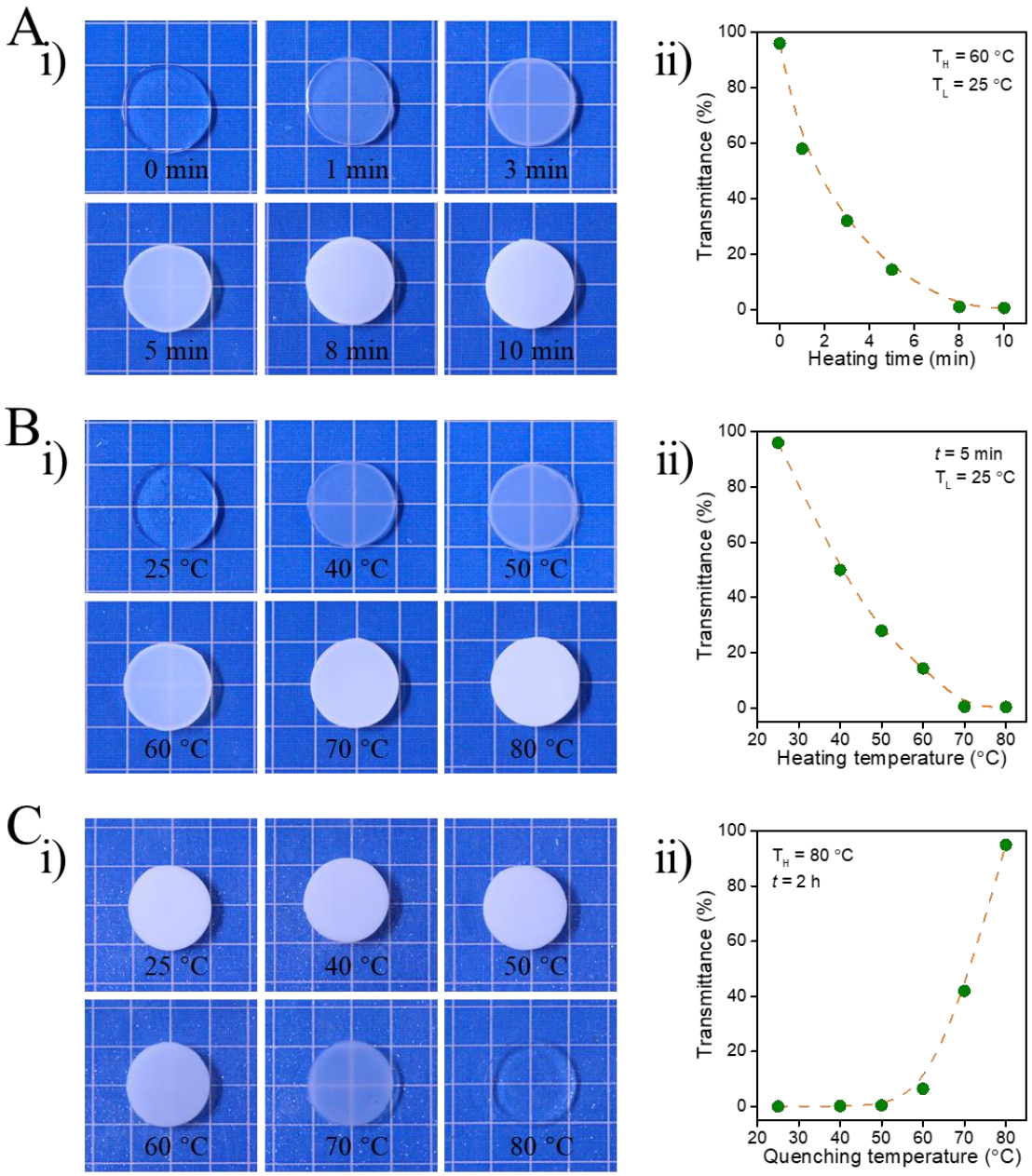

Fig. 3.4. Optical images to exhibit PA gels with various transmittance by tuning thermal history. **(A)** Optical images of PA gels quenched to T_L = 25 °C for 1 min after heating at T_H = 60 °C for different time *t* **(i)** and corresponding transmittance at 550 nm **(ii)**. **(B)** Optical images of PA gels quenched to T_L = 25 °C for 1 min after heating at different temperature T_H for *t* = 5 min **(i)** and corresponding transmittance at 550 nm **(ii)**. **(C)** Optical images of PA gels quenched to different low temperature T_L for 1 min after

heating at T_H = 80 °C for *t* = 2 h **(i)** and corresponding transmittance at 550 nm **(ii)**. All background lattices are 5 mm.

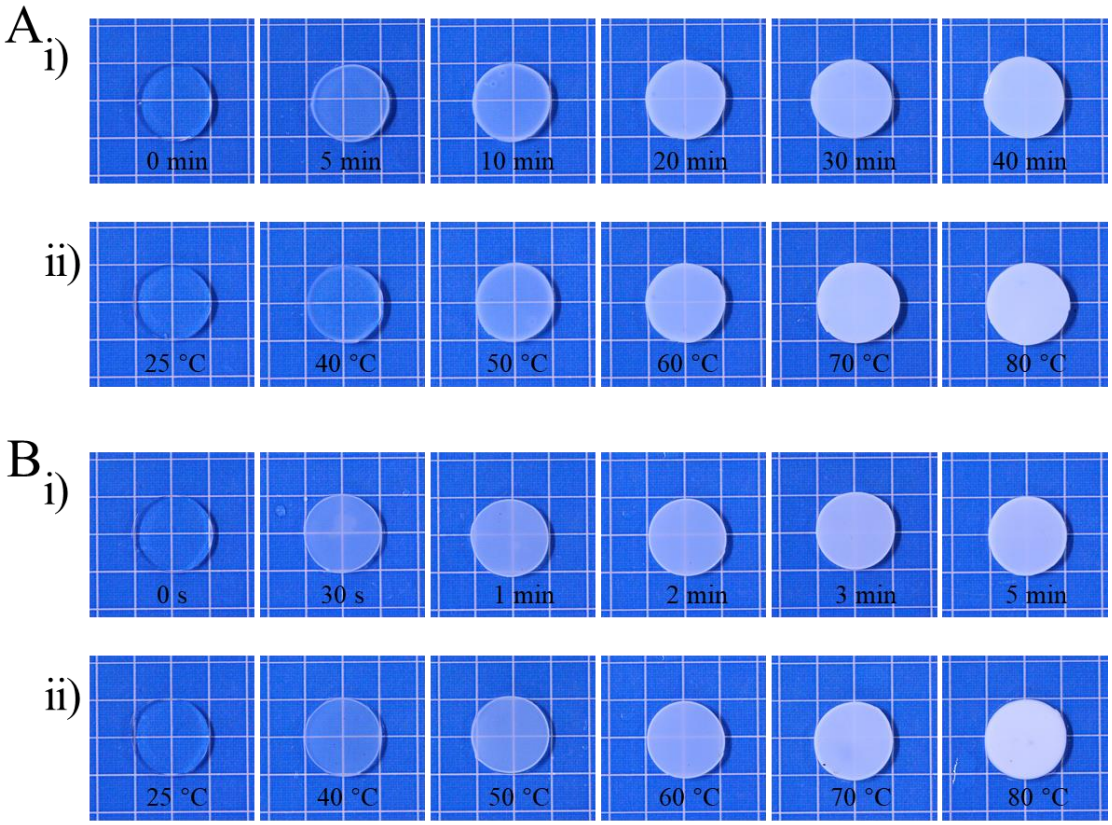

Fig. 3.5. Optical images to show the universality of thermal history dependent transparency change in other DB gels. **(A)** Optical images of P(NaSS-*co*-MATAC) gels containing ionic bonds quenched to T_L = 25 °C for 1 min after **(i)** heating at T_H = 60 °C for different time *t*, and **(ii)** heating at different temperature T_H for *t* = 20 min. **(B)** Optical images of P(UMA-*co*-MAAc) gels containing hydrogen bonds quenched to 25 °C for 1 min after **(i)** heating at T_H = 60 °C for different time *t*, and **(ii)** heating at different temperature T_H for *t* = 2 min. All background lattices are 5 mm.

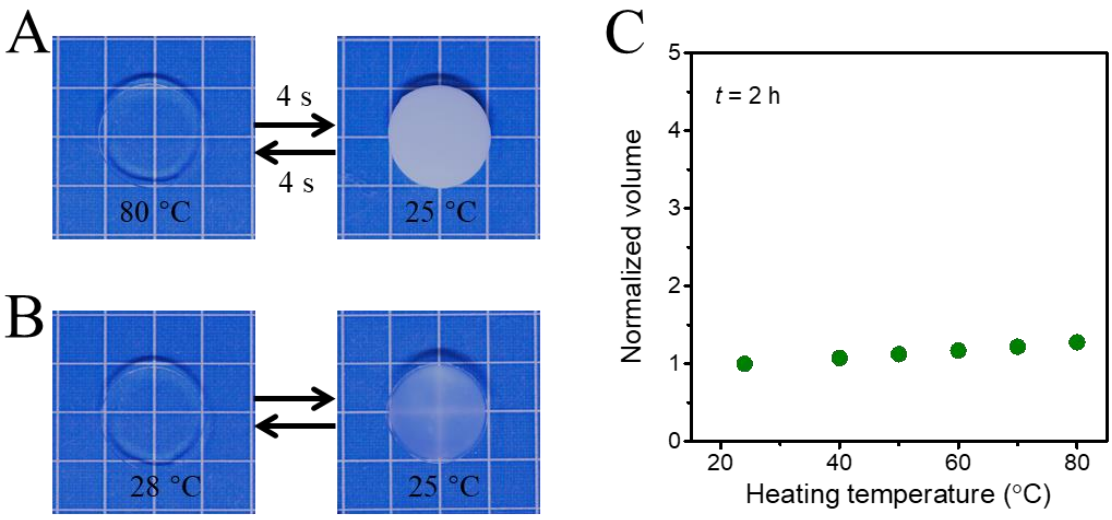

Fig. 3.6. Advantages of transparency change by using PA gels. **(A)** Quick response. A PA gel is initially heated at T_H = 80 °C for t = 2 h; then, this PA gel is moved to T_L = 25 °C and turns to turbid within 4 s, and it becomes transparent when moved back to 80 °C within 4 s. The transparency change only takes several seconds. **(B)** High sensitivity. A PA gel is initially heated at T_H = 28 °C for t = 4 h; then, this PA gel is moved to T_L = 25 °C and occurs obvious transparency change, and it returns to transparent when moved back to 28 °C. The temperature difference of 3 °C is sufficient to induce distinct transparency change for observing by naked eyes. All background lattices are 5 mm. **(C)** Normalized volume change versus heating temperature. The gels are heated at different temperature T_H for t = 2 h before testing the volume, and the volume is normalized by the volume of the sample at 25 °C equilibrium state.

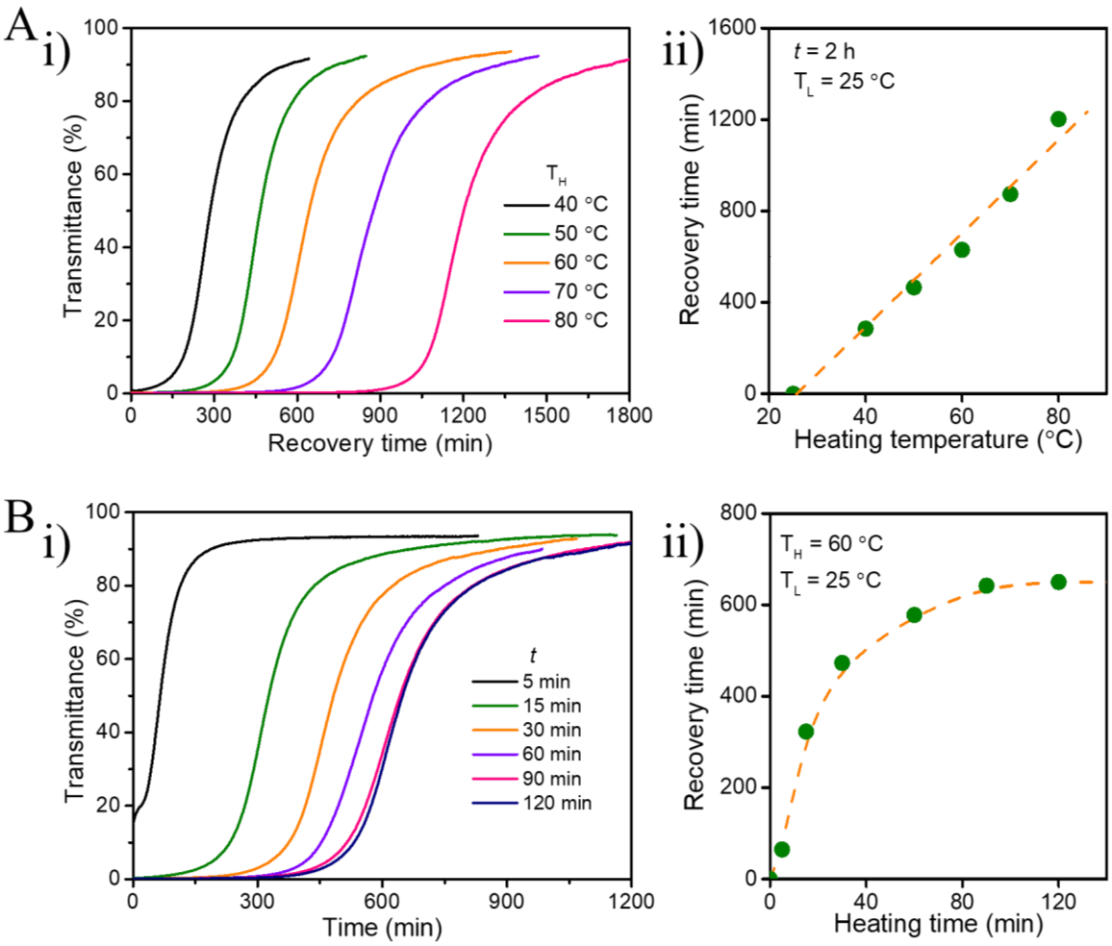

Fig. 3.7. Spontaneous opaque-to-transparency transition of PA gels with different thermal history. **(A)** Transmittance change in recovery process of PA gels quenching to T_L = 25 °C after heating at different temperature T_H for t = 2 h **(i)**, and corresponding characteristic recovery time t_c **(ii)**. **(B)** Transmittance change in recovery process of PA gels quenching to T_L = 25 °C after heating at T_H = 60 °C for different heating time t **(i)**, and corresponding characteristic recovery time t_c **(ii)**. The characteristic recovery time was defined as the corresponding time at the inflection point of transmittance curve. All recorded transmittance change is at wavelength of 550 nm.

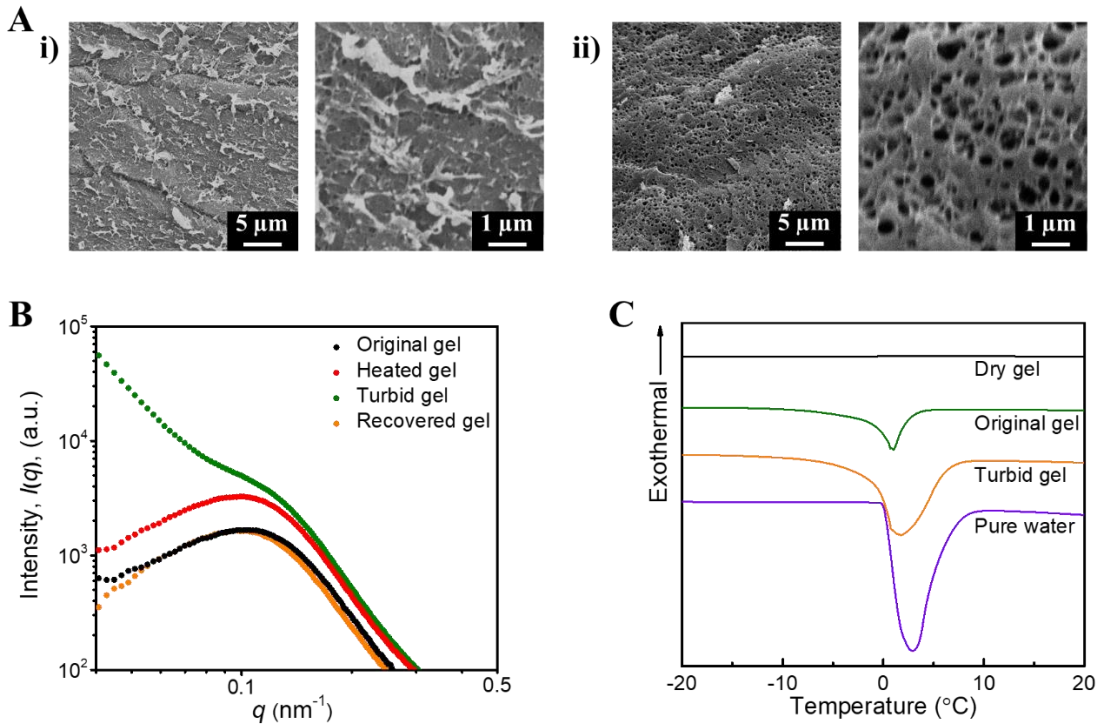

D

Code	ΔH_m (J/g)	W_{WC} (%)	W_{poly} (%)	W_{FW} (%)	W_{BW} (%)	W_{FW}/W_{poly}	W_{BW}/W_{poly}
Original gel	59.76 ± 1.06	45.67 ± 0.32	54.33 ± 0.32	18.11 ± 0.32	27.56 ± 0.64	0.33 ± 0.01	0.50 ± 0.02
Turbid gel	97.25 ± 0.36	55.03 ± 0.75	44.97 ± 0.75	29.47 ± 0.11	25.56 ± 0.86	0.66 ± 0.02	0.56 ± 0.04

Fig. 3.8. Structure and structural evolution of PA gels in transparency-change process. **(A)** SEM images of cross section of **(i)** the original gel and **(ii)** the turbid gel in **Fig. 3.1B**. **(B)** 1D SAXS profiles of original, heated, turbid, and recovered gels. **(C)** DSC curves recorded in heating scans for dry, original, and turbid gels and pure water. **(D)** Contents of various types of water and polymer in original and turbid gels. ΔH_m, the melting enthalpy, and ΔH_m of pure water is 330.00 J/g; W_T, the total water content, measured by a moisture balance MOC-120H; W_{poly}, the content of polymer, defined by $W_{poly} = 1 - W_{WC}$; W_{FW}, the content of free water, calculated from DSC data; W_{BW}, the content of bound water, defined as $W_{BW} = W_T - W_{FW}$.

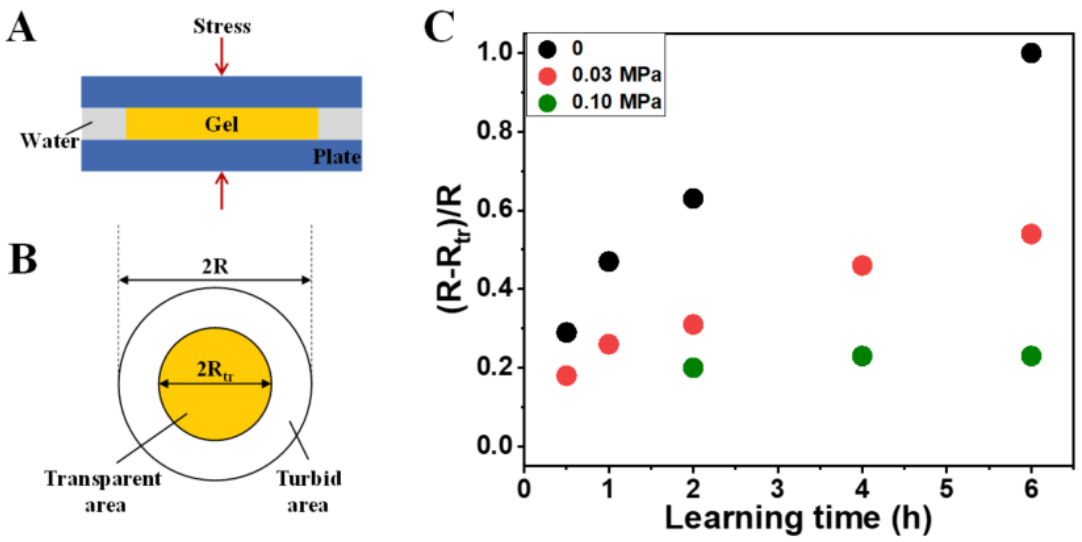

Fig. 3.9. Prohibition of water absorption by applying stress. **(A)** Scheme of sandwiched PA gel with pressure. The initial radius and thickness of sample are 5 and 1.15 mm, respectively. **(B)** Method to determine the length ratio between the opaque region to the entire sample, $\beta = (R-R_{tr})/R$, where R and R_{tr} are the radiuses of entire sample and transparent region, respectively. R and R_{tr} were measured with the gels after jumping temperature from 80 to 25 °C for 1 min. **(C)** Change of $(R-R_{tr})/R$ with learning time t_L under different stress.

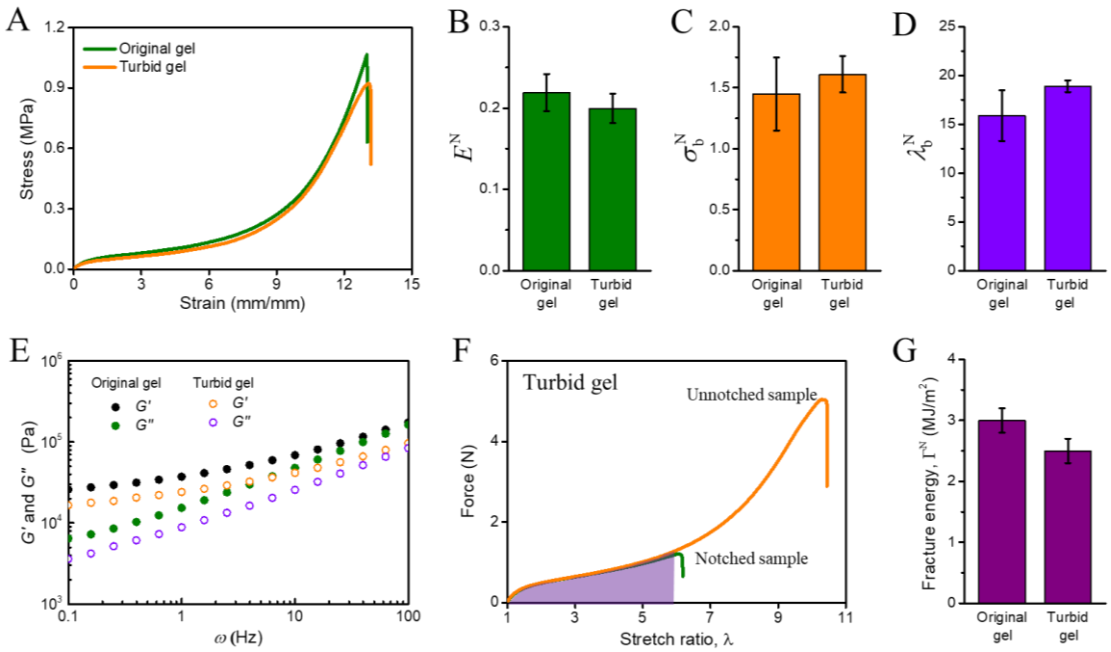

Fig. 3.10. Comparison of mechanical behaviors between original and turbid gels. a-d) Uniaxial tensile test: **(A)** Stress-strain curves, and results of **(B)** Young's modulus E^N, **(C)** fracture stress σ_b^N, and **(D)** fracture stretch ratio λ_b^N at the virtual reference state ($\Phi_P = 1$). **(E)** Frequency dependence of storage modulus G′ and lose modulus G″ at 25 °C. **(F)** Force-stretch ratio (λ) curves of notched and unnotched samples for the turbid gel. **(G)** Fracture energy Γ^N of the original gel and turbid gel at the virtual reference state ($\Phi_P = 1$).

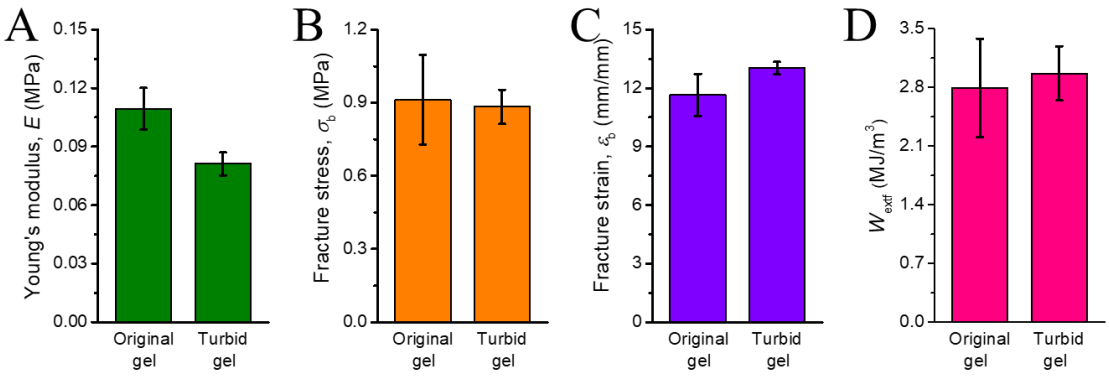

Fig. 3.11. Tensile property of original gel and turbid gel. **(A)** Young's modulus E, **(B)** fracture stress σ_b, **(C)** fracture strain ε_b, and **(D)** work of extension at fracture W_{extf}.

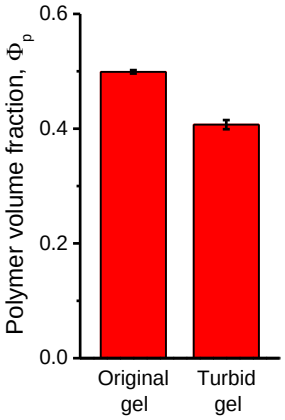

Fig. 3.12. Polymer volume fraction of original gel and turbid gel.

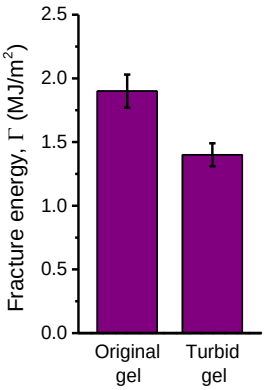

Fig. 3.13. Fracture energy Γ of original gel and turbid gel.

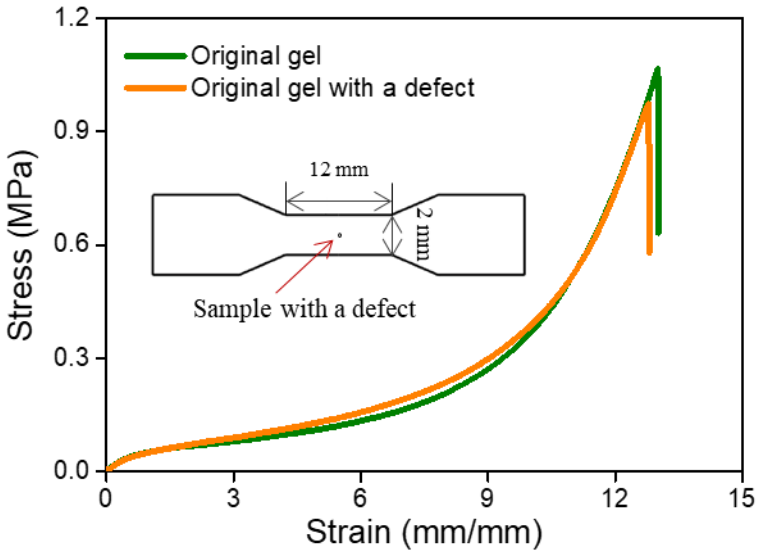

Fig. 3.14. Comparison of uniaxial tensile test of original gels with and without a defect. Inset shows a defect in the middle of the dumbbell sample, and the defect is formed by a needle with 0.25 mm diameter piercing through the sample. The original gels with and without a defect show the nearly same tensile behavior. It indicates the small defect makes no obvious effect on the tensile behavior of the PA gels, showing good crack resistant. Therefore, numerous water aggregations in turbid gel probably behave like small defects, but they have no obvious influences on the tensile behavior as well.

Charter 4-Asymmetric swelling/shrinking kinetics

4.1 Introduction

Due to conventional thermal responsive chemical gels without physical bonds, we can summarize some common rules about the swelling/shrinking kinetics based on previous works [132, 133], which has listed as below:

1. The motion equation of gels can be employed to describe both swelling and shrinking kinetics of disk-shaped gels.

2. Within the experimental accuracy the cooperative diffusion coefficient (D_{co}) does not depend on the gel size and on the extent of swelling realized by temperature jumps of different magnitude.

3. The cross-linking density, which determines the equilibrium swelling degree, makes its strong influence on D_{co}.

4. Comparing the swelling and the shrinking kinetics, the swelling and shrinking are not symmetric processes. The shrinking usually takes much longer than the swelling; the cooperative diffusion coefficient for shrinking (D_{sh}) is smaller by 1 or 2 orders of magnitude than that for swelling (D_{sw}). This difference is due to microsyneresis, that is, polymer-diluent incompatibility on a microscale. Consequently, upon cooling, all the gels exhibit optical and structural changes that can be observed by the naked eyes.

Inspired by previous research, in this chapter we find the swelling and shrinking kinetics in DB gels are also asymmetric ($D_{sh} << D_{sw}$). Especially, we demonstrate that this asymmetry is dependent on the frustrated structure, another heterogenous structure

in PA gels, and the ionic bonds also plays an important role. Finally, we know this asymmetry is another necessary condition to design hydrogel materials with dynamic memorizing-forgetting behavior.

4.2 Measurement

Water content measurement. The water content, or the water weight percentage of gel was measured with an electronic moisture balance (MOC-120H, SHIMADZU Co.). The gels were first weighted at 25 °C; then the temperature was increased to 120 °C for gel drying until no weight changes. The water content was calculated as the ratio of the lost weight to the initial weight of the gel.

Differential scanning calorimetry (DSC). DSC analysis was performed by employing a Model DSC22 instrument (SII Nano Technology Inc.) connected to a thermal analysis system (SSC 5100). The samples (8-12 mg) were first cooled to -80 °C with a cooling rate of 50 °C/min, and maintained at -80 °C for 10 min; then heated to 25 °C with a heating rate of 5 °C/min to observe the melting behavior of water in PA gels. For comparison, the dry PA gels and pure water were also performed under the same thermal procedure. The dry sample was obtained by evaporating the water in the gel at an elevated temperature of 120 °C [99]. Every sample was repeatedly tested for 3 times.

4.3 Swelling/shrinking kinetics and cooperative diffusion coefficients

We first show the thermal-induced swelling/shrinking behavior of a P(NaSS-*co*-DMAEA-Q)-2.0-0.1 gel. When the gel, of 25 mm radius and 1.15 mm thickness, is moved from a 25 °C bath to an 80 °C bath, it swells gradually and reaches equilibrium after 0.6 h, showing an increase of only 7 % in radius and 17 % in weight (**Figs. 3.1** and **3.2**). By quenching to 25 °C, the gel gradually recovers to its original size after a prolonged time by releasing water (**Figs. 3.1** and **3.2**). The recoveries of sample size and transparency in the cold bath are strongly coupled (**Fig. 3.2**).

The shrinking time required in the cold bath (t_F = 28 h) is much longer than the swelling time in the hot bath (t_L = 0.6 h) (**Figs. 3.1** and **3.2**). The relatively fast swelling and slow shrinking indicate the strong asymmetric diffusion kinetics of water. Therefore, the cooperative diffusion coefficient D_{co} of gel is determined by measuring the swelling and shrinking kinetics of disc-shape samples with varying values of thickness according to the theory developed by Tanaka *et al* [134]. For a gel with a disk-like shape of infinite diameter, the equation of motion is [135]

$$\left|\frac{d_t - d_\infty}{d_0 - d_\infty}\right| \cong \frac{8}{\pi^2}\exp(-\frac{t_v}{\tau}), \qquad \textbf{(4.1)}$$

where d_0, d_t, and d_∞ indicate the thickness values of the gels at the beginning, at time t_v, and at equilibrium, respectively, and τ is the characteristic time. In our experiments, the diameter of the gel is significantly larger than the thickness; therefore, **Equation (4.1)** can be applied. As the gel maintains the same shape during swelling, the thickness and radius ratios of the sample are always the same [136]; therefore, **Equation (4.1)** can be

re-written as

$$\left|\frac{R_t - R_\infty}{R_0 - R_\infty}\right| \cong \frac{8}{\pi^2}\exp(-\frac{t_v}{\tau}), \qquad \textbf{(4.2)}$$

where R_0, R_t, and R_∞ indicate the radius of the gels at the beginning, at t_v, and at equilibrium, respectively.

Size and appearance change of common chemical hydrogels without physical bonds at cooling and heating. To check the size and appearance change of common nonthermal-sensitive chemical hydrogels at heating or cooling, we chose two representative hydrogels, Polyacrylamide (PAAm) hydrogel and double-network (DN) hydrogel for study in this experiment. The PAAm gel was prepared by UV polymerization of a mixed solutions containing 2 M AAm monomers, 1 mol% UV initiator (α-keto), and 0.1 mol% chemical crosslinker (MBAA). The DN gel was prepared by two steps. The first network was synthesized by UV polymerization of mixed solutions containing 1 M 2-acrylamido-2-methylpropanesulfonic acid, 1 mol% α-keto, and 4 mol% MBAA. After polymerization, the first network was immersed in precursor aqueous solution containing 2 M AAm, 0.1 mol% α-keto, and 0.01 mol% MBAA for 1 day. Then, the gel was UV polymerized again to form the DN gel. Both PAAm gel and DN gel were immersed in large amount of water for at least 5 days to remove the unreacted reagents before using.

We performed the swelling/shrinking experiments of PAAm and DN gels in pure water. The gels were initially equilibrated in a 25 °C water bath. The size and radius of these two gels are the same, which are 25 and 4.0 mm, respectively. We first moved

these gels to an 80 °C water bath and observed the size change. After 30 min at 80 °C, we removed the gel to a 25 °C water bath and observed the size change. Unlike the PA gels containing dynamic ionic bonds, there is no observable appearance change at cooling, for both PAAm and DN gels, as shown in **Figs. 4.1A** and **4.1B**. There is also no observable size change of these two gels at cooling and heating (**Figs. 4.1C-F**), suggesting that the physical bonds play a key role in the formation of frustrated structure as well as the water absorption and release.

Swelling kinetics of PA gels. PA gels with a radius of 25 mm were moved from a 25 °C to an 80 °C water bath and the radius change at the 80 °C bath was recorded. Five different samples with d_∞ ranging from 0.37 to 2.49 mm were used. The relative change of radius of these gels, $(R_t-R_\infty)/(R_0-R_\infty)$, as a function of time is shown in **Fig. 4.2**. All the curves can be fitted well using **Equation (4.2)** and the characteristic swelling time, τ_{sw}, can be obtained [135, 137]. τ_{sw} depends on d_∞, following a power relationship, $\tau_{sw} \sim d_\infty^{1.97}$ (**Fig. 4.3**). The exponent 1.97 is significantly close to 2, confirming that the swelling kinetics is governed by the cooperative diffusion process [137].

Shrinking kinetics of PA gels. The gel was initially heated at 80 °C for 2 h, then quenched to 25 °C, and the radius change at 25 °C was recorded. Similarly, the relative change of radius was fitted with **Equation (4.2)** to obtain the characteristic shrinking time, τ_{sh} (**Fig. 4.4**). τ_{sh} also depends on d_∞, following the power relationship, $\tau_{sh} \sim d_\infty^{1.96}$ (**Fig. 4.5**). The exponent 1.96 is almost equal to 2, demonstrating that the volume shrinking is also controlled by the cooperative diffusion process.

Cooperative Diffusion coefficient of PA gels. For a disk-like sample, D_{co} is defined as [135]

$$D_{co} = \frac{(d_\infty/2)^2}{(\pi/2)^2\tau} = \frac{d_\infty^2}{\pi^2\tau}. \qquad \textbf{(4.3)}$$

With this equation, D_{co} of the swelling (D_{sw}) process at 80 °C and that of the shrinking (D_{sh}) process at 25 °C can be calculated, which are measured as $(2.3\pm0.3)\times10^{-10}$ and $(3.8\pm0.7)\times10^{-12}$ m^2/s, respectively. Therefore, for a temperature difference $\Delta T = 55$ °C, the ratio D_{sw}/D_{sh} of the PA gel is as high as 61 (**Fig. 4.6**), showing an obvious swelling/shrinking asymmetry.

4.4 Mechanism of asymmetry in swelling/shrinking

4.4.1 Dependence of frustrated structure

The slow shrinking process may be caused by the formation of more bound water, skin layer, or structure frustration in the turbid gel. To check the content of bound water in turbid and transparent gels, DSC testing was performed on the transparent gel shown in **Fig. 3.1(i)** and the turbid gel shown in **Fig. 3.1(iii)**. During DSC measurement, the gels were first cooled to -80 °C at a cooling rate of 50 °C/min and then held at this temperature for 10 min to allow the crystallization of free water but not the bound water; after that, the gels were heated to 25 °C at a heating rate of 5 °C/min to melt the crystals formed by the free water. **Fig. 4.7A** shows the DSC data of these two gels during heating from -80 to 25 °C, from which the contents of free water (W_F's) are calculated. The total water contents (W_T) of turbid and transparent gels are obtained with an electronic

moisture balance device, which are 46 and 56 %, respectively (**Fig. 4.7B**). W_F's for transparent and turbid gels are about 18 and 30 %, respectively (**Fig. 4.7C**). The contents of bound water (W_B's) can be calculated with the equation of $W_B = W_T - W_F$, which are about 28 and 26 % for the transparent and the turbid gels, respectively (**Fig. 4.7D**). This result suggests that the free water changes a lot while the bound water almost does not change when the gel changes from transparent to turbid, which is consistent with the result as shown in **Fig. 3.8**. The cut cross section of sample totally turns to turbid quickly when being cooled (**Fig. 3.1(iii)**), excluding the possibility of the formation of skin layer on the surface of the gel. Therefore, the frustrated structure caused by sudden cooling, as seen by the instant transparent to opaque change of gel at cooling, should be responsible for the slow shrinking kinetics.

The formation of frustrated structure can be rationalized with the following picture. When the sample is heated to T_L = 80 °C, the number of associated ionic bonds in the gel decreases and the osmotic pressure of gel increases, which leads to the swelling of gel. After jumping the temperature to 25 °C, the number of associated bonds increases quickly (the average association time of ionic bonds is several microseconds at 25 °C) [138] while the absorbed water at 80 °C cannot be expelled out of the gel instantly, as the thermal diffusion coefficient ($D_{th} = 1.2\times10^{-7}$ m^2/s at 25 °C, details see following discussion) is much larger than the D_{co} of the gel (**Fig. 4.6**). Therefore, water is trapped between the aggregated polymers to form a transient frustrated structure. There are two timescales that influence the formation of the frustrated structure. One is the time required for heat conduction from the surface to the center of gel; the other is the time

required for local water diffusion to form trapped water aggregates. First, we calculate the heat conduction time from the surface to the center of gel. D_{th} of the PA gel is obtained as follows:

$$D_{th} = \frac{\lambda}{\rho C_p}. \qquad \textbf{(4.4)}$$

Here, ρ = 1.19×10^3 kg/m^3, λ = 0.605 W/(m·K), and C_p = 4.136×10^3 J/(kg·K) are the density, thermal conductivity, and heat capacity, respectively [42, 139]. D_{th} = 1.2×10^{-7} m^2/s at 25 °C, which is significantly larger than D_{co} at the same temperature (**Fig. 4.6**). Then, we estimate the temperature change at the center of the gel after temperature jumping, for the case of T_L = 80 °C and T_F = 25 °C. For a disk-like sample with a diameter that is significantly larger than the thickness, the following equation can be established [140] by assuming that:

1. the thickness does not change;

2. the heat conduction is constant along the thickness;

3. the thermal contact resistance and heat convection on the water-gel interface do not exist;

4. the thermal conductivities of gel and water are the same, which are reasonable for hydrogels [139].

$$\Gamma = \frac{d_\infty^2}{8D_{th}}[In(T_L - T_F) - In(T - T_F)]. \qquad \textbf{(4.5)}$$

Here, d_∞ = 1.15 mm is the thickness of the gel at equilibrium and Γ is the time when the temperature at the center part reaches a value of temperature T. **Fig. 4.8** presents the

evolution of Γ as a function of T. Only about 2 s is required for T to reach 40 °C and about 6 s is required for T to reach 26 °C.

For the local water diffusion to form water aggregates with structural length around 300 nm (**Fig. 3.7A**), the characteristic time can be estimated using **Equation (4.3)**, which is in the order of tens of microseconds, by considering d_∞ = 150 nm and D_{co} = 3.8×10^{-12} m^2/s. Thus, the formation rate of structure frustration is primarily limited by heat conduction. This is also consistent with our experimental observation that the timescale for the gel to become completely opaque is almost the same as the timescale for heat conduction from the surface to the center of the gel. It is surprising that the formation of such a prominent frustrated structure is caused by a considerably small amount (17 *wt*%) of extra water in the sample.

4.4.2 Heterogeneity of frustrated structure

From **Figs. 3.6** and **3.7**, we have demonstrated that the transparent gel has a period heterogeneous structure with a characteristic length of about 60 nm (**Fig. 3.6**); the turbid gel has two heterogeneous, containing the 60 nm length and new large-scale length of 300 nm. We furtherly discussed the asymmetric swelling/shrinking kinetics is due to the formation of this 300 nm heterogeneous frustrated structure (**Fig. 3.7**). Therefore, we consider that the length of this frustrated structure is critical to the asymmetry of swelling/shrinking kinetics of PA gels. In order to investigate how the frustrated structure influences the asymmetry of swelling/shrinking kinetics, we constructed a

series of P(NaSS-*co*-DMAEA-Q) gels with various crosslinkers as shown in **Table 2.1**.

Fig. 4.9 shows the optical images of the samples with different crosslinkers at different states, and **Fig. 4.10** represents the 1D SAXS profiles and the characteristic length d_0 of the samples at 25 °C equilibrium state. Based on our previous work [95, 96], we know the optical appearance of the samples is highly dependent the characteristic length. For example, the P(NaSS-*co*-DMAEA-Q)-2.5-0 gels without crosslinker at 25 °C equilibrium state has a characteristic length around 170 nm (**Fig. 4.10**), showing turbid appearance. When the content of crosslinker is between 0.1 and 0.5 %, their characteristic length is under 60 nm, showing transparent appearance (**Fig. 4.10(B)**). The gels turn to homogeneous when the crosslinker is larger than 0.5 nm, also showing transparent (**Figs. 4.9** and **4.10(A)**).

The optical appearances of the gels after quenching to 25 °C are distinctly different because of the formation of frustrated structure. The transparency of these gels becomes higher with the increase of crosslinkers. When the crosslinker is 1.0 %, the gels are semi-transparent, and the gels become turbid or transparent when the crosslinker is less or higher than 1.0 %, respectively. This result indicates the structural strength of frustrated structure decreases as the gels keeps transparent when the crosslinker is larger than 3 %. In other hands, the polymer distribution of PA gel with different crosslinkers at equilibrium is homogeneous or periodic at the hundred nm scale.

As the structural strength of frustrated structure is larger than the observation window of SAXS testing (*e.g.*, 300 nm, as shown in **Fig. 3.6**), or the frustrated structure possibly has no periodic structure with characteristic length, we performed SEM to

observe the cross-section structure of the samples. **Fig. 4.11** shows the morphology of frustrated structure in PA gels with various crosslinkers. From **Fig. 4.11**, we can see the polymer distribution becomes more and more homogeneous with the increase of the content of crosslinker. When the content of crosslinker is less than 0.3 %, we can find the porous sizes are very different and their contribution is disorder; this indicates the polymer distribution is very heterogeneous at micrometer scale. When the content of crosslinker is between 0.5 and 1 %, the frustrated structure forms by the homogeneous porous-like structure. When the content of crosslinker is larger than 3 %, the cross section is very smooth, showing the homogeneous polymer distribution at micrometer scale, and no obvious frustrated structure forms.

According to above analysis, we think the asymmetry of swelling/shrinking kinetics get worse with increasing the content of crosslinker. **Figs. 4.12** and **4.13** exhibits the swelling and shrinking kinetics of PA gels with different crosslinkers, respectively. Based on the relative change of radius was fitted with **Equation (4.2)** as shown in **Figs. 4.12** and **4.13**, we obtain the characteristic swelling τ_{sw} and shrinking time τ_{sh}. As we demonstrated before, the swelling and shrinking of PA gels are water diffusion controlled. We can calculate the cooperative diffusion coefficients for swelling D_{sw} and shrinking D_{sh} by using **Equation (4.3)** (**Fig. 4.14(A)**).

As **Fig. 4.14(A)** shown, the value of D_{sw} has no obvious change as no new structure forms in swelling process (**Fig. 3.6**). The slight increase of D_{sw} for PA gels with 3 and 5 % crosslinker is due to the increase of volume fraction of polymer because the decreased total water content [133]. D_{sh} increases sharply with increased crosslinker,

because the formation of frustrated structure is confined by the increased crosslinker, and the distribution of polymer becomes more and more homogeneous (**Fig. 4.11**). **Fig. 4.14(B)** shows the value of D_{sw}/D_{sh} as a function of the content of crosslinker. We can see the asymmetry of swelling/shrinking kinetics become worse as the confined formation of frustrated structure. When the crosslinker is larger than 3 %, D_{sw}/D_{sh} trends to constant, and does not turn to 1. This means the swelling is also faster than the shrinking process, because the crosslinker just limits the formation of frustrated structure, not forbids.

4.4.3 Role of dynamic bonds

The asymmetry of swelling/shrinking behavior changes with the density of ionic bonds, *i.e.*, the ionic bond strength (**Fig. 4.15**), further supporting the above analysis. To study the effect of density of ionic bonds which depends the ionic bond strength on swelling/shrinking kinetics of PA gels, we performed the swelling/shrinking experiments of PA gels in NaCl aqueous solution instead of pure water. The ions of NaCl in solution weaken the ionic bond strength and decrease the effective crosslinking density of ionic bonds [42]. The NaCl concentration was changed from 0 to 0.1 M, because the ionic bond strength changes significantly [42] while the gel size changes slightly in this salt concentration range. When the NaCl concentration is 0.1 M, the increase in radius is only about 5 % compared with the original gel in pure water. The swelling kinetics of the gels in NaCl solutions were measured with the following protocols. We first put the gels in NaCl solutions of 7 °C to reach equilibrium, and then

jumped the temperature to 25 °C to observe the size change of gels (**Fig. 4.15A**). The shrining kinetics of the gels were measured with the same way. The only difference is that we first put the gels in NaCl solutions of 80 °C to reach equilibrium, and then jumped the temperature to 25 °C to observe the size change (**Fig. 4.15B**). As shown in **Fig. 4.15**, all the curves can be well fitted using the **Equation (4.2)**. The characteristic swelling time, τ_{sw}, increases from 0.59 to 1.72 h, while the characteristic shrinking time, τ_{sh}, decreases from 9.03 to 2.39 h, by increasing NaCl concentration from 0 to 0.1 M. Accordingly, the ratio of D_{sw}/D_{sh} (= τ_{sh}/τ_{sw}) decreases with increasing NaCl concentration, from 15.3 to 1.4. This means that the asymmetry of swelling/shrinking decreases with decreasing the ionic bond strength, and *vice versa*.

4.4.3 Comparison with conventional thermal responsive hydrogels

The thermal-response behavior of our gels containing dynamic bonds is distinctly different from conventional thermal-sensitive gels with UCST or lower critical solution temperature (LCST) [26, 30, 33] in which the transparent-to-opaque transition only occurs at the critical temperature specific to the materials. These gels, also showing an asymmetric swelling/shrinking behavior [132, 133], and in principle, can act as dynamic memory but only working at their critical temperatures. Moreover, the large volume change (tens or hundreds of times in volume) at the critical temperature [31, 38] brings difficulty to construct memory devices.

4.5 Figures and tables

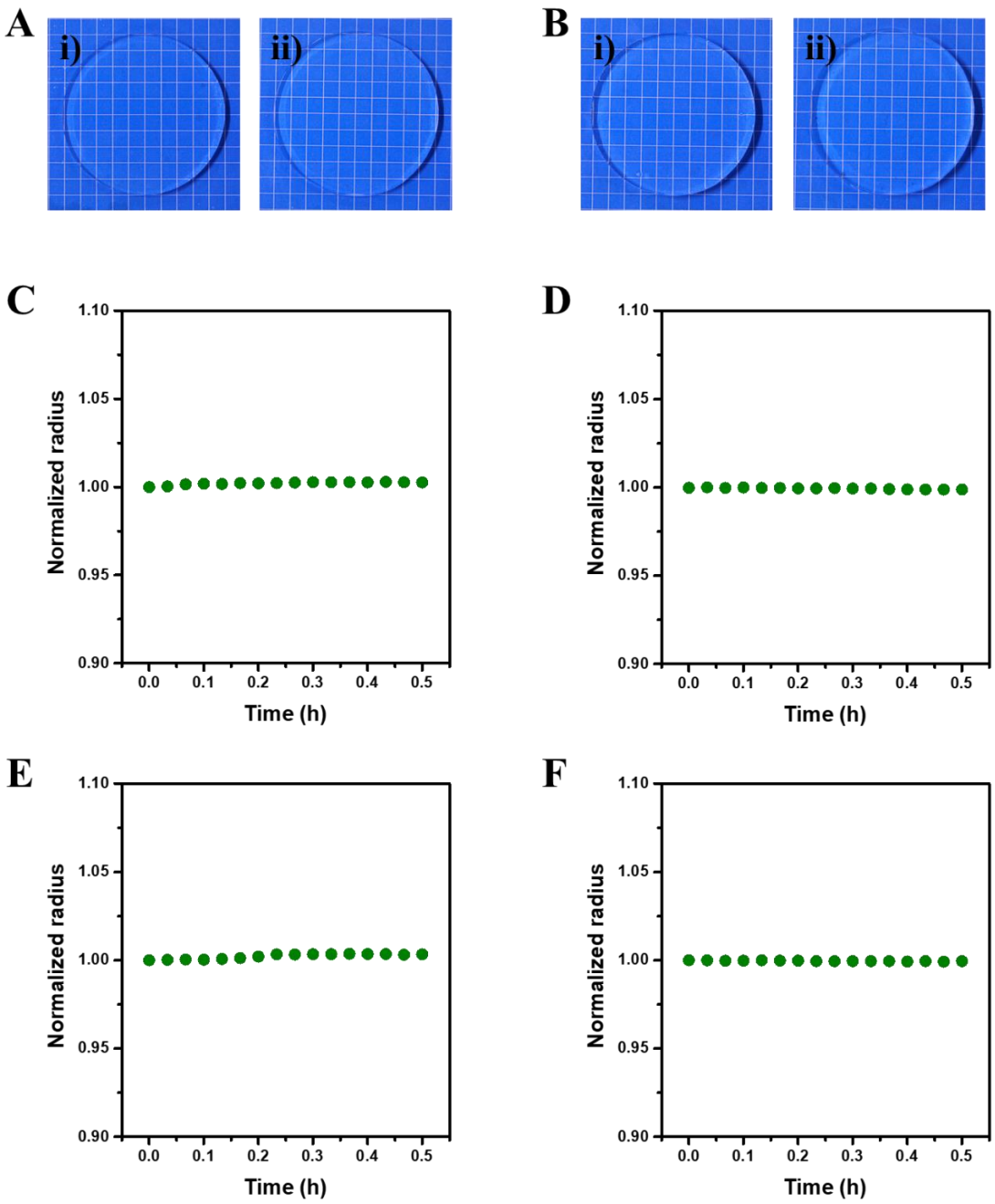

Fig. 4.1. Appearance and size change of PAAm and DN gels at cooling and heating. **(A)** Optical appearance of PAAm gels **(i)** equilibrated at 25 °C and **(ii)** immediately after jumping temperature from 80 to 25 °C. **(B)** Optical appearance of DN gels **(i)** equilibrated at 25 °C and **(ii)** immediately after jumping temperature from 80 to 25 °C.

The background lattice in **(A)** and **(B)** is 5 mm. **(C, D)** Normalized radius change of PAAm gels **(C)** after jumping temperature from 25 to 80 °C and **(D)** after jumping temperature from 80 to 25 °C. **(E, F)** Normalized radius change of DN gels **(E)** after jumping temperature from 25 to 80 °C and **(F)** after jumping temperature from 80 to 25 °C.

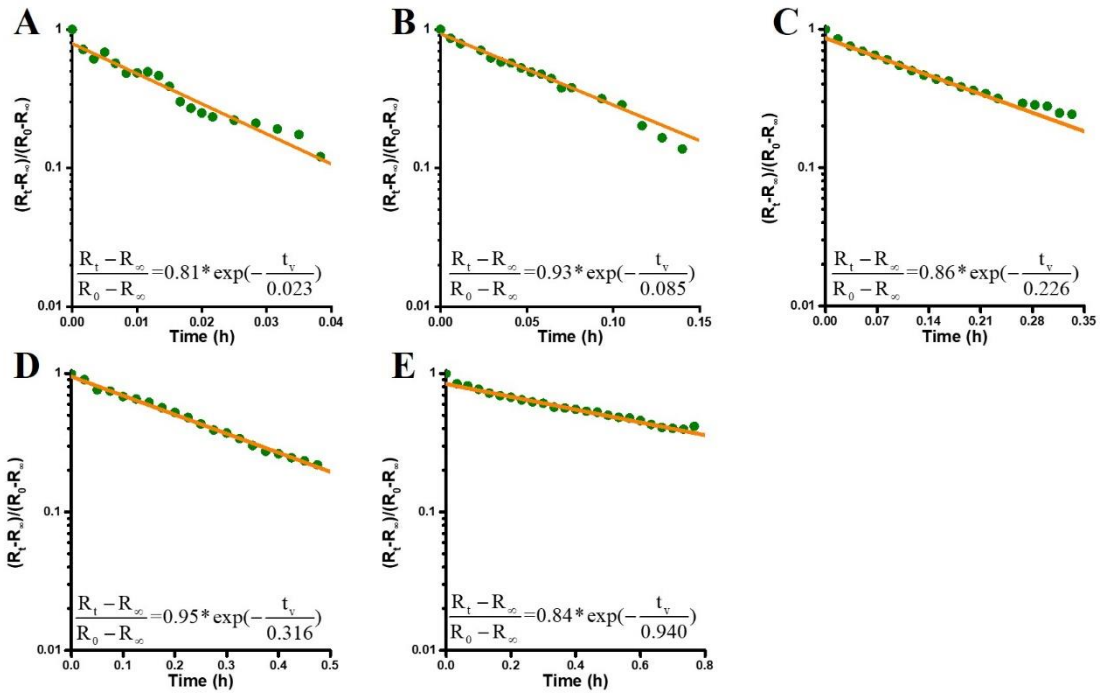

Fig. 4.2. Swelling kinetics. Relative change of radius of PA gels with different d_∞, **(A)** 0.37, **(B)** 0.78, **(C)** 1.23, **(D)** 1.68, and **(E)** 2.49 mm, as a function of time for a temperature jump from T_F = 25 °C to T_L = 80 °C. The orange lines indicate the fitting results with the equations shown in the figures.

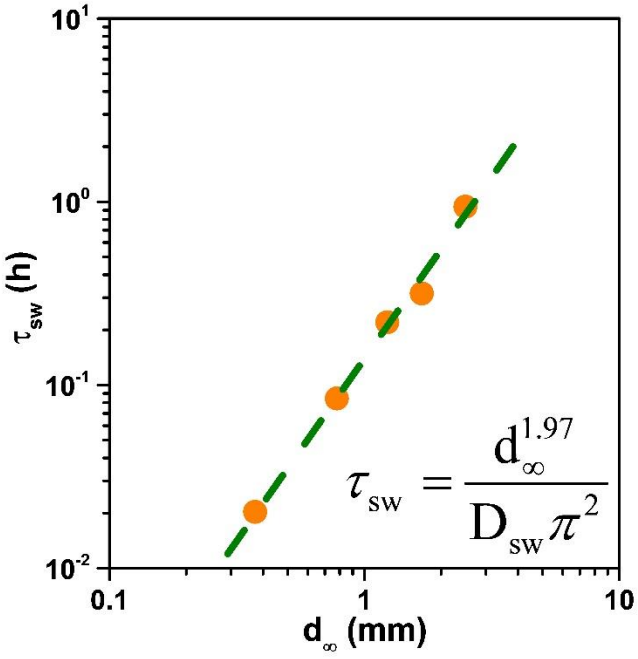

Fig. 4.3. Change of τ_{sw} corresponding to d_∞ for a temperature jump from T_F = 25 °C to T_L = 80 °C. D_{sw} is $(2.3\pm0.3)\times10^{-10}$ m^2/s.

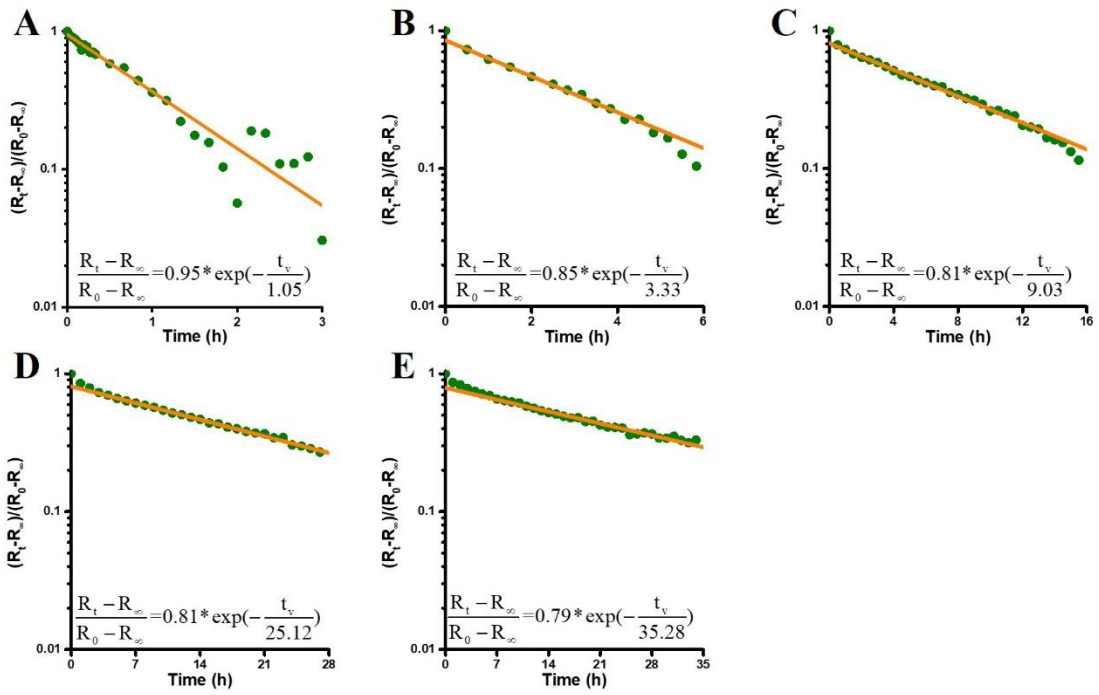

Fig. 4.4. Shrinking kinetics. Relative change of radius of PA gels as a function of time for a temperature jump from T_L = 80 °C to T_F = 25 °C after heating at 80 °C for 2 h. Five samples with d_∞ of **(A)** 0.35, **(B)** 0.73, **(C)** 1.15, **(D)** 1.58, and **(E)** 2.34 mm were used. The orange lines indicate the fitting results with the equations shown in the figures.

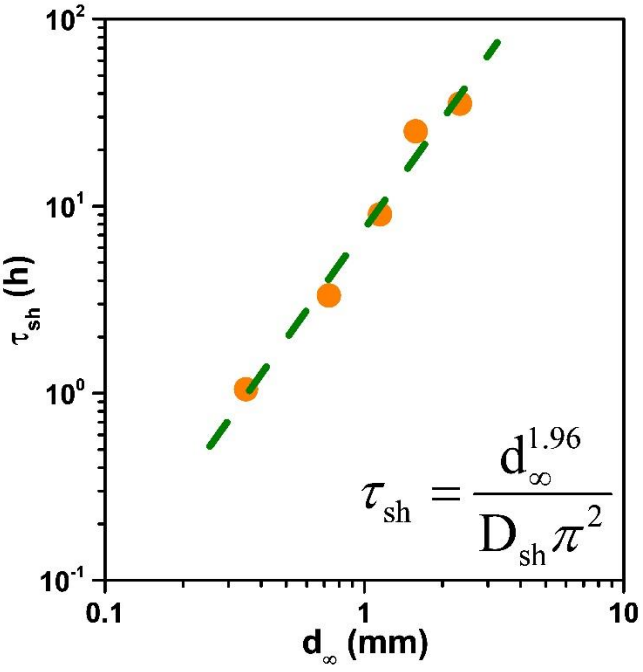

Fig. 4.5. Change of τ_{sh} corresponding to d_∞ for a temperature jump from T_L = 80 °C to T_F = 25 °C after heating at 80 °C for 2 h. D_{sh} is $(3.8\pm0.7)\times10^{-12}$ m^2/s.

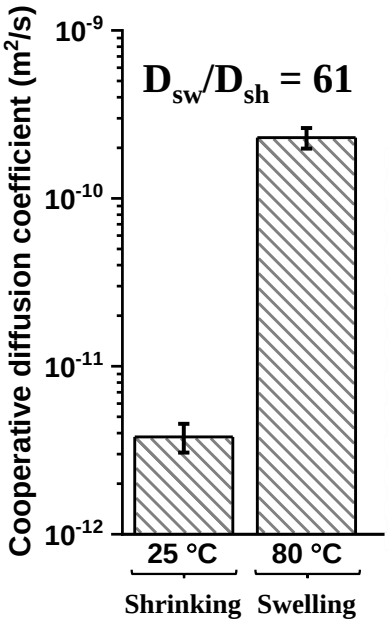

Fig. 4.6. Cooperative diffusion coefficients of PA gel for shrinking at 25 °C (D_{sh}) and swelling at 80 °C (D_{sw}).

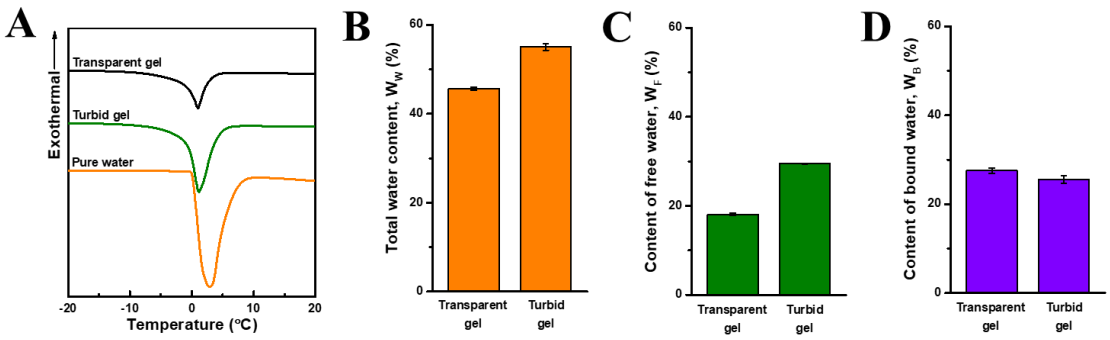

Fig. 4.7. Contents of free water and bound water in PA gels. **(A)** DSC curves recorded in heating scans for the transparent gel shown in **Fig. 3.1(i)**, the turbid gel shown in **Fig. 3.1(iii)**, and pure water. **(B-D)** Contents of total water **(B)**, free water **(C)**, and bound water **(D)** in transparent gel and turbid gel in relative to the total weight of the gels.

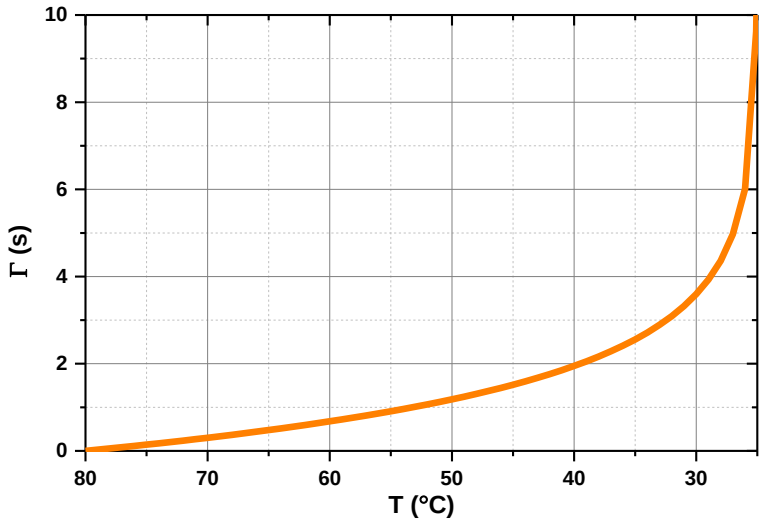

Fig. 4.8. Calculated time Γ required for the temperature at the center part of the gel to reach a value of temperature T.

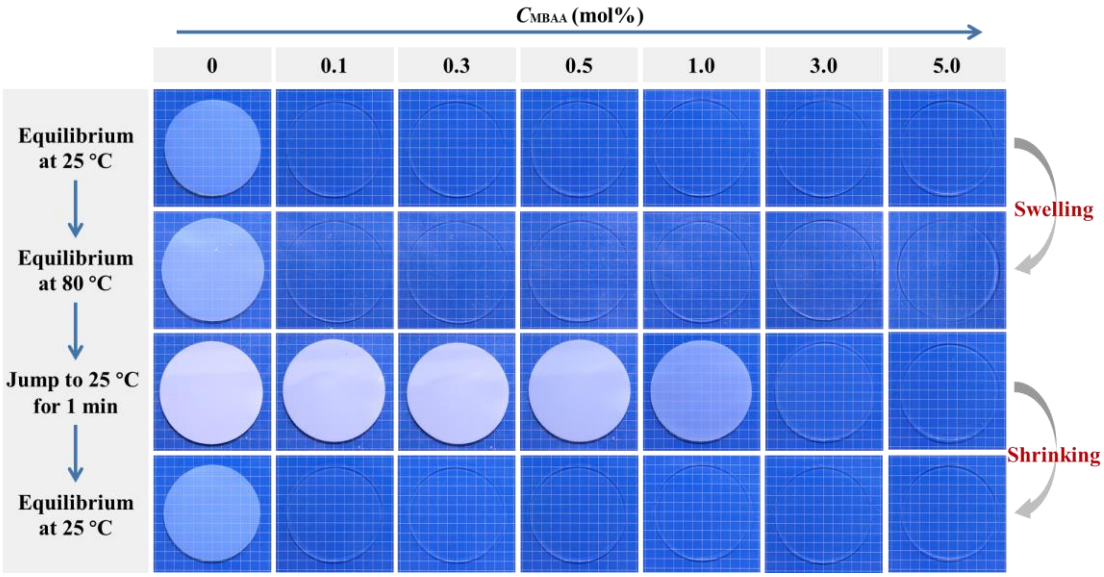

Fig. 4.9. Optical images of the samples with different crosslinkers at different states.

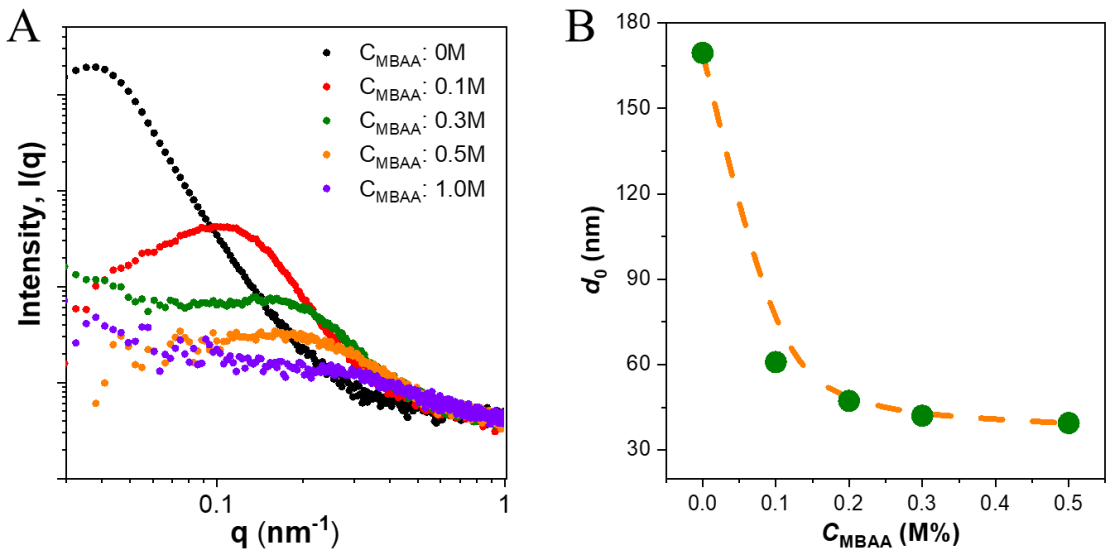

Fig. 4.10. (A) 1D SAXS profiles and **(B)** characteristic length d_0 of PA gels with different crosslinkers.

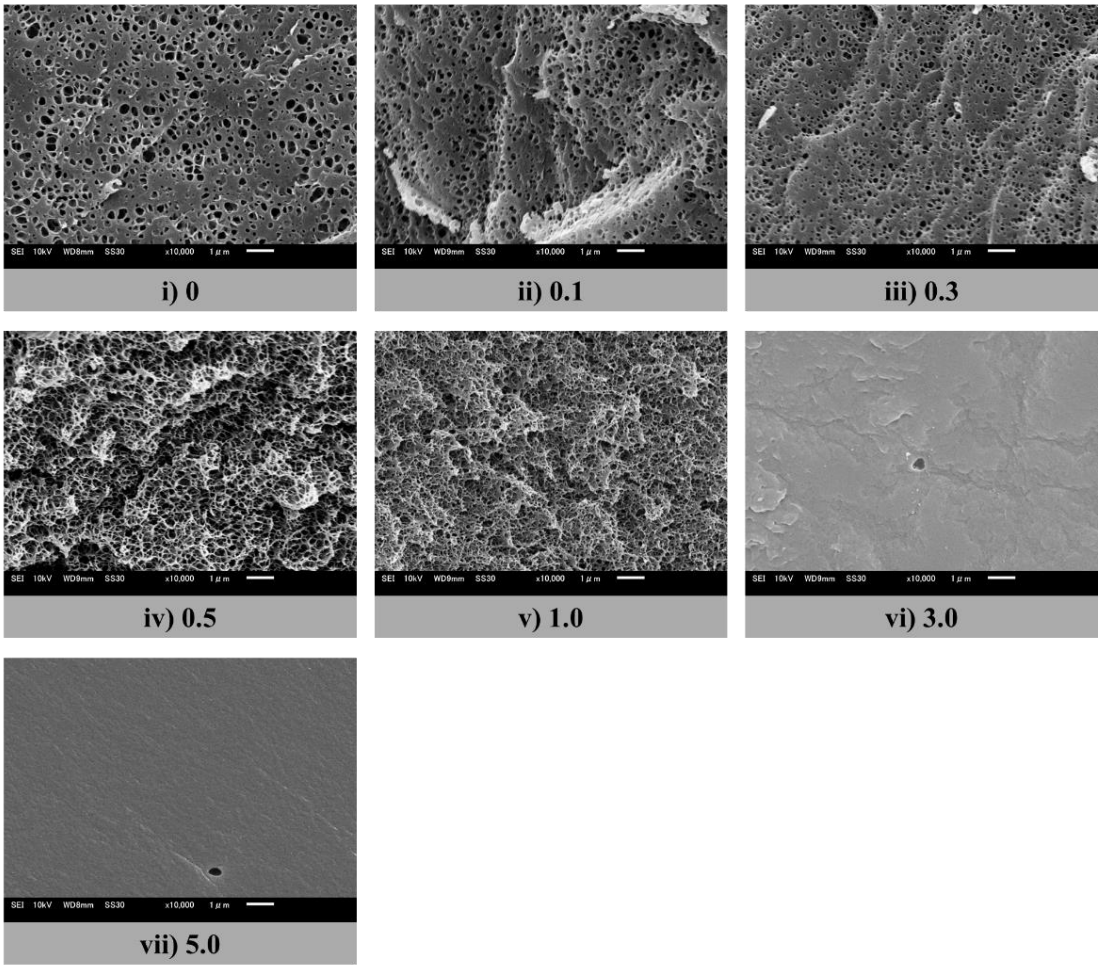

Fig. 4.11. Morphology of frustrated structure of PA gels with different crosslinkers. SEM photographs of the cross section of PA gels with different crosslinkers: **(i)** 0 %, **(ii)** 0.1 %, **(iii)** 0.3 %, **(iv)** 0.5 %, **(v)** 1.0 %, **(vi)** 3.0 %, and **(vii)** 5.0, and (B) the transparent PA gels with different crosslinkers: **(i)** 0 %, **(ii)** 0.1 %, **(iii)** 0.3 %, **(iv)** 0.5 %, **(v)** 1.0 %, **(vi)** 3.0 %, and **(vii)** 5.0.

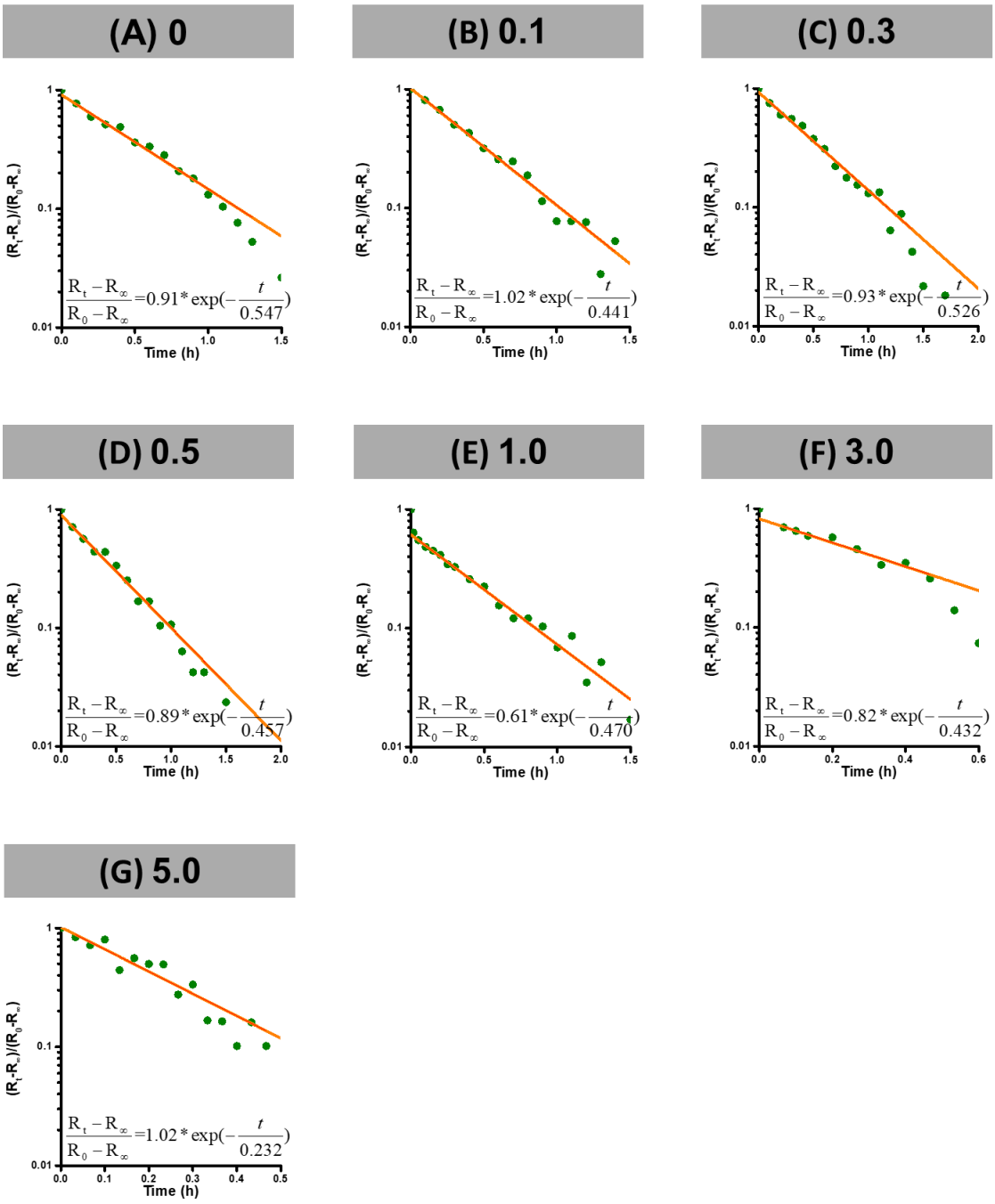

Fig. 4.12. Swelling kinetics. Relative change of radius of PA gels with different with different crosslinkers of **(A)** 0 %, **(B)** 0.1 %, **(C)** 0.3 %, **(D)** 0.5 %, **(E)** 1.0 %, **(F)** 3.0 %, and **(G)** 5.0 %, as a function of time for a temperature jump from T_F = 25 °C to T_L = 80 °C. The orange lines indicate the fitting results with the equations shown in the figures.

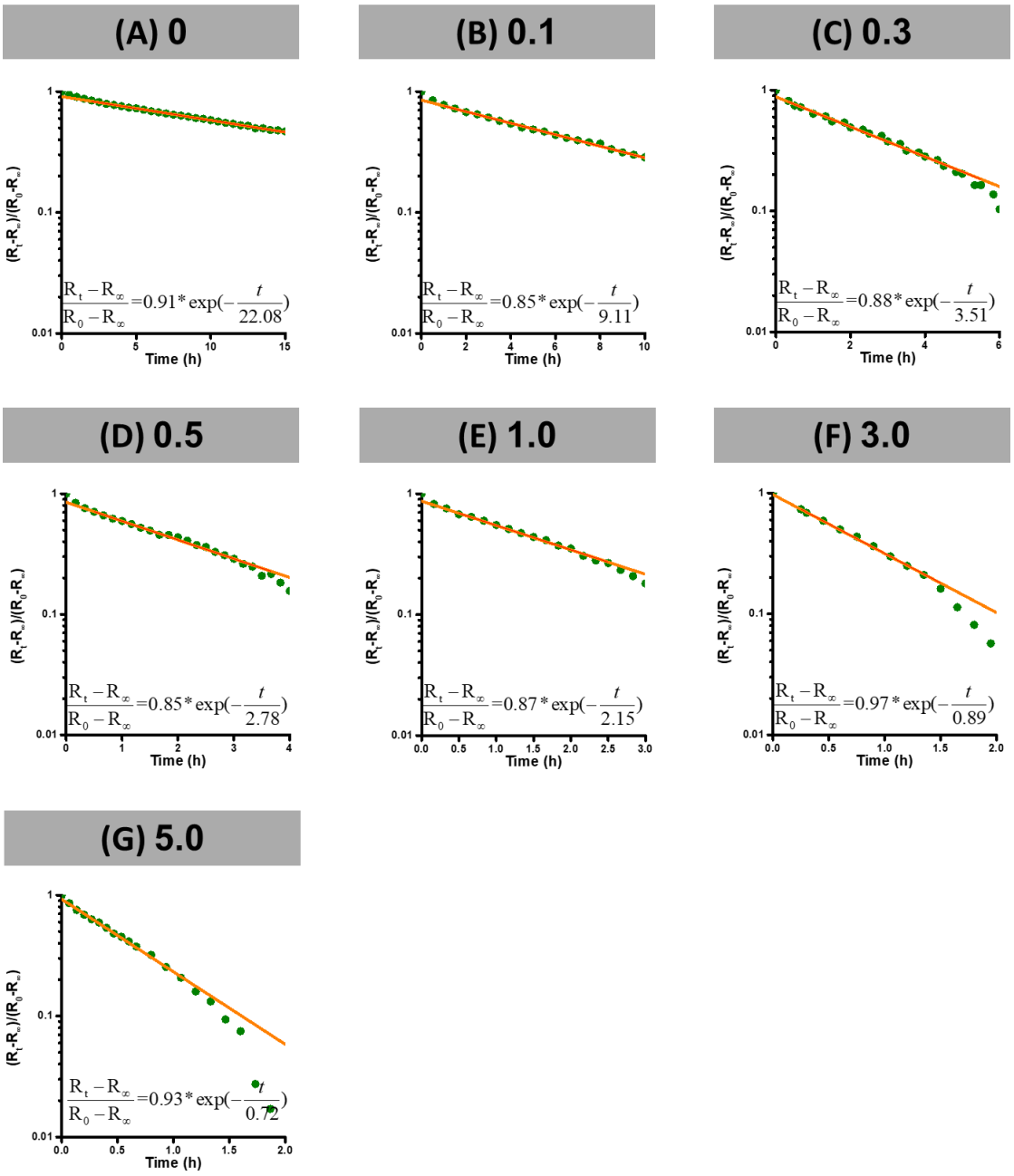

Fig. 4.13. Shrinking kinetics. Relative change of radius of PA gels as a function of time for a temperature jump from T_L = 80 °C to T_F = 25 °C after heating at 80 °C for 2 h. Five samples with different crosslinkers of **(A)** 0 %, **(B)** 0.1 %, **(C)** 0.3 %, **(D)** 0.5 %, **(E)** 1.0 %, **(F)** 3.0 %, and **(G)** 5.0 % were used. The orange lines indicate the fitting results with the equations shown in the figures.

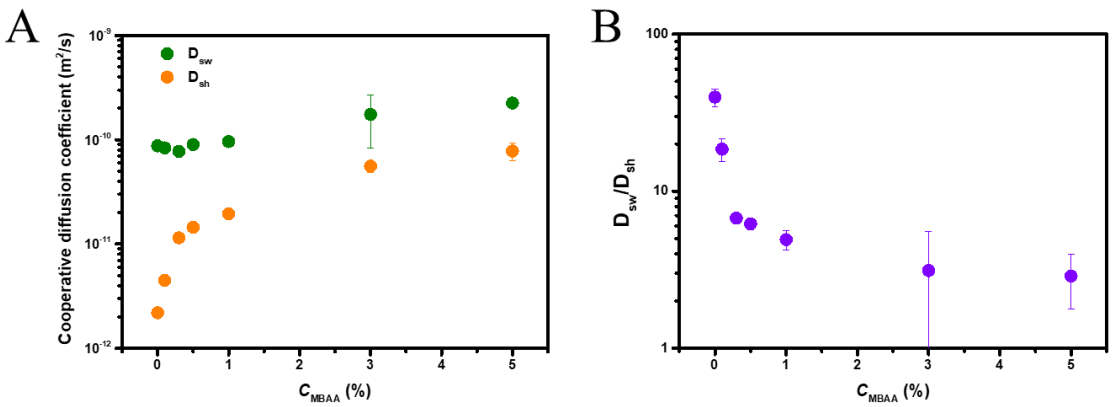

Fig. 4.14. Cooperative diffusion coefficient of PA gels with different crosslinkers. **(A)** Cooperative diffusion coefficient for swelling (D_{sw}) and shrinking (D_{sh}) as a function of crosslinker. **(B)** Swelling/shrinking asymmetry (D_{sw}/D_{sh}) as a function of crosslinker.

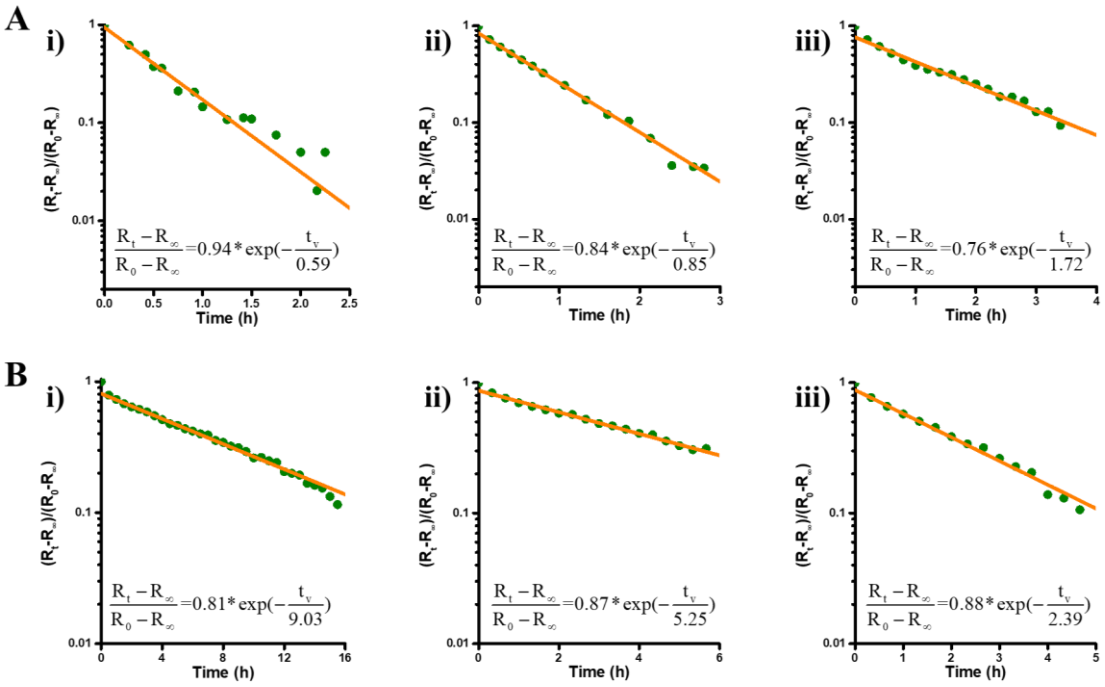

Fig. 4.15. Swelling and shrinking kinetics of PA gels in various concentrations of NaCl aqueous solutions. **(A)** Relative change of the radius of PA gels as function of time after jumping temperature from 7 to 25 °C in NaCl solutions with concentrations of **(i)** 0 M, **(ii)** 0.05 M, and **(iii)** 0.1 M. **(B)** Relative change of the radius of PA gels as function of time after jumping temperature from 80 to 25 °C in NaCl solutions with concentrations of **(i)** 0 M, **(ii)** 0.05 M, and **(iii)** 0.1 M. The orange lines indicate the fitting results with the equations shown in the figures. The equilibrium thicknesses of these gels in 0, 0.05, and 0.1 M NaCl solutions at 25 °C are 1.15, 1.18, and 1.21 mm, respectively.

Charter 5-Application in dynamic memory with forgetting ability

5.1 Introduction

The memorizing-forgetting behavior in the human brains, stored in soft and wet matter, is a dynamic and nonequilibrium process [141-144]. The acquisition of information, or learning, forms cellular memory traces in the brain, and the traces spontaneously decay over time [145, 146]. It is considered that forgetting may be the default mode of the brain, which filters out noise and unimportant information to achieve high efficiency [144]. In this dynamic process, certain mediators such as dopamine and proteins are essential in structuring cellular memory traces (**Scheme 5.1A**) [145].

Creating dynamic memory based on out of equilibrium process of soft matter, similar to the brains, is a grand challenge. So far, only several attempts were made along this line, mainly in solutions, utilizing sophisticated chemistry and experimental setup [147-150]. In this work, we propose a very simple approach to develop dynamic memory that exhibits memorizing-forgetting behavior by utilizing hydrogels, in analogy to the human brain. We show that the hydrogels containing dynamic bonds (DB gels) can encode two-dimensional (2D) information through thermal learning and the information spontaneously forgets at a forgetting time that is proportional to the learning strength (learning time and temperature). The principle of memorizing-forgetting is based on asymmetric water absorption and release of dynamic bond hydrogels in response to thermal stimulus.

5.2 Design principle

The cognitive view divides the memory process of brain into three stages: encoding, storage, and retrieval [151], while the nature of forgetting is the decay of encoded memory trace [144]. To achieve dynamic memorizing-forgetting behavior, our strategy is utilizing asymmetric and spontaneous structure transformation process of soft materials. When a soft material in equilibrium state is applied with a stimulus (learning), the change of thermodynamic environment results in the formation of an excited state (encoding information). When the stimulus is removed, the excited state returns to the initial equilibrium structure (forgetting by decaying of stored information, **Scheme 5.1B**). To apply such a general stimuli-responsive process for dynamic memorizing-forgetting, we require a strongly asymmetric but correlated kinetics between encoding and forgetting. That is, a relatively faster kinetics to form the excited structure (encoding or learning time) and a slower kinetics to recover to the original structure (storage or forgetting time); the recovery time (forgetting time) needs to be dependent on stimulus strength (learning strength). Moreover, a mechanism is necessary to facilely retrieve the stored information that decays with time.

Our idea is to use thermal swelling hydrogels to construct soft and dynamic memory. Hydrogels have similar soft and wet nature as well as permeability to small molecules as biological tissues [152], and these materials have been used to mimic muscle growth [153] and associative learning [147]. The most common feature specific to hydrogels is the reversible swelling and shrinking in response to various stimuli, such as pH and temperature [154-156]. To demonstrate this principle, we consider the

swelling and shrinking kinetics of a hydrogel of thickness d in response to thermal stimulus. We use two water baths of different temperatures, T_L and T_F, for thermal learning and forgetting, respectively, where $T_L > T_F$. The gel is initially equilibrated in the cold bath; then it is moved to the hot bath for a thermal learning time t_L; finally, it is moved back to the cold bath. Hereafter we denote this thermal learning process as T_L-t_L-T_F. When placed in the hot bath, the gel swells by absorbing water, and it shrinks when being moved back to the cold bath by releasing water. The kinetics of swelling and shrinking are governed by the cooperative diffusion coefficients of hydrogel, D_{sw} and D_{sh}, respectively. The time for gel to reach swelling equilibrium in the hot bath is $\tau_e \approx d^2/4D_{sw}$ [135, 137]. When thermal learning time t_L is shorter than τ_e, the gel does not reach swelling equilibrium, and water absorption only occurs in the surface layers of sample with thickness d_{sw} (< d/2). Therefore, only these layers shrink at cooling. Under such a condition, the time for swelling in the hot bath t_L and shrinking in the cold bath t_F are correlated through d_{sw} by $t_L \approx d_{sw}^2 / D_{sw}$ and $t_F \approx d_{sw}^2 / D_{sh}$. The water releasing time in the cold bath can be considered as the forgetting time t_F of sample with thermal learning. Accordingly, the ratio of forgetting time to learning time is

$$t_F/t_L = D_{sw}/D_{sh} \ (t_L < \tau_e). \qquad \textbf{(5.1)}$$

Equation (5.1) indicates that, if a hydrogel has a strong asymmetric swelling/shrinking kinetics by thermal stimulus ($D_{sw}/D_{sh} >> 1$), it might show a memorizing-forgetting behavior, with a forgetting time (shrinking time) proportional to but much longer than the thermal learning time (swelling time) ($t_F/t_L >> 1$). The ratio t_F/t_L can be considered as the learning efficiency. In principle, **Equation (5.1)** only holds before reaching the

learning saturation time ($t_L < \tau_e$). When the learning time t_L is longer than τ_e, the memory saturates and the longest forgetting time is about $d^2/4D_{sh}$, independent of the learning time. The saturated learning time and longest forgetting time can be tuned by sample thickness d.

To achieve the strongly asymmetric water absorption-release kinetics in response to thermal stimulus, we adopt hydrogels containing physical interactions, like hydrogen bonds and Coulombic interactions [42-44, 93]. Different from the common chemical gels that do not contain physical bonds and show no observable size and appearance change with temperature (**Fig. 4.1**), many of these physical gels swell at heating and shrink at cooling, and the shrinking kinetics is slower than the swelling kinetics [133, 157]. As the thermal conduction rate is significantly faster than the water diffusion rate, abrupt cooling induces a large-scale frustrated structure in these physical gels, which often appears as an immediate transparent-to-opaque change in the gels by cooling [90]. That is, the gel is transparent when being equilibrated in the cold bath or being suddenly put in the hot bath (**Scheme 5.1C(i, ii)**), but immediately turns opaque when being placed back to the cold bath owing to the large-scale frustrated structure formation (**Scheme 5.1C(iii)**). The turbidity of the opaque state decays with time in accompany with water release (**Scheme 5.1C(iv)**), and finally recovers to transparent when reaching the equilibrium again. Thus, the thermal-stimulus encoded information can be retrieved from the opaque state of gels, and the forgetting time corresponds to the time recovers to transparent. The learning temperature T_L and forgetting temperature T_F can be arbitrarily chosen, independent of the specific chemical structure of hydrogels.

5.3 Information storage by thermal learning

Based on the asymmetric water absorption-release kinetics and the thermal-history-dependent turbidity change of the PA gel, we can construct dynamic memory devices. To spatially control the thermal learning process, we use a mask with a hollow-out pattern featuring 2D information to be memorized. The gel pre-equilibrated in the cold bath at T_F is sandwiched between two plates with a slight compression, and one of the plates is the mask with the hollow-out pattern. Then, the sample is immersed in the hot bath for thermal learning at T_L. During thermal learning, the gel can only absorb water in the hollowed region, which memorizes the 2D information of the mask (**Fig. 5.1A**). After that, the sample is moved to the cold bath and taken out from the plates to retrieve the memorized information.

Fig. 5.1B shows a series of memorized information obtained through an 80 °C-5 min-25 °C learning process by using different masks, such as a word "GEL," patterns of "umbrella," "fish," and "twig". The memorized information is highly stretchable, and the stretched information is fully recoverable after releasing load, benefiting from the high stretchability and self-recovery of PA gels [42, 99]. As the sample becomes opaque whenever experiences a sudden cooling, independent on the specific temperature and structure of materials [33], the choice of T_L and T_F is arbitrary, provided the difference between T_L and T_F is sufficiently large (**Fig. 5.2**). As shown in **Figs. 5.2A** and **5.2B**, T_F can be higher or lower than 25 °C. In addition, the turbidity change is sensitive to temperature. A 3 °C temperature jump, from T_L = 28 °C to T_F =

25 ℃, is enough to induce the turbidity change for memorizing and retrieving information (**Fig. 5.2C**).

The memorized information in PA gels does not lose when the environmental temperature temporarily fluctuates (**Fig. 5.1C**), which is similar to the nonvolatility of memory materials in computers [158]. **Fig. 5.1C(i)** exhibits an example of memory nonvolatility at a high temperature. A PA gel is initially performed with a 60 ℃-10 min-25 ℃ learning process to memorize an airplane pattern; then, it was moved to the 60 ℃ bath. Within 2 s, the airplane pattern disappears and the entire gel becomes fully transparent. After moved back to the 25 ℃ bath, interestingly, the airplane pattern emerges again. This process can be repeated several times. Here we should mention that the time for the fluctuation treatment of the gel in the 60 ℃ bath must be very short to have negligible water absorption. Otherwise, the gel would absorb considerable amount of water and the entire gel would turn to turbid after moving back to the 25 ℃ bath. Similarly, **Fig. 5.1C(ii)** exhibits an example of memory nonvolatility at a low temperature. The airplane pattern is memorized upon 60 ℃-3 min-25 ℃ learning process; then, the gel is moved to a 4 ℃ bath for 20 s. The entire gel becomes turbid, which interferes with the airplane pattern. However, after moved back into the 25 ℃ bath, this airplane pattern re-appears clearly as the rest parts of gel become transparent.

5.4 Dynamic memorizing-forgetting behavior

The memorized information decays spontaneously, without any external stimuli. **Fig. 5.3A** shows an example of the forgetting process of PA gel after experiencing an 80 °C-5 min-25 °C learning process. The memorized airplane pattern decays and finally disappears within 4.5 h at 25 °C, and the entire gel becomes fully transparent. The forgetting time that the memorized information completely disappears depends on the learning strength, that is, the learning time and learning temperature. **Figs. 5.3B** and **5.3C** show the effect of learning time t_L on forgetting time t_F. T_L and T_F are fixed at 80 and 25 °C, respectively, and t_L is changed from 2 to 11 min. For t_L = 2 min, the initial memorized airplane pattern is translucent, indicating a relatively weak memory. By contrast, the initial memorized airplane pattern for t_L = 9 min is opaque, suggesting a relatively strong memory. The forgetting time increases almost linearly with learning time, from 115 to 715 min by increasing learning time from 2 to 11 min. The measured ratio of forgetting time to learning time, t_F/t_L, keeps almost constant value of 63, independent of learning time t_L ($t_L < \tau_e$ = 14 min, **Fig. 4.2**). This is reasonably consistent with the ratio D_{sw}/D_{sh} = 61 **(Fig. 4.6**), confirming the validity of **Equation (5.1)**. **Figs. 5.3D** and **5.3E** show that the forgetting time increases with the learning temperature, for fixed t_L = 5 min and T_F = 25 °C. t_F/t_L increases with the increase of T_L for a fixed T_F, due to the increase of temperature difference. These results show that learning with longer t_L or learning at higher T_L and retrieving at lower T_F leads to a stronger memory and *vice versa*. This behavior is similar to the memory in the human brain, where the

memory strength or forgetting time increases with learning time [159] or/and the magnitude of emotional stimulus [160].

5.5 Sequential forgetting

The dependence of memory on learning time and learning temperature allows us to program the memorizing-forgetting process in PA gels as a smart display of information. **Fig. 5.4** gives two typical examples to demonstrate sequential forgetting by programing learning time and learning temperature. We set T_L = 60 °C and T_F = 25 °C, and endow the learning time of letters "G," "E," and "L" for 26, 18, and 12 min, respectively. This is achieved by supplying water for different time during thermal learning (**Fig. 5.4A(i)**): The hollowed-out areas of "E" and "L" are initially covered by a plate, and only the letter "G" can contact with water at T_L = 60 °C for 8 min; then, both "G" and "E" are allowed to contact with water at T_L = 60 °C for 6 min; finally, all three letters "G," "E," and "L" are allowed to contact with water at T_L = 60 °C for 12 min. **Fig. 5.4A(ii)** shows the sequential forgetting process at T_F = 25 °C: The letter "L" disappears after about 3.0 h; then, "E" disappears after about 5.5 h; finally, "L" disappears after about 8.5 h. Using the same method, we set the learning temperature for "G," "E," and "L" as 45, 60, and 80 °C, respectively, while maintaining t_L = 20 min and T_F = 25 °C (**Fig. 5.4B(i)**), and a sequential forgetting behavior is also achieved (**Fig. 5.4B(ii)**).

5.6 Universal in hydrogels containing dynamic bonds

The principle proposed in this work for constructing dynamic memorizing-forgetting behavior is universal, as it is applicable to many other DB gels. Indeed, we have confirmed that PA gels made from two other cationic and anionic monomer combinations (*e.g.*, P(NaSS-*co*-MATAC) and P(NaSS-*co*-MATAC)) also show similar dynamic memorizing-forgetting behavior (**Figs. 5.5A** and **5.5B**). Furthermore, such behavior is not limited to gels with ionic bonds; gels with other dynamic bonds, such as hydrogen bonds, also show dynamic memorizing-forgetting behavior (*e.g.*, P(UMA-*co*-MAAc) as shown in **Fig. 5.5C**).

5.6 Figures and tables

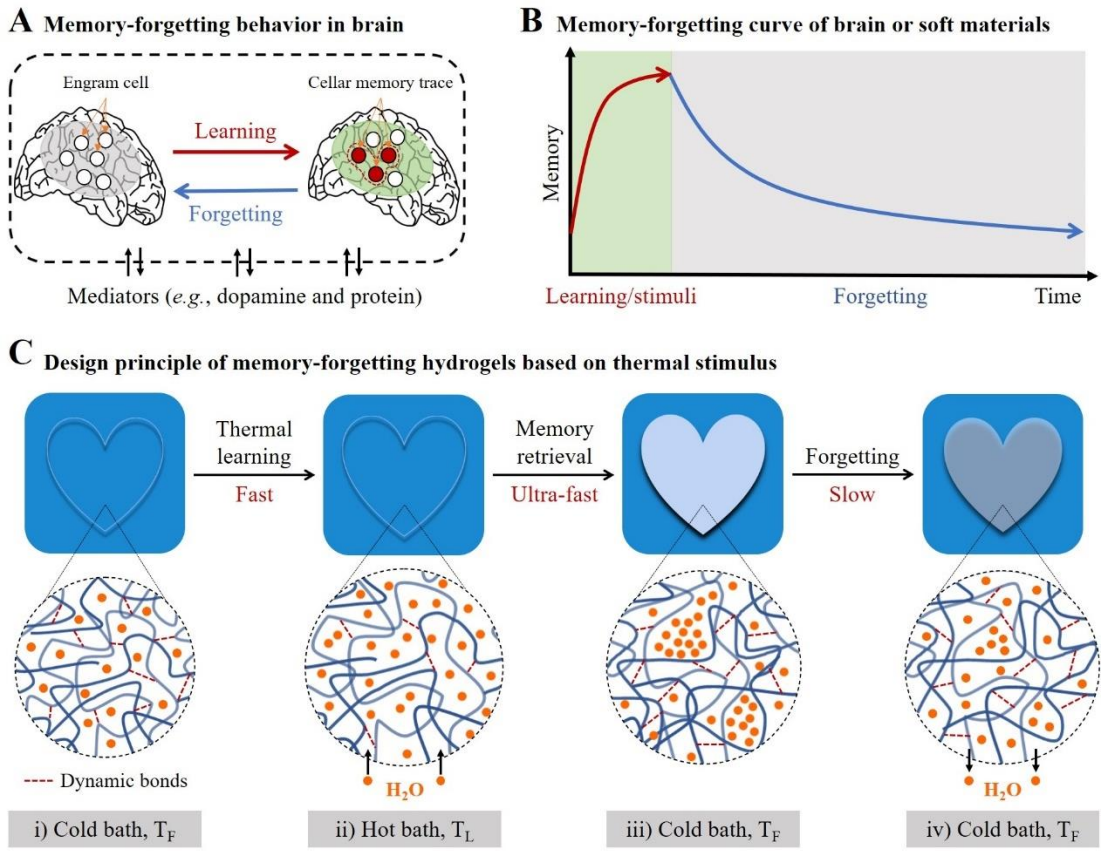

Scheme 5.1. Conceptual scheme of dynamic memorizing-forgetting behavior from human to soft materials. **(A)** Memorizing-forgetting behavior in brain. Certain mediates such as dopamine and protein are involved in the process of forming memory through learning, and the memory decays gradually and spontaneously with time, exhibiting a dynamic forgetting. **(B)** Memorizing-forgetting curve of brain or soft materials. The memorizing-forgetting behavior of soft materials is based on its nonequilibrium process in response to stimuli. Stimuli-on induces quick formation of memory, which gradually decays with time after stimuli-off. **(C)** Design principle of dynamic memorizing-forgetting hydrogels based on thermal stimulus. We use a hydrogel containing abundant dynamic bonds. The gel has unique nonequilibrium features: It swells fast in a hot bath

(learning temperature T_L) and shrinks slowly in a cold bath (forgetting temperature T_F). Moreover, the gel instantly turns from transparent to opaque (memory retravel) when being switched from the hot bath to the cold bath due to structure frustration. Consequently, the thermal history of the gel can be memorized and detected by its opaque appearance. With the shrinking progress toward the equilibrium, the gel gradually recovers to transparent, exhibiting a spontaneous and slow forgetting of the thermal history. The forgetting time (t_F) in the cold bath is correlated to the thermal learning time (t_L) in the hot bath as $t_F/t_L = D_{sw}/D_{sh}$, where D_{sw} and D_{sh} are the cooperative diffusion coefficients corresponding to swelling and shrinking, respectively. The fast water absorbing and slow releasing kinetics of the gel, corresponding to $D_{sw}/D_{sh} >> 1$, result in the fast learning and slow forgetting behaviors.

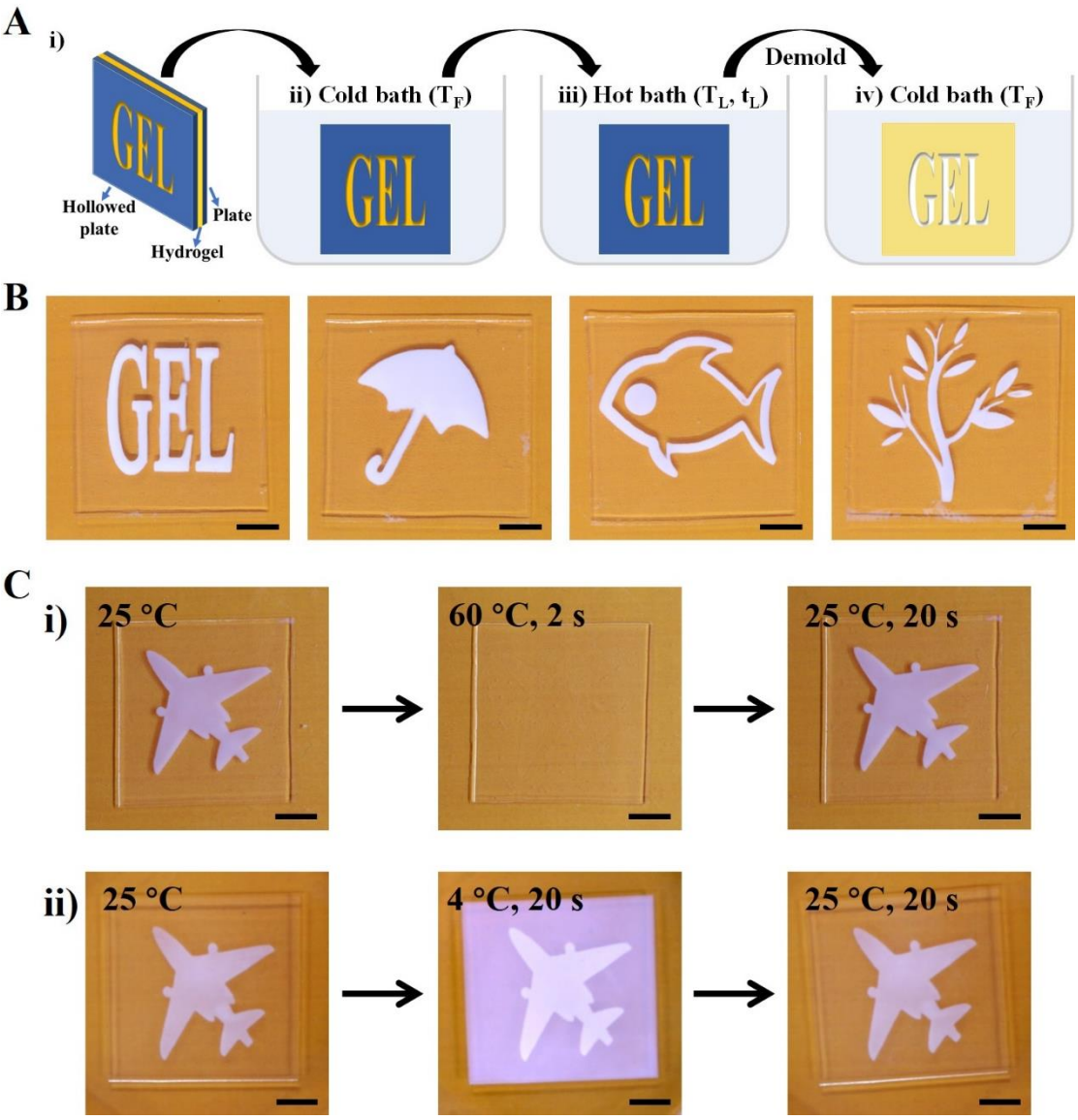

Fig. 5.1. Thermal learning and memory of PA gels. **(A)** Thermal learning process T_L-t_L-T_F. **i)** A PA gel is sandwiched between two plates with a slight compression and one plate is a mask having a hollowed-out area featuring the memorized information; **ii)** the sandwiched sample is put into a cold bath of temperature T_F for equilibrium; **iii)** the sample is then moved into a hot bath of temperature T_L for a time t_L for learning information, during which the hollow area absorbs water; **iv)** after thermal learning, the two mold plates are removed and the gel is placed into the cold bath to retrieve the

memorized information. **(B)** Various memorized information through different masks with the same 80 ℃-5 min-25 ℃ learning process. The photos are captured after jumping temperature from 80 to 25 ℃ for 1 min. **(C)** Results to demonstrate the memory nonvolatility against high and low temperature perturbation. **i)** High temperature perturbation. The gel is first performed a 60 ℃-10 min-25 ℃ learning process to memorize an airplane pattern. Then, the gel is put into a 60 ℃ bath and the pattern disappears within 2 s. After putting the gel back to the 25 ℃ bath, the airplane pattern remerges again. **ii)** Low temperature perturbation. The gel is performed a 60 ℃-3 min-25 ℃ learning process. Then, it is put into a 4 ℃ bath for 20 s and the surrounding region becomes opaque. After putting back to the 25 ℃ bath, the surrounding noise disappears, and the airplane pattern remerges clearly again. All scale bars are 1 cm.

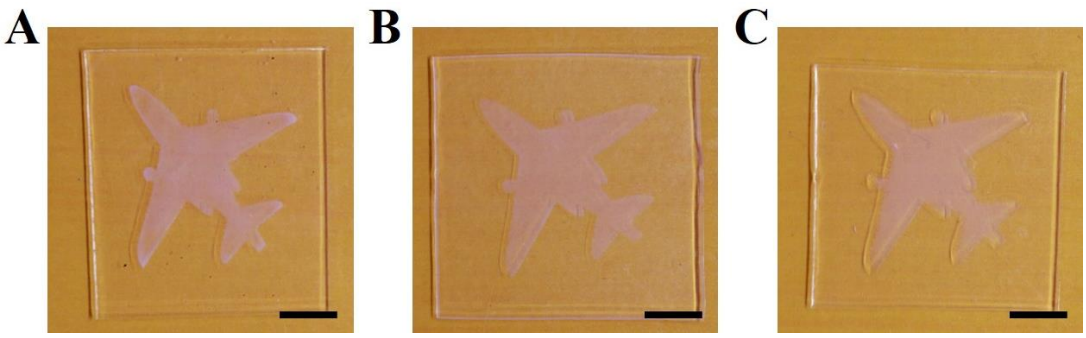

Fig. 5.2. Memorized information embedded upon PA gels under different learning processes. **(A)** 80 °C-6 min-40 °C learning process, **(B)** 25 °C-20 min-8 °C learning process, and **(C)** 28 °C-12 h-25 °C learning process. All pictures were captured after jumping the temperature to T_F for 1min; here, all scale bars are 1 cm. The initial temperature before thermal learning for **(B)** is 8 °C, and for other samples, it was 25 °C.

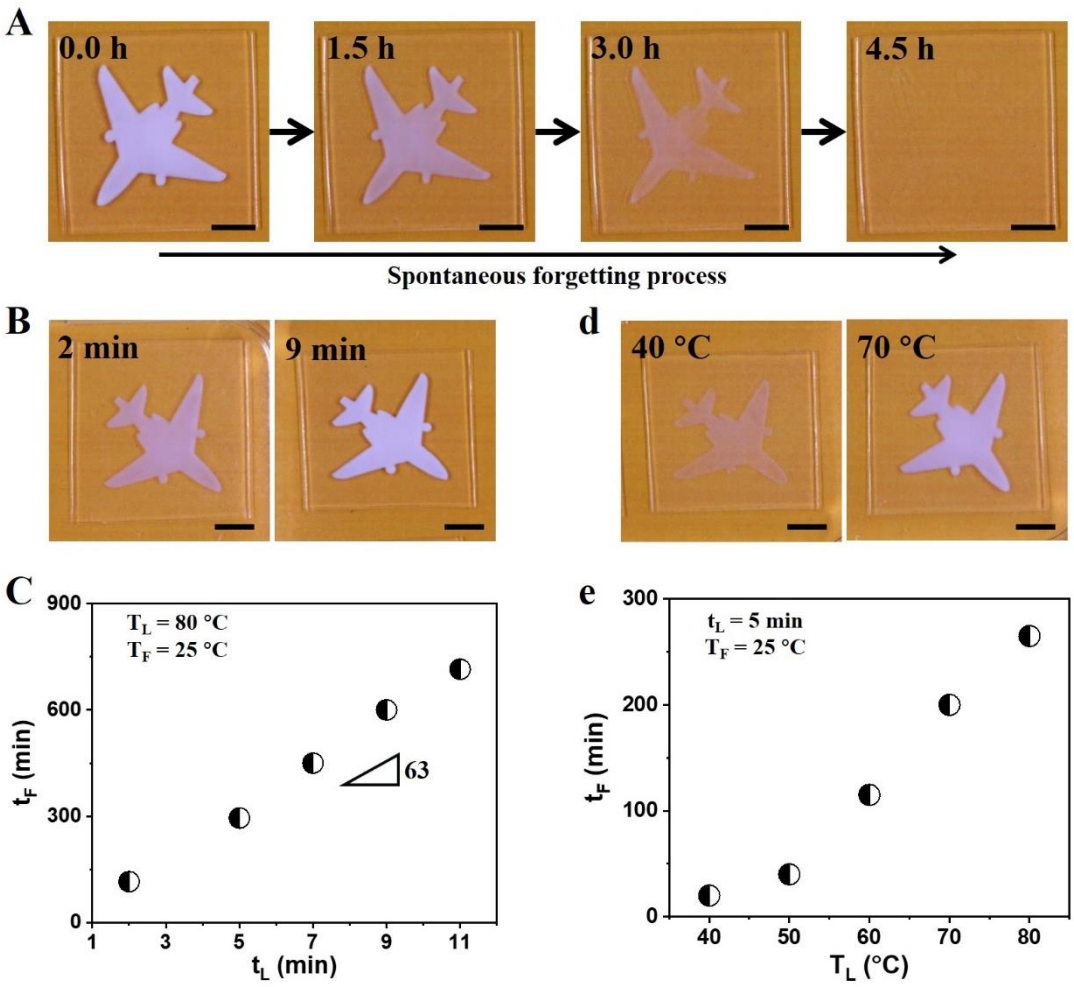

Fig. 5.3. Spontaneous forgetting process of PA gels. **(A)** Example to show spontaneous forgetting process of a gel experienced an 80 °C-5 min-25 °C learning process to memorize an airplane pattern. The elapsed time after cooling in 25 °C bath is shown in the photos. **(B, C)** Effect of thermal learning time t_L on memory strength **(B)** and forgetting time t_F **(C)** for the same T_L and T_F. The time in the images is the learning time t_L. **(D, E)** Effect of thermal learning temperature T_L on memory strength **(D)** and forgetting time t_F **(E)** for the same t_L and T_F. The temperature in the images is the learning temperature T_L. In all experiments, t_L shorter than the equilibrium swelling time of sample and the forgetting time t_F is determined by the recovery time from opaque to transparent. All scale bars are 1 cm.

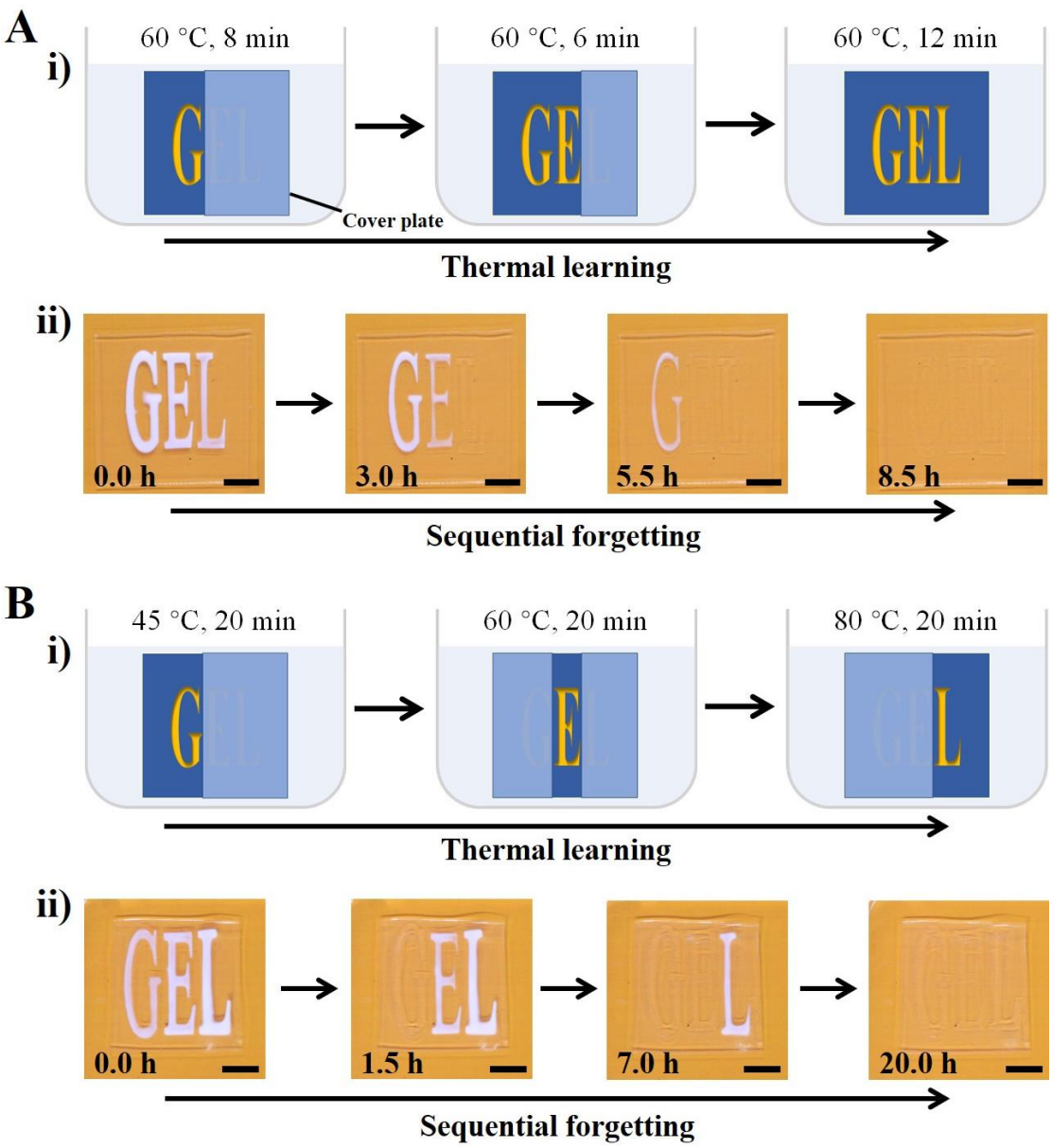

Fig. 5.4. Programmable forgetting process of PA gels. By using additional plates to selectively cover the hollowed-out area for prohibiting water uptake, the gels show programmable forgetting behaviors. **(A)** Sequential forgetting process by tuning the thermal learning time. **i)** The learning times for "G," "E," and "L" are 26, 18, and 12 min, respectively. **ii)** The optical images of gel during spontaneous sequential forgetting in a 25 °C bath. **(B)** Sequential forgetting process by tuning the thermal learning temperature. **i)** The learning temperatures for "G," "E," and "L" are 45, 60, and 80 °C,

respectively. **ii)** The optical images of gel during spontaneous sequential forgetting in a 25 °C bath. All scale bars are 1 cm.

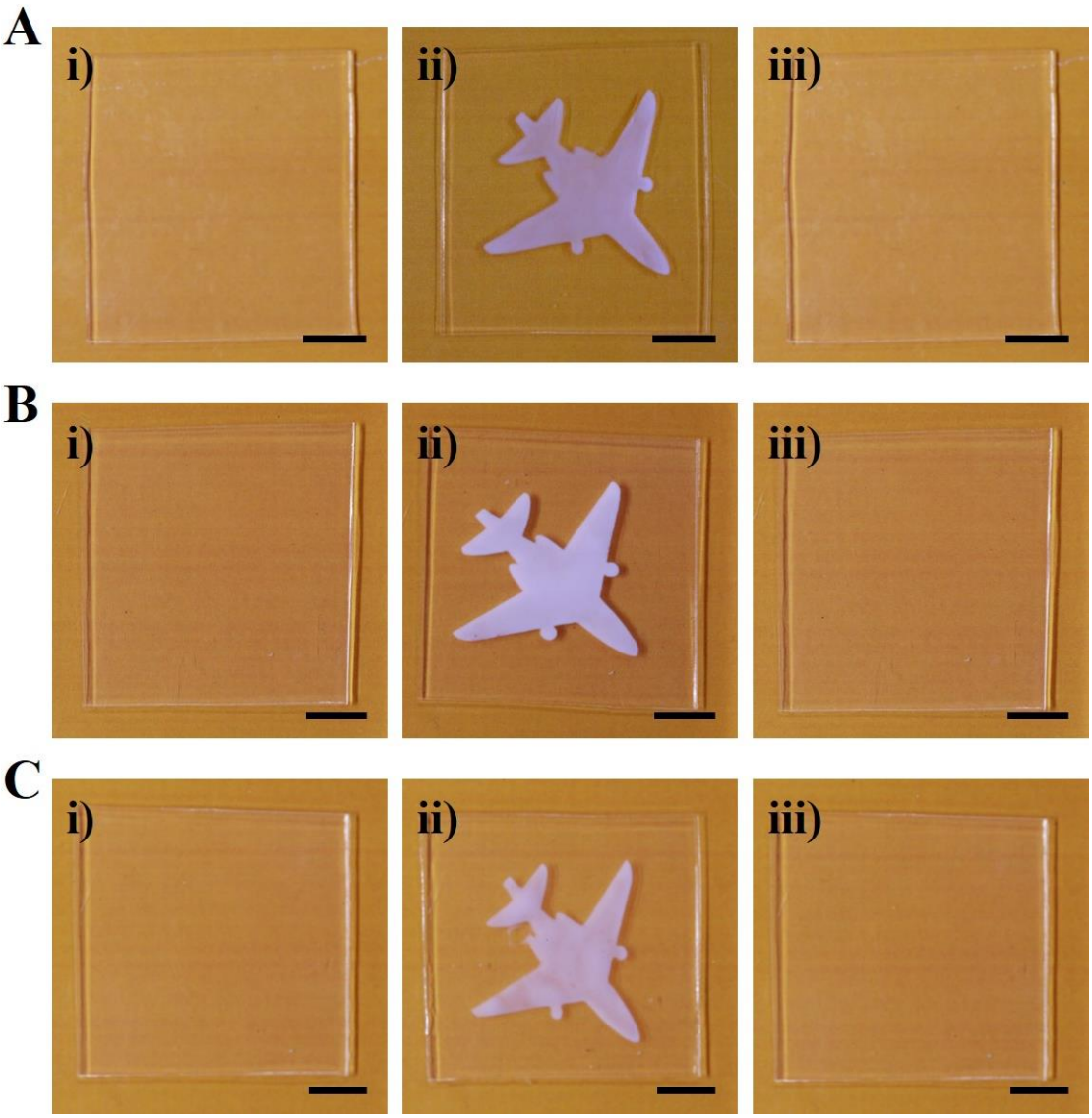

Fig. 5.5. Universality of memorizing-forgetting behavior in other hydrogels with physical interactions. **(A)** P(NaSS-*co*-MATAC) gel. **i)** The original gel at 25 °C; **ii)** the gel after the 80 °C-15 min-25 °C learning process for 1min; **iii)** forgetting in the 25 °C bath for 3 h. **(B)** P(NaSS-*co*-MPTC) gel. **i)** The original gel at 25 °C; **ii)** The gel after the 80 °C-2 h-25 °C learning process for 1min; **iii)** forgetting at the 25 °C bath for 6 h. **(C)** P(UMA-*co*-MAAc) gel. **i)** The original gel in the 25 °C bath; **ii)** the gel after the 80 °C-2 min-25 °C learning process for 1min; **iii)** forgetting in the 25 °C bath for 14.5 h. **(D)** Chemical structures of the monomers that were used to synthesize the above

hydrogels. The formulations of these hydrogels are listed in **Table 2.1**. All scale bars are 1 cm.

Charter 6-Applications in drug release, thermal imagery, and security paper

6.1 Introduction

As demonstrated above, PA gels as a new type of thermal responsive materials have many advantages. The first is the quick and asymmetric thermal response. The transparent gel turns to turbid within 4 s at cooling, but the time is nearly 30 h for the turbid gel recovering to transparent (**Fig. 3.1B**). The second is no critical temperature, and one can tune the cloudy temperature by programing thermal history (**Fig. 3.2**). The third is high sensitivity. Tiny change of temperature at cooling, for example, a temperature difference of 3 °C, can induce a remarkable transparency change of the gel (**Fig. 3.6B**). The fourth is the tiny size change. The maximum size change of the gel in this study is only 8 % compared with the original gel (**Fig. 3.6C**). The fifth is the constant mechanical performance. The turbid and transparent gels have almost the same mechanical performance (**Fig. 3.10**). These advantages endow PA gels a new type of promising thermal responsive materials. Here we give several conceptual applications of this thermal responsive behavior, such as in drug release, thermal imagery, and security paper.

6.2 Drug release

As the formation of frustrated structure can induce a slow water release process in

PA gels, we consider using this structure to prolong drug release process from the gel. To demonstrate this idea, we loaded dye molecules Rhodamine B (RB) in PA gels and compare the RB release kinetics for samples with and without thermal learning. RB has a characteristic absorbance at 554 nm in UV-*vis* spectrum (**Fig. 6.1A**), which provides an easy way to quantify the release process. Before this measurement, we made a calibration curve of UV absorption intensity at 554 nm versus RB concentration by measuring the UV spectrum of RB aqueous solutions with different concentrations (**Figs. 6.1A** and **6.1B**).

Two disk-like PA gels with 5 mm radius and 1.15 mm thickness were soaked into large amount of 10^{-4} M RB solution for 2 days to reach equilibrium. Then one gel was directly moved into the bottom of a quartz cuvette filled with 2 ml pure water, and the RB release was measured by recording the UV absorbance at 554 nm of the solution with time. While the other gel was first undergone an 80 °C-2 h-25 °C learning process in 10^{-4} M RB solution to form the frustrated structure before the RB release, and then the RB release was measured with the same experimental conditions as that of the gel without thermal learning. **Fig. 6.1C** presents the released amount of RB with time. The released amount of RB for the gel without thermal learning almost approaches the plateau at the time of 500 min. The gel with thermal learning reaches the same plateau value, while the time is prolonged to about 2700 min. This demonstrates that the RB release rate of the gel with thermal learning is significantly slower than that of the gel without thermal learning. We use a parameter, $t_{1/2}$, to quantify the release rate, where $t_{1/2}$ is the time when the released amount of RB reaches the half of the equilibrium

release value. The $t_{1/2}$ for the gels without and with thermal learning are 75 and 438 min, respectively. Therefore, through thermal learning, we can distinctly prolong the drug release process from the gel. Furthermore, it is also possible to spatially program the release rate through programing the thermal learning region of gel, as like in **Fig. 5.1**.

6.3 Thermal imagery

As shown in **Fig. 6.2A**, a PA gel is sealed into a water chamber consisting of two glasses separated by a rubber spacer; then we put a cylindrical cold source (diameter of 35 mm) with a constant temperature of 5 °C on the center of the chamber to cool the gel; after a certain time, we remove the cold source and take the optical and infrared images of the sealed sample immediately. **Fig. 6.2B** show the optical and infrared images of the gels with different contacting time, respectively. The temperature decreases along the radial direction from the center of the gel due to the heat transfer. This temperature gradient is well represented by the turbidity change of the gels from the center to the edge. Quantitative analysis shows that the temperature and the turbidity nearly have a liner relationship (**Fig. 6.2C**). This result suggests that the PA gels have a great potential in thermal imagery, where the transparency change can be directly used to reflect the temperature change.

6.4 Security paper

Another application is that the PA gel can be used as security paper for recording

temporary information. We use an ice stick as a pen (ice pen), to write information on the surface of a PA gel. The temperature difference between the ice (0 °C) and the gel (25 °C) induces obvious transparency change. Meanwhile, the contacting time between the ice and the surface of gel is very short, thus the turbid surface recovers to original appearance soon, resulting to a quick and autonomic disappearance of the recorded information (**Fig. 6.3A(i)**). For example, we write a letter "L" on the surface of the gel; after 30 s, we write another letter "S", and L almost disappears at this time; then, we write a letter "W" after waiting another 30 s, and S almost disappears; finally, W also disappears, and the PA gels turns to transparent as the original one (**Fig. 6.3A(ii)**). The recorded information also can be erased immediately after writing by wiping the surface of the gel with warm water. We quickly write a word "GEL" on the surface of PA gels, and then use a water wiper with a temperature of 40 °C. The word disappears immediately after wiping, and other information can be recorded repeatedly (**Fig. 6.3B**).

6.5 Figures and tables

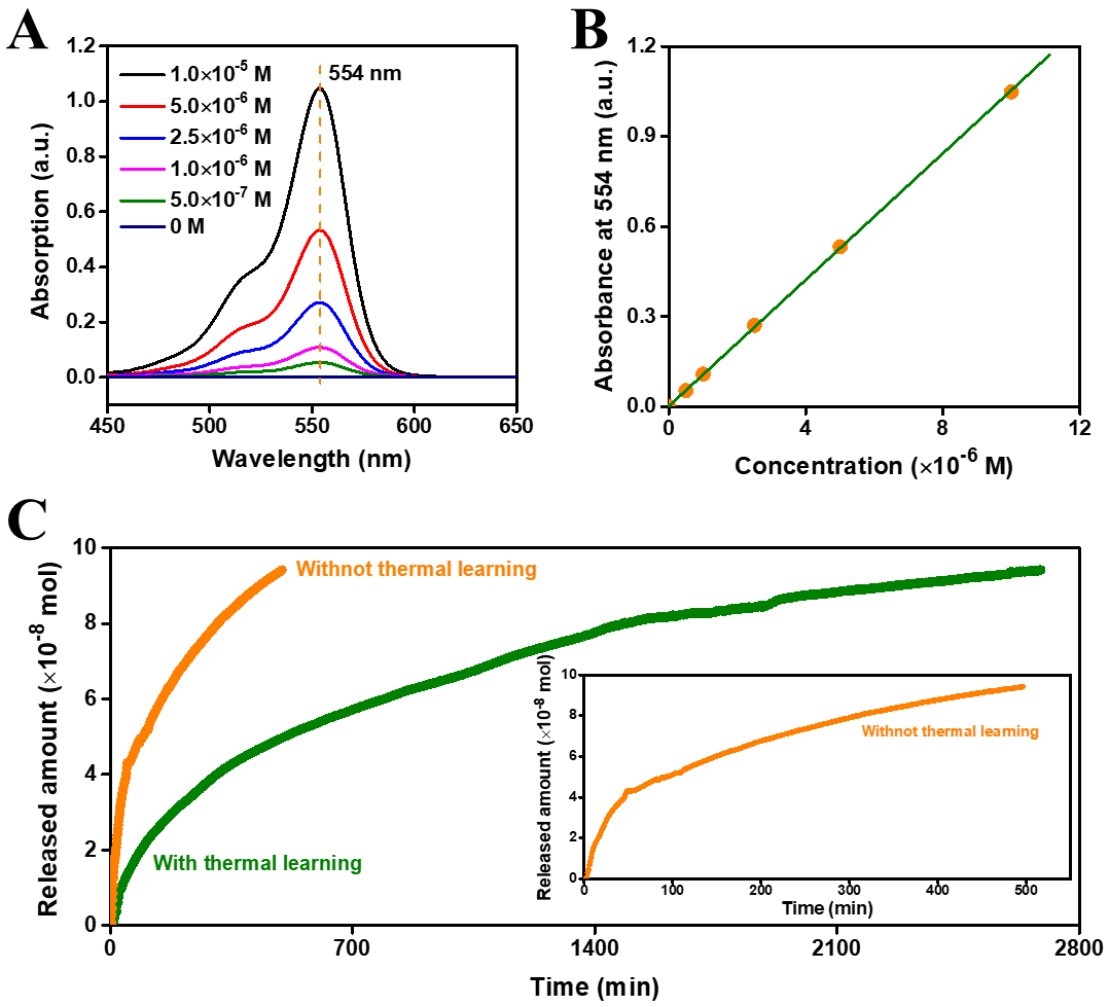

Fig. 6.1. Effect of thermal learning on the release rate of Rhodamine B (RB). **(A)** UV-*vis* absorption spectrum of RB aqueous solutions with various RB concentrations. **(B)** Calibration curve of UV absorption peak at 554 nm versus RB concentration. **(C)** Release amount of RB as a function of time for the gels with an 80 °C-2 h-25 °C learning process and without thermal learning. The inset shows the enlarged curve of the gel without thermal learning. The inset shows the enlarged curve of the gel without thermal learning.

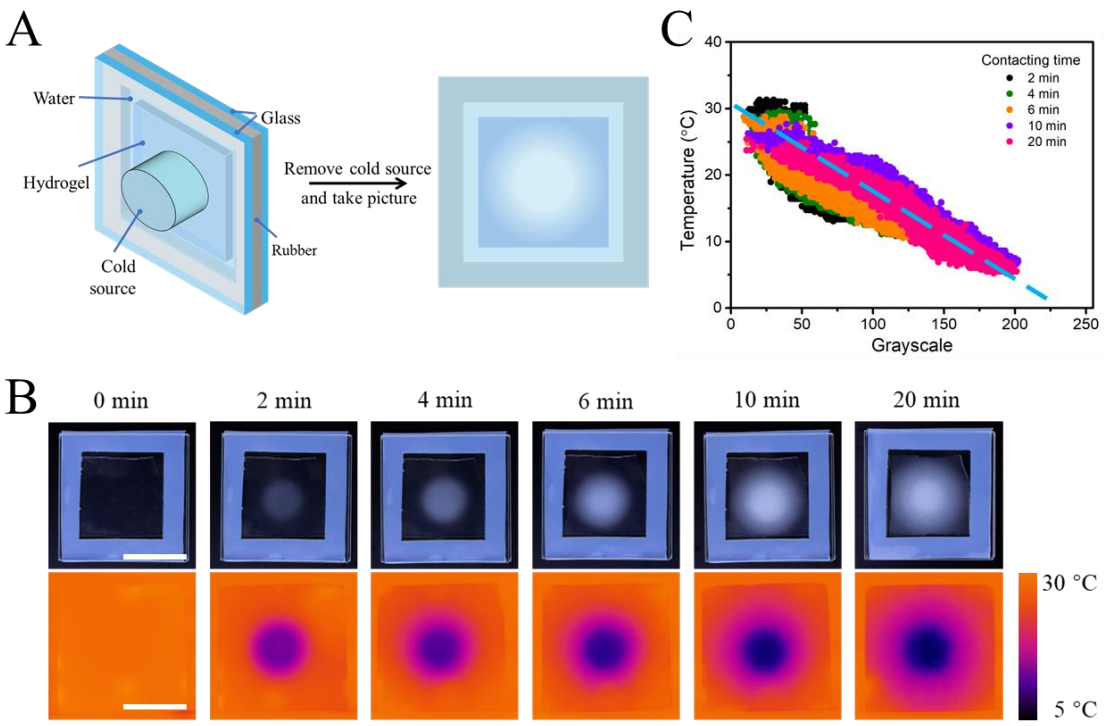

Fig. 6.2. Application of the thermal responsive behavior of PA gel in 2D thermal imagery. a) Scheme to show the experimental procedure: A PA gel with thickness of 1.2 mm, was sealed in a water chamber consisting of two transparent glasses separated by a rubber spacer; then, one surface of the sealed sample was attached with a cylindrical cold source with a diameter of 35 mm and a constant temperature of 5 °C; after contacting with a certain time, the cold source was removed and the optical and infrared images were taken immediately. b) Optical (upper) and infrared (lower) images of the sealed sample with different contacting time. The infrared images were taken by an infrared thermometer (Optris, Germany), and the working distance was approximately 25 cm. c) Relationship between the turbidity and temperature of gels with different contacting time. The turbidity is represented by the 8-bit grayscale (GS) of the optical image, where GS = 0 means “black” and GS = 255 means “white”. Scale bars, 5 cm.

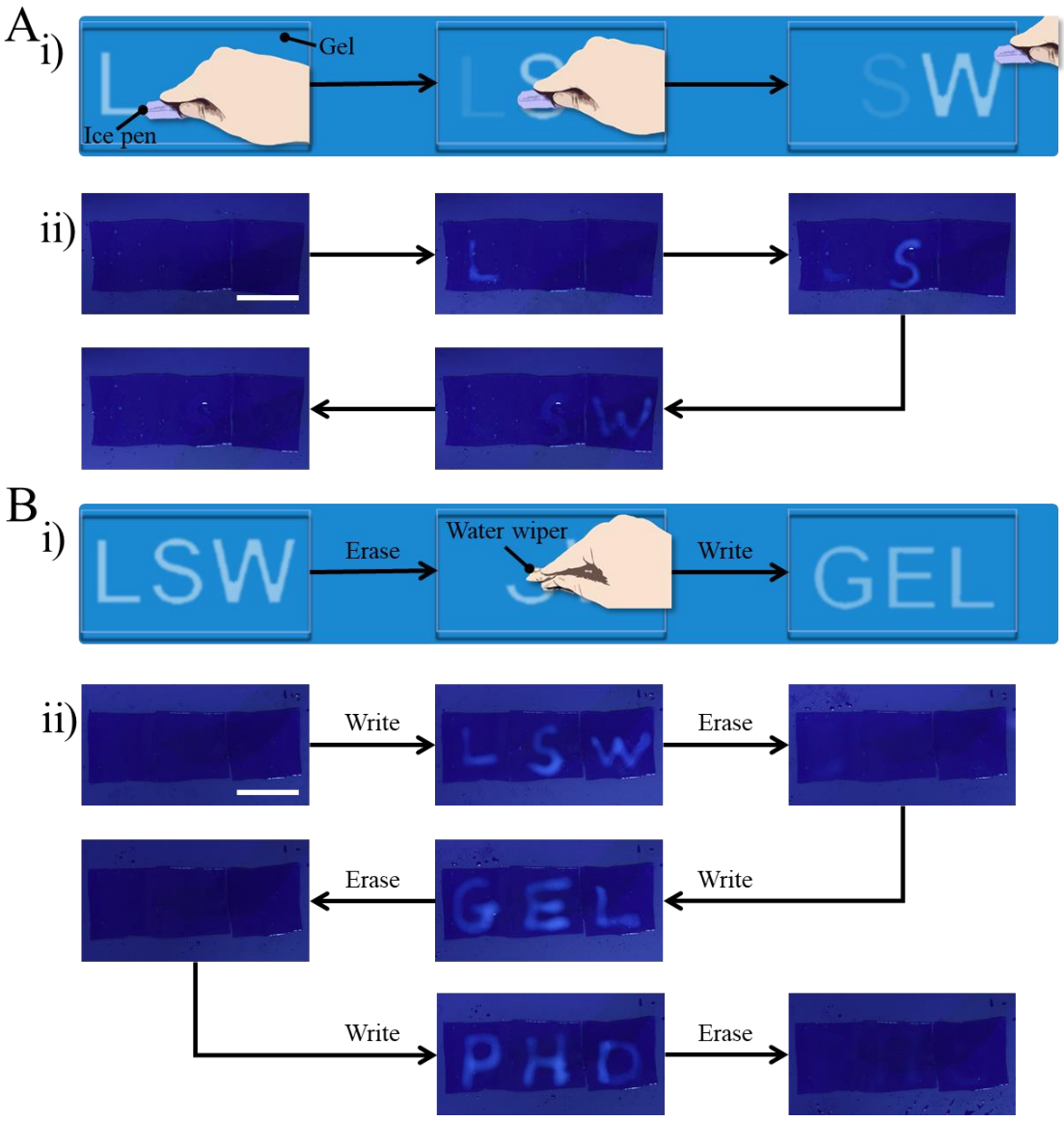

Fig. 6.3. Application of thermal responsive behavior of PA gel as security paper for recording temporary information. a) Autonomic disappearance of the recorded temporary information. i) Scheme to show the experimental procedure: An ice stick, behaving as a pen, is used to write the information on the surface of the PA gel. As the ice temperature (0 °C) is much lower than the gel temperature (around 25 °C) and the contacting time is short, the gel has obvious transparency change to record information yet the recorded information quickly decays. ii) An example to show the autonomic disappearance of the recorded information of PA gels. A letter "L" is initially written on

the surface of the gel; after 30 s, “S” is written, and L nearly disappears at this time; then, “W” is written after waiting another 30 s, and S almost disappears; finally, W also disappears, and the PA gel turns to transparent as before. b) Erasing the recorded information by a water wiper. i) Scheme to show the experimental procedure: A letter string “LSW” is written on the surface of gel continuously, and this letter string can be erased quickly by wiping the surface of gel with warm water. Consequently, the gel can be reused again. ii) An example to show the quick erasure of the recorded information and re-writing process. A letter string of LSW is written on the gel; then this letter string is erased by a water wiper with 40 °C. After that, the letter strings of “GEL” and “PHD” are recorded and erased in sequence with the same procedure. Scale bars, 5 cm.

Charter 7-Conclusion

In summary, this dissertation demonstrated a new type of thermal responsive behavior in self-healing hydrogels containing dynamic bonds (DB gels). This thermal responsive behavior originates from the structure frustration upon cooling, which is distinctly different from the temperature-induced polymer solubility change in conventional thermal responsive hydrogels. The DB gels can respond to arbitrary temperature at cooling, with negligible changes in size and mechanical performance. In addition, this new responsive behavior is universal in DB gels and independent on the specific chemistry. Furthermore, it has advantages of fast response and high sensitivity. Several conceptual applications of this behavior in intelligent display device, drug release, thermal imagery, and security paper are demonstrated. The concept of using DB gels as new thermal responsive hydrogels proposed here widely expands the applications of thermal responsive materials, especially in the field where small changes in size and mechanical performance are required. Conclusions of this dissertation are listed as follows.

In **Chapter 3**, we demonstrated that the transparency change in DB gels, such as ionic bonds and hydrogen bonds, was thermal history dependent. The cooling rate, heating temperature, and cooling temperature all influence the transparency of the gels after cooling. The transparent-to-opaque transition of the gels is fast and does not have a specific critical temperature, unlike the UCST and LCST gels. The gel with turbid appearance, induced by the formation of frustrated structure, is unstable and in

nonequilibrium state, and spontaneously occurs opaque-to-transparent transition from the surface to the center of the gel. Interestingly, even though the frustrated structure endows the opaque appearance to the gels, it makes no obvious influences on the mechanical performance.

In **Chapter 4**, the asymmetry of swelling kinetics during heating and shrinking kinetics during recovery was investigated. The cooperative diffusion coefficient for swelling is nearly 2 orders larger than that for shrinking. The formation of this obvious asymmetry is attribute to the formation of large-scale frustrated structure, not the formation of skin layer or more bound water. When the heterogeneity of this frustrated structure decreases, the asymmetry of swelling/shrinking kinetics turns to worse. Moreover, this asymmetry decreases with decreasing the ionic bond strength in PA gels, and *vice versa*. These results indicate the asymmetry is controllable by tuning the component of the gels or the strength of dynamic bonds.

In **Chapter 5**, the memorizing-forgetting behavior is achieved based on fast swelling kinetics and slow shrinking kinetics upon thermal stimulus (**Chapter 4**), as well as thermal history dependent transparency change of these gels (**Chapter 3**). More importantly, the recovery time of transparency and size is highly coupled. The gels containing dynamic bonds can memorize 2D information by thermal learning. Subsequently, the memorized information spontaneous decays, and the forgetting time is proportional to the thermal learning time, in analogy to the behavior of brain. The memory is stable against temperature fluctuation and large stretching; moreover, the forgetting process is programmable.

In **Chapter 6**, we further expand the applications of this thermal history dependent responsive behavior in DB gels, such as in drug release, thermal imagery, and security paper. The applications of using the DB gels revealed here inspire more researches on this unusual thermal responsive behavior.

We believe this thermal history dependent responsive behavior in DB gels opens an opportunity to develop intelligent device with brain-like memorizing-forgetting behavior, controllable drug release, 2D thermal imagery, and security paper for recording temporary information. This new thermal responsive behavior, distinct from that in the UCST and LCST gels, is expected to inspire further research on developing thermal responsive smart materials based on the nonequilibrium process of soft matter.

References

[1] D. Gan, T. Xu, W. Xing, X. Ge, L. Fang, K. Wang, F. Ren, X. Lu. Mussel-inspired contact-active antibacterial hydrogel with high cell affinity, toughness, and recoverability. *Adv. Funct. Mater.* 2019, **29**, 1805964.

[2] Y. Zhu, J. Zhang, J. Song, J. Yang, Z. Du, W. Zhao, H. Guo, C. Wen, Q. Li, X. Sui, L. Zhang. A multifunctional pro-healing zwitterionic hydrogel for simultaneous optical monitoring of ph and glucose in diabetic wound treatment. *Adv. Funct. Mater.* 2019, **30**, 1905493.

[3] C. Cui, T. Wu, F. Gao, C. Fan, Z. Xu, H. Wang, B. Liu, W. Liu. An autolytic high strength instant adhesive hydrogel for emergency self-rescue. *Adv. Mater.* 2018, **28**, 1804925.

[4] Y. Zhao, Z. Li, S. Song, K. Yang, H. Liu, Z. Yang, J. Wang, B. Yang, Q. Lin. Skin-inspired antibacterial conductive hydrogels for epidermal sensors and diabetic foot wound dressings. *Adv. Funct. Mater.* 2019, **29**, 1901474.

[5] Z. He, C. Wu, M. Hua, S. Wu, D. Wu, X. Zhu, J. Wang, X. He. Bioinspired multifunctional anti-icing hydrogel. *Matter* 2020, **2**, 723-734.

[6] S. Wei, W. Lu, X. Le, C. Ma, H. Lin, B. Wu, J. Zhang, P. Theato, T. Chen. Bioinspired synergistic fluorescence-color switchable polymeric hydrogel actuator. *Angew. Chem. Int. Ed.* 2019, **58**, 16243-16251.

[7] W. Huang, D. Restrepo, J.-Y. Jung, F.Y. Su, Z. Liu, R.O. Ritchie, J. McKittrick, P. Zavattieri, D. Kisailus. Multiscale toughening mechanisms in biological materials and bioinspired designs. *Adv. Mater.* 2019, **31**, 1901561.

[8] Y. Chen, J. Meng, Z. Gu, X. Wan, L. Jiang, S. Wang. Bioinspired multiscale wet adhesive surfaces: Structures and controlled adhesion. *Adv. Funct. Mater.* 2019, **30**, 1905287.

[9] J.C. Yang, J. Mun, S.Y. Kwon, S. Park, Z. Bao, S. Park. Electronic skin: Recent progress and future prospects for skin-attachable devices for health monitoring, robotics, and prosthetics. *Adv. Mater.* 2019, **31**, 1904765.

[10] B. Lu, H. Yuk, S. Lin, N. Jian, K. Qu, J. Xu, X. Zhao. Pure PEDOT:PSS hydrogels. *Nat. Commun.* 2019, **10**, 1043.

[11] C. Keplinger, J.-Y. Sun, C.C. Foo, P. Rothemund, G.M. Whitesides, Z. Suo. Stretchable, transparent, ionic conductors. *Science* 2013, **341**, 984.

[12] A. Inoue, H. Yuk, B. Lu, X. Zhao. Strong adhesion of wet conducting polymers on diverse substrates. *Sci. Adv.* 2020, **6**, 5394.

[13] S. Huang, Y. Liu, Y. Zhao, Z. Ren, C.F. Guo. Flexible electronics: Stretchable electrodes and their future. *Adv. Funct. Mater.* 2018, **29**, 1805924.

[14] H. Chen, F. Yang, Q. Chen, J. Zheng. A novel design of multi-mechanoresponsive and mechanically strong hydrogels. *Adv. Mater.* 2017, **29**, 1606900.

[15] X. Chang, Y. Geng, H. Cao, J. Zhou, Y. Tian, G. Shan, Y. Bao, Z.L. Wu, P. Pan. Dual-crosslink physical hydrogels with high toughness based on synergistic hydrogen bonding and hydrophobic interactions. *Macromol. Rapid Commun.* 2018, **39**, 1700806.

[16] X. Le, W. Lu, J. Zheng, D. Tong, N. Zhao, C. Ma, H. Xiao, J. Zhang, Y. Huang, T. Chen. Stretchable supramolecular hydrogels with triple shape memory effect. *Chem. Sci.* 2016, **7**, 6715-6720.

[17] Z. Zhao, S. Zhuo, R. Fang, L. Zhang, X. Zhou, Y. Xu, J. Zhang, Z. Dong, L. Jiang, M. Liu. Dual-programmable shape-morphing and self-healing organohydrogels through orthogonal supramolecular heteronetworks. *Adv. Mater.* 2018, **30**, 1804435.

[18] Y. Zhang, H. Gao, H. Wang, Z. Xu, X. Chen, B. Liu, Y. Shi, Y. Lu, L. Wen, Y. Li, Z. Li, Y. Men, X. Feng, W. Liu. Radiopaque highly stiff and tough shape memory hydrogel microcoils for permanent embolization of arteries. *Adv. Funct. Mater.* 2018, **28**, 1705962.

[19] Z.J. Wang, C.N. Zhu, W. Hong, Z.L. Wu, Q. Zheng. Cooperative deformations of periodically patterned hydrogels. *Sci. Adv.* 2017, **3**, 1700348.

[20] Z.J. Wang, W. Hong, Z. Wu, Q. Zheng. Site-specific pre-swelling-directed morphing structures of patterned hydrogels. *Angew. Chem. Int. Ed.* 2017, **56**, 15974-15978.

[21] D. Chen, Y. Zhang, C. Ni, C. Ma, J. Yin, H. Bai, Y. Luo, F. Huang, T. Xie, Q. Zhao. Drilling by light: Ice-templated photo-patterning enabled by a dynamically crosslinked

hydrogel. *Mater. Horiz.* 2019, **6**, 1013-1019.

[22] L. Hua, M. Xie, Y. Jian, B. Wu, C. Chen, C. Zhao. Multiple-responsive and amphibious hydrogel actuator based on asymmetric UCST-type volume phase transition. *ACS Appl. Mater. Interfaces* 2019, **11**, 43641-43648.

[23] W. Lu, X. Le, J. Zhang, Y. Huang, T. Chen. Supramolecular shape memory hydrogels: A new bridge between stimuli-responsive polymers and supramolecular chemistry. *Chem. Soc. Rev.* 2017, **46**, 1284-1294.

[24] S.-k. Ahn, R.M. Kasi, S.-C. Kim, N. Sharma, Y. Zhou. Stimuli-responsive polymer gels. *Soft Matter* 2008, **4**, 1151-1157.

[25] M.A. Haq, Y. Su, D. Wang. Mechanical properties of PNIPAM based hydrogels: A review. *Mater. Sci. Eng. C* 2017, **70**, 842-855.

[26] Z. Hu, Y. Chen, C. Wang, Y. Zheng, Y. Li. Polymer gels with engineered environmentally responsive surface patterns. *Nature* 1998, **393**, 149-152.

[27] P. Muthiah, S.M. Hoppe, T.J. Boyle, W. Sigmund. Thermally tunable surface wettability of electrospun fiber mats: Polystyrene/poly (N - isopropylacrylamide) blended versus crosslinked poly [(*N* - isopropylacrylamide) - *co* - (methacrylic acid)]. *Macromol. Rapid Commun.* 2011, **32**, 1716-1721.

[28] Y. Oni, W. Soboyejo. Swelling and diffusion of PNIPA-based gels for localized chemotherapy and hyperthermia. *Mater. Sci. Eng. C* 2012, **32**, 24-30.

[29] H.N. Kim, S. Yang. Responsive smart windows from nanoparticle–polymer composites. *Adv. Funct. Mater.* 2019, **30**, 1902597.

[30] D. Roy, W.L.A. Brooks, B.S. Sumerlin. New directions in thermoresponsive polymers. *Chem. Soc. Rev.* 2013, **42**, 7214-7243.

[31] O. Erol, A. Pantula, W. Liu, D.H. Gracias. Transformer hydrogels: A review. *Adv. Mater. Technol.* 2019, **4**, 1900043.

[32] A. Asadujjaman, B. Kent, A. Bertin. Phase transition and aggregation behaviour of an UCST-type copolymer poly(acrylamide-*co*-acrylonitrile) in water: effect of acrylonitrile content, concentration in solution, copolymer chain length and presence of electrolyte. *Soft Matter* 2017, **13**, 658-669.

[33] J. Seuring, S. Agarwal. Polymers with upper critical solution temperature in aqueous solution. *Macomol. Rapid Commun.* 2012, **33**, 1898-1920.

[34] W. Fu, B. Zhao. Thermoreversible physically crosslinked hydrogels from UCST-type thermosensitive ABA linear triblock copolymers. *Polym. Chem.* 2016, **7**, 6980-6991.

[35] H. Ye, C. Owh, X.J. Loh. A thixotropic polyglycerol sebacate-based supramolecular hydrogel showing UCST behavior. *RSC Adv.* 2015, **5**, 48720-48728.

[36] M. Xia, Y. Cheng, Z. Meng, X. Jiang, Z. Chen, P. Theato, M. Zhu. A novel nanocomposite hydrogel with precisely tunable UCST and LCST. *Macromol. Rapid*

Commun. 2015, **36**, 477-482.

[37] F. Liu, S. Jiang, L. Ionov, S. Agarwal. Thermophilic films and fibers from photo cross-linkable UCST-type polymers. *Polym. Chem.* 2015, **6**, 2769-2776.

[38] Y. Xu, O. Ghag, M. Reimann, P. Sitterle, P. Chatterjee, E. Nofen, H. Yu, H. Jiang, L.L. Dai. Development of visible-light responsive and mechanically enhanced "smart" UCST interpenetrating network hydrogels. *Soft Matter* 2017, **14**, 151-160.

[39] N. Shimada, S. Kidoaki, A. Maruyama. Smart hydrogels exhibiting UCST-type volume changes under physiologically relevant conditions. *RSC Adv.* 2014, **4**, 52346-52348.

[40] H. Katono, K. Sanui, N. Ogata, T. Okano, Y. Sakurai. Thermo-responsive swelling and drug release switching of interpenetrating polymer networks composed of poly(acrylamide-*co*-butyl methacrylate) and poly (acrylic acid). *J. Control. Release* 1991, **16**, 215-228.

[41] C. Echeverria, D. López, C. Mijangos. Ucst responsive microgels of poly(acrylamide−acrylic acid) copolymers: Structure and viscoelastic properties. *Macromolecules* 2009, **42**, 9118-9123.

[42] T.L. Sun, T. Kurokawa, S. Kuroda, A.B. Ihsan, T. Akasaki, K. Sato, M.A. Haque, T. Nakajima, J.P. Gong. Physical hydrogels composed of polyampholytes demonstrate high toughness and viscoelasticity. *Nat. Mater.* 2013, **12**, 932-937.

[43] J.-Y. Sun, X. Zhao, W.R.K. Illeperuma, O. Chaudhuri, K.H. Oh, D.J. Mooney, J.J. Vlassak, Z. Suo. Highly stretchable and tough hydrogels. *Nature* 2012, **489**, 133-136.

[44] X. Dai, Y. Zhang, L. Gao, T. Bai, W. Wang, Y. Cui, W. Liu. A mechanically strong, highly stable, thermoplastic, and self-healable supramolecular polymer hydrogel. *Adv. Mater.* 2015, **27**, 3566-3571.

[45] W. Wang, Y. Zhang, W. Liu. Bioinspired fabrication of high strength hydrogels from non-covalentinteractions. *Prog. Polym. Sci.* 2017, **71**, 1-25.

[46] D.L. Taylor, M. in het Panhuis. Self-healing hydrogels. *Adv. Mater.* 2016, **28**, 9060-9093.

[47] Z. Wei, J.H. Yang, J. Zhou, F. Xu, M. Zrínyi, P.H. Dussault, Y. Osada, Y.M. Chen. Self-healing gels based on constitutional dynamic chemistry and their potential applications. *Chem. Soc. Rev.* 2014, **43**, 8114-8131.

[48] Q. Zhou, X. Dong, Y. Xiong, B. Zhang, S. Lu, Q. Wang, Y. Liao, Y. Yang, H. Wang. Multi-responsive lanthanide-based hydrogel with encryption, naked eye sensing, shape memory, self-healing, and antibacterial activity. *ACS Appl. Mater. Interfaces* 2020, **12**, 28539-28549.

[49] Z. Zhang, L. Wang, H. Yu, F. Zhang, L. Tang, Y. Feng, W. Feng. Highly transparent, self-healable, and adhesive organogels for bio-inspired intelligent ionic skins. *ACS Appl. Mater. Interfaces* 2020, **12**, 15657-15666.

[50] P. Wei, T. Chen, G. Chen, H. Liu, I.T. Mugaanire, K. Hou, M. Zhu. Conductive self-healing nanocomposite hydrogel skin sensors with antifreezing and thermoresponsive properties. *ACS Appl. Mater. Interfaces* 2020, **12**, 3068-3079.

[51] X. Su, H. Wang, Z. Tian, X. Duan, Z. Chai, Y. Feng, Y. Wang, Y. Fan, J. Huang. A solvent co-cross-linked organogel with fast self-healing capability and reversible adhesiveness at extreme temperatures. *ACS Appl. Mater. Interfaces* 2020, **12**, 29757-29766.

[52] S. Park, B.-G. Shin, S. Jang, K. Chung. Three-dimensional self-healable touch sensing artificial skin device. *ACS Appl. Mater. Interfaces* 2020, **12**, 3953-3960.

[53] Y. Li, X. Li, S. Zhang, L. Liu, N. Hamad, S.R. Bobbara, D. Pasini, F. Cicoira. Autonomic self-healing of PEDOT:PSS achieved via polyethylene glycol addition. *Adv. Funct. Mater.* 2020, **30**, 2002853.

[54] B. Fan, K. Zhang, Q. Liu, R. Eelkema. Self-Healing Injectable Polymer Hydrogel via Dynamic Thiol-Alkynone Double Addition Cross-Links. *ACS Macro Lett.* 2020, **9**, 776-780.

[55] X. Ding, G. Li, P. Zhang, C. Xiao. Constructing Thermally Reversible Dynamic Hydrogels via Catalysis-Free Knoevenagel Condensation. *ACS Macro Lett.* 2020, **9**, 830-835.

[56] L. Zhang, Z. Liu, X. Wu, Q. Guan, S. Chen, L. Sun, Y. Guo, S. Wang, J. Song, E.M. Jeffries, C. He, F.-L. Qing, X. Bao, Z. You. A highly efficient self-healing elastomer

with unprecedented mechanical properties. *Adv. Mater.* 2019, **31**, 1901402.

[57] Y.J. Wang, X.N. Zhang, Y. Song, Y. Zhao, L. Chen, F. Su, L. Li, Z.L. Wu, Q. Zheng. Ultrastiff and tough supramolecular hydrogels with a dense and robust hydrogen bond network. *Chem. Mater.* 2019, **31**, 1430-1440.

[58] H. Tan, Q. Lyu, Z. Xie, M. Li, K. Wang, K. Wang, B. Xiong, L. Zhang, J. Zhu. Metallosupramolecular photonic elastomers with self-healing capability and angle-independent color. *Adv. Mater.* 2019, **31**, 1805496.

[59] C. Shao, L. Meng, M. Wang, C. Cui, B. Wang, C.-R. Han, F. Xu, J. Yang. Mimicking dynamic adhesiveness and strain-stiffening behavior of biological tissues in tough and self-healable cellulose nanocomposite hydrogels. *ACS Appl. Mater. Interfaces* 2019, **11**, 5885-5895.

[60] H. Liao, X. Guo, P. Wan, G. Yu. Conductive MXene nanocomposite organohydrogel for flexible, healable, low-temperature tolerant strain sensors. *Adv. Funct. Mater.* 2019, **29**, 1904507.

[61] C.H. Li, J.L. Zuo. Self-Healing Polymers Based on Coordination Bonds. *Adv Mater* 2019, e1903762.

[62] Z. Jiang, B. Diggle, I.C.G. Shackleford, L.A. Connal. Tough, self-healing hydrogels capable of ultrafast shape changing. *Adv. Mater.* 2019, **31**, 1904956.

[63] J.-B. Hou, X.-Q. Zhang, D. Wu, J.-F. Feng, D. Ke, B.-J. Li, S. Zhang. Tough self-

healing elastomers based on the host-guest interaction of polycyclodextrin. *ACS Appl. Mater. Interfaces* 2019, **11**, 12105-12113.

[64] R. Du, Z. Xu, C. Zhu, Y. Jiang, H. Yan, H.-C. Wu, O. Vardoulis, Y. Cai, X. Zhu, Z. Bao, Q. Zhang, X. Jia. A highly stretchable and self-healing supramolecular elastomer based on sliding crosslinks and hydrogen bonds. *Adv. Funct. Mater.* 2019, **30**, 1907139.

[65] C. Dang, M. Wang, J. Yu, Y. Chen, S. Zhou, X. Feng, D. Liu, H. Qi. Transparent, highly stretchable, rehealable, sensing, and fully recyclable ionic conductors fabricated by one-step polymerization based on a small biological molecule. *Adv. Funct. Mater.* 2019, **29**, 1902467.

[66] Y. Chen, W. Wang, D. Wu, H. Zeng, D.G. Hall, R. Narain. Multiresponsive and self-healing hydrogel via formation of polymer-nanogel interfacial dynamic benzoxaborole esters at physiological pH. *ACS Appl. Mater. Interfaces* 2019, **11**, 44742-44750.

[67] L. Chen, T.L. Sun, K. Cui, D.R. King, Y. Saruwatari, J.P. Gong. Facile synthesis of novel elastomers with tunable dynamics for toughness, self-healing and adhesion. *J. Mater. Chem. A* 2019, **7**, 17334-17344.

[68] N. An, X. Wang, Y. Li, L. Zhang, Z. Lu, J. Sun. Healable and mechanically super-strong polymeric composites derived from hydrogen-bonded polymeric complexes. *Adv. Mater.* 2019, **31**, 1904882.

[69] R. Zheng, Y. Wang, C. Jia, Z. Wan, J. Luo, H.A. Malik, X. Weng, J. Xie, L. Deng.

Intelligent biomimetic chameleon skin with excellent self-healing and electrochromic properties. *ACS Appl. Mater. Interfaces* 2018, **10**, 35533-35538.

[70] Y.N. Ye, M. Frauenlob, L. Wang, M. Tsuda, T.L. Sun, K. Cui, R. Takahashi, H.J. Zhang, T. Nakajima, T. Nonoyama, T. Kurokawa, S. Tanaka, J.P. Gong. Tough and self-recoverable thin hydrogel membranes for biological applications. *Adv. Funct. Mater.* 2018, **28**, 1801489.

[71] L. Wang, F. Deng, W. Wang, A. Li, C. Lu, H. Chen, G. Wu, K. Nan, L. Li. Construction of injectable self-healing macroporous hydrogels via a template-free method for tissue engineering and drug delivery. *ACS Appl. Mater. Interfaces* 2018, **10**, 36721-36732.

[72] M.W. Urban, D. Davydovich, Y. Yang, T. Demir, Y. Zhang, L. Casabianca. Key-and-lock commodity self-healing copolymers. *Science* 2018, **362**, 220-225.

[73] M.E. Smithmyer, C.C. Deng, S.E. Cassel, P.J. LeValley, B.S. Sumerlin, A.M. Kloxin. Self-healing boronic acid-based hydrogels for 3D co-cultures. *ACS Macro Lett.* 2018, **7**, 1105-1110.

[74] A. Sinclair, M.B. O'Kelly, T. Bai, H.-C. Hung, P. Jain, S. Jiang. Self-healing zwitterionic microgels as a versatile platform for malleable cell constructs and injectable therapies. *Adv. Mater.* 2018, **30**, 1803087.

[75] Y. Shi, Y. Zhang, L. Jia, Q. Zhang, X. Xu. Stretchable and self-healing integrated all-gel-state supercapacitors enabled by a notch-insensitive supramolecular hydrogel

electrolyte. *ACS Appl. Mater. Interfaces* 2018, **10**, 36028-36036.

[76] T. Long, Y. Li, X. Fang, J. Sun. Salt-mediated polyampholyte hydrogels with high mechanical strength, excellent self-healing property, and satisfactory electrical conductivity. *Adv. Funct. Mater.* 2018, **28**, 1804416.

[77] S. Liu, W. Guo. Anti-biofouling and healable materials: Preparation, mechanisms, and biomedical applications. *Adv. Funct. Mater.* 2018, **28**, 1800596.

[78] Q. Li, Y.-W. Zhang, C.-F. Wang, D.A. Weitz, S. Chen. Versatile hydrogel ensembles with macroscopic multidimensions. *Adv. Mater.* 2018, **30**, e1803475.

[79] S.-Y. Kwak, J.P. Giraldo, T.T.S. Lew, M.H. Wong, P. Liu, Y.J. Yang, V.B. Koman, M.K. McGee, B.D. Olsen, M.S. Strano. Polymethacrylamide and carbon composites that grow, strengthen, and self-repair using ambient carbon dioxide fixation. *Adv. Mater.* 2018, **30**, 1804037.

[80] X. He, L. Liu, H. Han, W. Shi, W. Yang, X. Lu. Bioinspired and microgel-tackified adhesive hydrogel with rapid self-healing and high stretchability. *Macromolecules* 2018, **52**, 72-80.

[81] Y. Deng, M. Huang, D. Sun, Y. Hou, Y. Li, T. Dong, X. Wang, L. Zhang, W. Yang. Dual physically cross-linked *κ*-carrageenan-based double network hydrogels with superior self-healing performance for biomedical application. *ACS Appl. Mater. Interfaces* 2018, **10**, 37544-37554.

[82] M. Cui, N.A. Nguyen, P.V. Bonnesen, D. Uhrig, J.K. Keum, A.K. Naskar. Rigid oligomer from lignin in designing of tough, self-healing elastomers. *ACS Macro Lett.* 2018, **7**, 1328-1332.

[83] Y. Cao, H. Wu, S.I. Allec, B.M. Wong, D.-S. Nguyen, C. Wang. A highly stretchy, transparent elastomer with the capability to automatically self-heal underwater. *Adv. Mater.* 2018, **30**, 1804602.

[84] Y.S. Zhang, A. Khademhosseini. Advances in engineering hydrogels. *Science* 2017, **356**, 500.

[85] J. Wu, L.-H. Cai, D.A. Weitz. Tough self-healing elastomers by molecular enforced integration of covalent and reversible networks. *Adv Mater* 2017, **29**, 1702616.

[86] Q. Rong, W. Lei, L. Chen, Y. Yin, J. Zhou, M. Liu. Anti-freezing, conductive self-healing organohydrogels with stable strain-sensitivity at subzero temperatures. *Angew. Chem. Int. Ed.* 2017, **56**, 14159-14163.

[87] H.J. Zhang, T.L. Sun, A.K. Zhang, Y. Ikura, T. Nakajima, T. Nonoyama, T. Kurokawa, O. Ito, H. Ishitobi, J.P. Gong. Tough physical double-network hydrogels based on amphiphilic triblock copolymers. *Adv. Mater.* 2016, **28**, 4884-4890.

[88] C.-H. Li, C. Wang, C. Keplinger, J.-L. Zuo, L. Jin, Y. Sun, P. Zheng, Y. iCao, F. Lissel, C. Linder, X.-Z. You, Z. Bao. A highly stretchable autonomous self-healing elastomer. *Nat. Chem.* 2016, **8**, 618-624.

[89] I. Jeon, J. Cui, W.R.K. Illeperuma, J. Aizenberg, J.J. Vlassak. Extremely stretchable and fast self-healing hydrogels. *Adv. Mater.* 2016, **28**, 4678-4683.

[90] A.B. Ihsan, T.L. Sun, T. Kurokawa, S.N. Karobi, T. Nakajima, T. Nonoyama, C.K. Roy, F. Luo, J.P. Gong. Self-healing behaviors of tough polyampholyte hydrogels. *Macromolecules* 2016, **49**, 4245-4252.

[91] C. Bilici, V. Can, U. Nöchel, M. Behl, A. Lendlein, O. Okay. Melt-processable shape-memory hydrogels with self-healing ability of high mechanical strength. *Macromolecules* 2016, **49**, 7442-7449.

[92] D. Wang, J. Guo, H. Zhang, B. Cheng, H. Shen, N. Zhao, J. Xu. Intelligent rubber with tailored properties for selfhealing and shape memory. *J. Mater. Chem. A* 2015, **3**, 12864-12872.

[93] F. Luo, T.L. Sun, T. Nakajima, T. Kurokawa, Y. Zhao, K. Sato, A.B. Ihsan, X. Li, H. Guo, J.P. Gong. Oppositely charged polyelectrolytes form tough, self-healing, and rebuildable hydrogels. *Adv. Mater.* 2015, **27**, 2722-2727.

[94] Z. Wang, W. Fan, R. Tong, X. Lu, H. Xia. Thermal-healable and shape memory metallosupramolecular poly(*n*-butyl acrylate-*co*-methyl methacrylate) materials. *RSC Adv.* 2014, **4**, 25486-25493.

[95] K. Cui, T.L. Sun, X. Liang, K. Nakajima, Y.N. Ye, L. Chen, T. Kurokawa, J.P. Gong. Multiscale energy dissipation mechanism in tough and self-healing hydrogels. *Phys. Rev. Lett.* 2018, **121**, 185501.

[96] K. Cui, Y.N. Ye, T.L. Sun, L. Chen, X. Li, T. Kurokawa, T. Nakajima, T. Nonoyama, J.P. Gong. Effect of structure heterogeneity on mechanical performance of physical polyampholytes hydrogels. *Macromolecules* 2019, **52**, 7369-7378.

[97] K. Cui, Y.N. Ye, T.L. Sun, C. Yu, X. Li, T. Kurokawa, J.P. Gong. Phase separation behavior in tough and self-healing polyampholyte hydrogels. *Macromolecules* 2020, **53**, 5116-5126.

[98] X. Li, K. Cui, T.L. Sun, L. Meng, C. Yu, L. Li, C. Creton, T. Kurokawa, J.P. Gong. Mesoscale bicontinuous networks in self-healing hydrogels delay fatigue fracture. *Proc. Natl. Acad. Sci. U. S. A.* 2020, **117**, 7606-7612.

[99] A.B. Ihsan, T.L. Sun, S. Kuroda, M.A. Haque, T. Kurokawa, T. Nakajima, J.P. Gong. A phase diagram of neutral polyampholyte–from solution to tough hydrogel. *J. Mater. Chem. B* 2013, **1**, 4555-4562.

[100] R. Takahashi, T.L. Sun, Y. Saruwatari, T. Kurokawa, D.R. King, J.P. Gong. Creating stiff, tough, and functional hydrogel composites with low-melting-point alloys. *Adv. Mater.* 2018, **30**, 1706885.

[101] Y. Song, W. Wei, X. Qu. Colorimetric biosensing using smart materials. *Adv. Mater.* 2011, **23**, 4215-4236.

[102] X. Yu, H. Cheng, M. Zhang, Y. Zhao, L. Qu, G. Shi. Graphene-based smart materials. *Nat. Rev. Mater.* 2017, **2**, 1-13.

[103] B.R. Donovan, V.M. Matavulj, S.-k. Ahn, T. Guin, T.J. White. All-optical control of shape. *Adv. Mater.* 2019, **31**, 1805750.

[104] Q. Zhao, X. Yang, C. Ma, D. Chen, H. Bai, T. Li, W. Yang, T. Xie. A bioinspired reversible snapping hydrogel assembly. *Mater. Horiz.* 2016, **3**, 422-428.

[105] C.-H. Zhu, Y. Lu, J. Peng, J.-F. Chen, S.-H. Yu. Photothermally sensitive poly(N-isopropylacrylamide)/graphene oxide nanocomposite hydrogels as remote light-controlled liquid microvalves. *Adv. Funct. Mater.* 2012, **22**, 4017-4022.

[106] Y.S. Kim, M. Liu, Y. Ishida, Y. Ebina, M. Osada, T. Sasaki, T. Hikima, M. Takata, T. Aida. Thermoresponsive actuation enabled by permittivity switching in an electrostatically anisotropic hydrogel. *Nat. Mater.* 2015, **14**, 1002-1007.

[107] X. Kuang, D.J. Roach, J. Wu, C.M. Hamel, Z. Ding, T. Wang, M.L. Dunn, H.J. Qi. Advances in 4D printing: Materials and applications. *Adv. Funct. Mater.* 2019, **29**, 1805290.

[108] K. Liu, Y. Zhang, H. Cao, H. Liu, Y. Geng, W. Yuan, J. Zhou, Z.L. Wu, G. Shan, Y. Bao, Q. Zhao, T. Xie, P. Pan. Programmable reversible shape transformation of hydrogels based on transient structural anisotropy. *Adv. Mater.* 2020, **32**, 2001693.

[109] P. Bertsch, L. Schneider, G. Bovone, M.W. Tibbitt, P. Fischer, S. Gstöhl. Injectable biocompatible hydrogels from cellulose nanocrystals for locally targeted sustained drug release. *ACS Appl. Mater. Interfaces* 2019, **11**, 38578-38585.

[110] P. Gupta, K. Vermani, S. Garg. Hydrogels: From controlled release to pH-responsive drug delivery. *Drug discov. today* 2002, **7**, 569-579.

[111] A. Kikuchi, T. Okano. Pulsatile drug release control using hydrogels. *Adv. Drug Deliv. Rev.* 2002, **54**, 53-77.

[112] Y. Ke, C. Zhou, Y. Zhou, S. Wang, S.H. Chan, Y. Long. Emerging thermal-responsive materials and integrated techniques targeting the energy-efficient smart window application. *Adv. Funct. Mater.* 2018, **28**, 1800113.

[113] T.G. La, X. Li, A. Kumar, Y. Fu, S. Yang, H.J. Chung. Highly flexible, multipixelated thermosensitive smart windows made of tough hydrogels. *ACS Appl. Mater. Interfaces* 2017, **9**, 33100-33106.

[114] Y. Hou, A.R. Matthews, A.M. Smitherman, A.S. Bulick, M.S. Hahn, H. Hou, A. Han, M.A. Grunlan. Thermoresponsive nanocomposite hydrogels with cell-releasing behavior. *Biomaterials* 2008, **29**, 3175-3184.

[115] A. Sidorenko, T. Krupenkin, J. Aizenberg. Controlled switching of the wetting behavior of biomimetic surfaces with hydrogel-supported nanostructures. *J. Mater. Chem.* 2008, **18**, 3841-3846.

[116] L. Chen, M. Liu, L. Lin, T. Zhang, J. Ma, Y. Song, L. Jiang. Thermal-responsive hydrogel surface: tunable wettability and adhesion to oil at the water/solid interface. *Soft Matter* 2010, **6**, 2708-2712.

[117] F. Zhao, X. Zhou, Y. Liu, Y. Shi, Y. Dai, G. Yu. Super moisture-absorbent gels for all-weather atmospheric water harvesting. *Adv. Mater.* 2019, **31**, 1806446.

[118] G.-F. Luo, W.-H. Chen, X.-Z. Zhang. 100th Anniversary of Macromolecular Science Viewpoint: Poly(N-isopropylacrylamide)-Based Thermally Responsive Micelles. *ACS Macro Lett.* 2020, **9**, 872-881.

[119] X. Chang, H. Mao, G. Shan, Y. Bao, P. Pan. Tuning the thermoresponsivity of amphiphilic copolymers via stereocomplex crystallization of hydrophobic blocks. *ACS Macro Lett.* 2019, **8**, 357-362.

[120] M. Dompé, F.J. Cedano-Serrano, O. Heckert, N. van den Heuvel, J. van der Gucht, Y. Tran, D. Hourdet, C. Creton, M. Kamperman. Thermoresponsive complex coacervate-based underwater adhesive. *Adv. Mater.* 2019, **31**, 1808179.

[121] H. Guo, N. Sanson, D. Hourdet, A. Marcellan. Thermoresponsive toughening with crack bifurcation in phase-separated hydrogels under isochoric conditions. *Adv. Mater.* 2016, **28**, 5857-5864.

[122] J. Seuring, S. Agarwal. Non-ionic homo- and copolymers with H-donor and H-acceptor units with an UCST in water. *Macromol. Chem. Phys.* 2010, **211**, 2109-2117.

[123] Z. Ye, S. Sun, P. Wu. Distinct cation–anion interactions in the UCST and LCST behavior of polyelectrolyte complex aqueous solutions. *ACS Macro Lett.* 2020, **9**, 974-979.

[124] M.I. Gibson, D. Paripovic, H.A. Klok. Size-Dependent LCST Transitions of Polymer-Coated Gold Nanoparticles: Cooperative Aggregation and Surface Assembly. *Adv. Mater.* 2010, **22**, 4721-4725.

[125] X.-Z. Zhang, J.-T. Zhang, R.-X. Zhuo, C.-C. Chu. Synthesis and properties of thermosensitive, crown ether incorporated poly (N-isopropylacrylamide) hydrogel. *Polymer* 2002, **43**, 4823-4827.

[126] Q. Yan, A.S. Hoffman. Synthesis of macroporous hydrogels with rapid swelling and deswelling properties for delivery of macromolecules. *Polymer* 1995, **36**, 887-889.

[127] K. Mayumi, J. Guo, T. Narita, C.Y. Hui, C. Creton. Fracture of dual crosslink gels with permanent and transient crosslinks. *Extreme Mech. Lett.* 2016, **6**, 52-59.

[128] R. Long, C.-Y. Hui. Fracture toughness of hydrogels: Measurement and interpretation. *Soft Matter* 2016, **12**, 8069-8086.

[129] J. Seuring, S. Agarwal. First example of a universal and cost-effective approach: Polymers with tunable upper critical solution temperature in water and electrolyte solution. *Macromolecules* 2012, **45**, 3910-3918.

[130] T.L. Sun, F. Luo, T. Kurokawa, S.N. Karobi, T. Nakajima, J.P. Gong. Molecular structure of self-healing polyampholyte hydrogels analyzed from tensile behaviors. *Soft Matter* 2015, **11**, 9355-9366.

[131] H. Itagaki, T. Kurokawa, H. Furukawa, T. Nakajima, Y. Katsumoto, J.P. Gong.

Water-induced brittle-ductile transition of double network hydrogels. *Macromolecules* 2010, **43**, 9495-9500.

[132] H. Tajima, Y. Yoshida, K. Yamagiwa. Experimental study of swelling and shrinking kinetics of spherical poly(*N*,*N*-diethylacrylamide) gel with continuous phase transition. *Polymer* 2011, **52**, 732-738.

[133] M. Zrinyi, J. Rosta, F. Horkay. Studies on the swelling and shrinking kinetics of chemically crosslinked disk-shaped poly (vinyl acetate) gels. *Macromolecules* 1993, **26**, 3097-3102.

[134] T. Tanaka, L.O. Hocker, G.B. Benedek. Spectrum of light scattered from a viscoelastic gel. *J. Chem. Phys.* 1973, **59**, 5151-5159.

[135] A. Peters, S.J. Candau. Kinetics of swelling of spherical and cylindrical gels. *Macromolecules* 1988, **21**, 2278-2282.

[136] M. Rubinstein, R.H. Colby. Polymer physics. Oxford university press, New York, 2003.

[137] T. Tanaka, D.J. Fillmore. Kinetics of swelling of gels. *J. Chem. Phys.* 1979, **70**, 1214-1218.

[138] C.K. Roy, H.L. Guo, T.L. Sun, A.B. Ihsan, T. Kurokawa, M. Takahata, T. Nonoyama, T. Nakajima, J.P. Gong. Self-adjustable adhesion of polyampholyte hydrogels. *Adv. Mater.* 2015, **27**, 7344-7348.

[139] S. Zhang, R. Zhao, J. Liu, J. Gu. Investigation on a hydrogel based passive thermal management system for lithium ion batteries. *Energy* 2014, **68**, 854-861.

[140] F.P. Incropera, D.P. DeWitt. Introduction to heat transfer. J. Wiley & sons, New York, 1990.

[141] N. Gorgoraptis, R.F.G. Catalao, P.M. Bays, M. Husain. Dynamic updating of working memory resources for visual objects. *J. Neurosci.* 2011, **31**, 8502-8511.

[142] K. Nader. Memory traces unbound. *Trends Neurosci.* 2003, **26**, 65-72.

[143] W.A. Wickelgren. Single-trace fragility theory of memory dynamics. *Mem. Cogn.* 1974, **2**, 775-780.

[144] O. Hardt, K. Nader, L. Nadel. Decay happens: The role of active forgetting in memory. *Trends Cogn. Sci.* 2013, **17**, 111-120.

[145] R.L. Davis, Y. Zhong. The biology of forgetting-a perspective. *Neuron* 2017, **95**, 490-503.

[146] S. Tonegawa, M. Pignatelli, D.S. Roy, T. JRyan. Memory engram storage and retrieval. *Curr. Opin. Neurobiol.* 2015, **35**, 101-109.

[147] H. Zhang, H. Zeng, A. Priimagi, O. Ikkala. Programmable responsive hydrogels inspired by classical conditioning algorithm. *Nat. Commun.* 2019, **10**, 3267.

[148] K. MacVittie, J. Halámek, V. Privman, E. Katz. A bioinspired associative memory system based on enzymatic cascades. *Chem. Commun.* 2013, **49**, 6962-6964.

[149] P.K. Kundu, D. Samanta, R. Leizrowice, B. Margulis, H. Zhao, M. Börner, T. Udayabhaskararao, D. Manna, R. Klajn. Light-controlled self-assembly of non-photoresponsive nanoparticles. *Nat. Chem.* 2015, **7**, 646-652.

[150] J.S. Mohammed, W.L. Murphy. Bioinspired design of dynamic materials. *Adv. Mater.* 2009, **21**, 2361-2374.

[151] E. Halgren, M.E. Smith. Cognitive evoked potentials as modulatory processes in human memory formation and retrieval. *Hum. Neurobiol.* 1987, **6**, 129-139.

[152] K.Y. Lee, D.J. Mooney. Hydrogels for tissue engineering. *Chem. Rev.* 2001, **101**, 1869-1880.

[153] T. Matsuda, R. Kawakami, R. Namba, T. Nakajima, J.P. Gong. Mechanoresponsive self-growing hydrogels inspired by muscle training. *Science* 2019, **363**, 504-508.

[154] Y. Osada, J.P. Gong. Soft and wet materials: polymer gels. *Adv. Mater.* 1998, **10**, 827-837.

[155] T. Tanaka, D. Fillmore, S.-T. Sun, I. Nishio, G. Swislow, A. Shah. Phase transitions in ionic gels. *Phys. Rev. Lett.* 1980, **45**, 1636-1639.

[156] M.A. Ward, T.K. Georgiou. Thermoresponsive polymers for biomedical applications. *Polymers-Basel* 2011, **3**, 1215-1242.

[157] M. Zrinyi, E. Wolfram. Experimental study of phase separation phenomena in

swollen polyvinyl acetate and polystyrene gels near the critical solution temperature. *J. Colloid Interface Sci.* 1982, **90**, 34-43.

[158] J.F. Scott, C.A.P. De Araujo. Ferroelectric memories. *Science* 1989, **246**, 1400-1405.

[159] F.I. Craik, R.S. Lockhart. Levels of processing: A framework for memory research. *J. Verbal Learn. Verbal Behav.* 1972, **11**, 671-684.

[160] B. Roozendaal, J.L. McGaugh. Memory modulation. *Behav. Neurosci.* 2011, **125**, 797-824.

Accomplishments

1. Papers

1.1. Original papers

1. **Chengtao Yu**, Honglei Guo, Kunpeng Cui, Xueyu Li, Ya Nan Ye, Takayuki Kurokawa, Jian Ping Gong. Hydrogels as dynamic memory with forgetting ability. ***Proc. Natl. Acad. Sci. U. S. A.*** 2020, 117, 18962-18968.
2. **Chengtao Yu**, Kunpeng Cui, Honglei Guo, Xueyu Li, Ya Nan Ye, Jian Ping Gong. Thermal history dependent responsive behavior of self-healing hydrogels. (In preparation)
3. **Chengtao Yu**, Kunpeng Cui, Honglei Guo, Xueyu Li, Ya Nan Ye, Jian Ping Gong. Structural heterogeneity dependent asymmetric swelling/shrinking kinetics in self-healing hydrogels. (In preparation)

1.2. Other papers

1. Xueyu Li, Kunpeng Cui, Tao Lin Sun, Lingpu Meng, **Chengtao Yu**, Liangbin Li, Costantino Creton, Takayuki Kurokawa, Jian Ping Gong. Mesoscale bicontinuous networks in self-healing hydrogels delay fatigue fracture. ***Proc. Natl. Acad. Sci. U. S. A.*** 2020, 117, 7606-7612.
2. Kunpeng Cui, Ya Nan Ye, Tao Lin Sun, **Chengtao Yu**, Xueyu Li, Takayuki Kurokawa, Jian Ping Gong. Phase separation behavior in tough and self-healing

polyampholyte hydrogels. ***Macromolecules*** 2020, 53, 5116-5126.

2. Conference presentations

1. **Chengtao Yu**, Kunpeng Cui, Liang Chen, Takahiro Matsuda, Jian Ping Gong. Stiff and tough physical hydrogel with excellent watery environment tolerance. 67th SPSJ Annual Meeting (September 2018, Sapporo).
2. **Chengtao Yu**, Honglei Guo, Kunpeng Cui, Liang Chen, Takahiro Matsuda, Jian Ping Gong. Highly stiff and tough physical hydrogel with excellent wet-environment tolerance. 68th SPSJ Annual Meeting (May 2019, Osaka).
3. **Chengtao Yu**, Honglei Guo, Kunpeng Cui, Xueyu Li, Ya Nan Ye, Jian Ping Gong. Bio-inspired memory-forgetting behaviors in physical hydrogels. 69th SPSJ Annual Meeting (May 2020, Fukuoka).

Acknowledgements

As time goes by, three-year learning passes like the arrow leaves the bow. Although the season is cycling from autumn to spring without ending, my age is leaving from junior to senior without suspending. I always dream my research to progress smoothly like my age, but it, in reality, behaves like the season that always turns back to where it starts. Therefore, I gradually understand what matters during this period is the things that I experienced and learned.

There is no doubt that I really enjoy my life in Hokkaido. Because of the marked diversity of latitude, the scenery here is very different from that in my hometown, especially the colorful leaves in autumn and the whirling snows in winter that I have never seen before. I feel so satisfied that I left many footprints in all directions of Hokkaido, from Kitami to Hakodate and from ishikari to Erimo. In June 2018, I bought a road bike, and cycled to peri-urban areas of Sapporo, such as Otaru, Eniwa, Ebetsu, and Jozankei. I have forgotten how many times I climbed from Zenibako to Asali or to Asalikawa Dam by bike. The only deficiency is that the wind is so heavy here, and so many times I cycled on the flat road, but felt like climbing.

Therefore, I am full of gratitude that Professor Jian Ping Gong give me an opportunity to pursue my PhD study in Hokkaido. Professor Gong keeps active, serious, and patient to research all the time. If there is no business trip, every workday she usually arrives her office at around 9:15 a.m. and leaves about 8:30 p.m. In order to keep awake in working, she always eats less at lunch. During this period of time, I

admire that her schedule is filled with various events, such as discussion, meeting, or writing. It is really difficult for a person to maintain the high efficiency in that case, but importantly she does. She pays attention to the details on experiments very much, and usually askes me the questions like "*what is the thickness of the sample*" and "*how about the testing temperature*". Based on her extensive experience and accumulation on soft matter, she is sensitive to hunt the critical problems and thinks much more comprehensive than us. Every time I discuss with her, she likes to draw a scheme to simplify the questions or list the related equations on the draft to explain my data. Sometimes she forgets the format of the equation, but she can leaf through *Polymer Physics*, written by Michael Rubinstein and Ralph H. Colby, to find it in a short time. She encourages students to face the problem in research and to explore the solutions. Carefully, she tries to remember the hobby of every member in LSW. She often asks me "*where did you go with your bike recently*" when I meet her. In my memory, this similar scene has occurred three times or more.

Meanwhile, I would like to thank Dr. Kunpeng Cui, who is our leader of viscoelastic-gel group and an assistant professor in our lab. He is good at studying the toughing mechanism of hydrogels and analyzing the polymer structure. He gives me a great help on the design of experiments and the data analysis. He also offers some constructive suggestions for my paper writing, and teaches me how to present the data better in the manuscript and make the logical line of the story clearer. His contributions make my research much deeper and more complete. Moreover, he and his family are kind to me, and I usually go to their home for dinner. They often pick me up and drive

out for relaxation together on the weekends.

Then, I would like to express my sincere thanks to Professor Takayuki Kurokawa, Tasuku Nakajima, Takayuki Nonoyama, and Daniel R. King, for helping me a lot on my study. For example, I often ask Dan-sensei some English grammars when I am writing my manuscript, because he is from Unite State and English is his mother language. I also thank Dr. Yoshinori Katsuyama and Ms. Yukiko Hane for their help with my experiments and devices. I really appreciate that the secretaries in LSW, Ms. Eiko Hasegawa, Yuki Ookubo, and Saeko Iseya, for providing lots of conveniences for me. I want to thank every member in LSW, both Japanese and international students, for taking care of me in my daily life, which makes me feel at home. Specially, I would like to thank Dr. Honglei Guo. At the beginning of my research, he provided a lot of help to me and taught me how to perform the experiments in our lab.

Besides, I want to thank our landlord, a Japanese gentleman, for providing so many conveniences in my daily life in Sapporo. He had been to China many times when he was young, and he knows Chinese culture, history and geography very well. Because of his kind and helpful qualities, more than half Chinese students in our lab are living in his building.

At last, I would like to express my deep thanks to my parents and fiancee, who always understand my choice and stand on my side all the time. I sincerely thank MEXT for providing the scholarship, and thank the staff at BL19U2 beamline of National Facility for Protein Science, Shanghai Synchrotron Radiation Facility, China for the assistant of data acquisition.

I want to conclude my thesis by a short story; as soon as I finished this thesis, believe it or not, I seemed to hear the words of the “old headmaster”:

“Boys, be enjoyable!”

Chengtao Yu

Laboratory of Soft & Wet Matter

Graduate School of Life Science

Hokkaido University

Sapporo, Japan

July 2020